Contract No:

This document was prepared in conjunction with work accomplished under Contract No. 89303321CEM000080 with the U.S. Department of Energy (DOE) Office of Environmental Management (EM).

Disclaimer:

This work was prepared under an agreement with and funded by the U.S. Government. Neither the U.S. Government or its employees, nor any of its contractors, subcontractors or their employees, makes any express or implied:

1) warranty or assumes any legal liability for the accuracy, completeness, or for the use or results of such use of any information, product, or process disclosed; or
2) representation that such use or results of such use would not infringe privately owned rights; or
3) endorsement or recommendation of any specifically identified commercial product, process, or service.

Any views and opinions of authors expressed in this work do not necessarily state or reflect those of the United States Government, or its contractors, or subcontractors.

Savannah River National Laboratory

FY21 LDRD ANNUAL REPORT

SRNL
SAVANNAH RIVER NATIONAL LABORATORY

LDRD
LABORATORY DIRECTED
RESEARCH & DEVELOPMENT

SRNL-STI-2022-00173

Disclaimer

This document was prepared by Battelle Savannah River Alliance, LLC (BSRA) under Contract No. 89303321CEM000080 with the U.S. Department of Energy (DOE). Release to and Use by Third Parties. As it pertains to releases of this document to third parties, and the use of or reference to this document by such third parties in whole or in part, neither BSRA nor DOE, nor their respective officers, directors, employees, agents, consultants or personal services contractors (i) make any warranty, expressed or implied, (ii) assume any legal liability or responsibility for the accuracy, completeness, or usefulness, of any information, apparatus, product or process disclosed herein or (iii) represent that use of the same will not infringe privately owned rights. Reference herein to any specific commercial product, process, or service by trademark, name, manufacture or otherwise, does not necessarily constitute or imply endorsement, recommendation, or favoring of the same by BSRA, DOE or their respective officers, directors, employees, agents, consultants or personal services contractors. The views and opinions of the authors expressed herein do not necessarily state or reflect those of BSRA, the United States Government or any agency thereof.

Message from the Laboratory Director

The Laboratory Directed Research and Development (LDRD) Program is important to the success of the Savannah River National Laboratory (SRNL). The program strengthens SRNL's scientific foundation, while positioning the laboratory to advance mission critical technologies.

In the past year, the Laboratory underwent an exciting transition, maturing to a stand-alone National Laboratory. With this change, the valuable contributions of the LDRD Program will grow the laboratory's presence in the global scientific and technical community. This unique change offers expanded opportunities for the laboratory, greater contributions to the DOE complex, and increased value to the nation.

A range of innovative science and engineering contributions have been discovered through LDRD supported research projects. In addition to scientific discoveries and engineering solutions, the program further expands SRNL's scientific and technical impact by yielding notable publications, supporting collaborations with external academic organizations, and integrating postdoctoral researchers and early career scientists.

To expand SRNL's pipeline of exceptional talent, in FY21 SRNL onboarded the first two Dwight D. Eisenhower Postdoctoral Researchers. Though this opportunity, Eisenhower postdoctoral researchers are supported by the LDRD program to investigate scientific challenges critical to the Nation.

I invite you to explore the pages of this Annual Report to learn more about the exciting innovative science and engineering contributions of SRNL researchers supported by the LDRD program.

Dr. Vahid Majidi

Laboratory Director

Savannah River National Laboratory

Overview

Research efforts to build upon the unique knowledge base of the Savannah River National Laboratory (SRNL) are funded through the Laboratory Directed Research and Development (LDRD) Program. The program yields foundational scientific research and development (R&D) essential to SRNL's core business areas, while aligning optimally and continuously with SRNL's Strategic Plan to provide long-term benefits to the Department of Energy (DOE), the National Nuclear Security Administration (NNSA), and other customers and stakeholders.

The three main objectives of the LDRD Program are:

As a multi-program laboratory, SRNL researchers investigate science and technology associated with a variety of DOE mission needs. All funded projects are aligned with at least one of SRNL's strategic goals, including:

- Provide applied science and engineering for the Office of Environmental Management's active clean-up sites and Office of Legacy Management's post closure management sites
- Provide science-based solutions for gaps identified in nonproliferation research and development and support the government in activities impacting national security
- Lead Science, Technology, and Engineering as the central technical authority for processing tritium loaded reservoirs and support production of plutonium pits
- Align science and energy security programs by focusing modern modeling, simulation, and data analytics tools on materials engineering and performance applications
- Build a workforce of the future

To enable science solutions and further the laboratory's strategic goals, specific core competencies are expanded and strengthened through the LDRD Program. Enabling core competencies include:

- Accelerating remediation, minimizing waste, and reducing risk
- Enabling next-generation nuclear materials processing and disposition
- Creating manufacturing solutions for the Office of Environmental Management, National Nuclear Security Administration, and energy security
- Assuring production and supply of strategic materials and weapons components
- Sensing, characterizing, assessing, and deterring nuclear proliferation
- Engineering new materials and their applications with data-driven modeling and simulations
- Securing connected control systems and associated data

LDRD BY THE *NUMBERS*

42
TOTAL # OF PROJECTS

41
PROJECTS INVOLVING EARLY CAREER STAFF

$9.074 M
TOTAL PROGRAM COST (NOT INCLUDING PM COSTS)

18
PROJECTS LED BY EARLY CAREER STAFF

20
POSTDOCTORAL RESEARCHERS FUNDED

24
PROJECTS SUPPORTING AT LEAST 1 POSTDOC

2
INVENTION DISCLOSURES

37
PEER-REVIEWED MANUSCRIPTS PUBLISHED

2
SCIENTIFIC JOURNAL COVERS

EXTERNAL ENTITIES ENGAGED

1. University of Georgia
2. University of South Carolina
3. Clemson University
4. New Mexico Institute of Mining and Technology
5. University of Nevada, Las Vegas
6. Coastal Carolina University
7. California State University, Northridge
8. Virginia Polytechnic Institute and State University
9. South Carolina Information & Intelligence Center
10. Glass WRX
11. Savannah River Nuclear Solutions
12. Savannah River Ecology Laboratory
13. Savannah River Consulting, LLC
14. Naval Research Labs

TABLE OF CONTENTS

EISENHOWER FELLOWSHIPS

The Dwight D. Eisenhower Postdoctoral Fellowship, a distinguished postdoctoral position at SRNL, attracts exemplary graduate students seeking experience at a National Laboratory. A unique position, Eisenhower Fellows are funded to investigate research they propose as part of the selection process. Their research efforts lead to solutions for complex energy and national defense challenges. The Fellowship is designed for pioneering researchers focused on expanding the boundaries of science and engineering. It is awarded to exceptional candidates who are able to demonstrate their scientific productivity through peer-reviewed publications and advanced research approaches to complex problems. This postdoctoral position is created to challenge the next generation of scientists and engineers to reexamine and push the norms, explore the unknown, and create new discoveries.

The Dwight D. Eisenhower Distinguished Postdoctoral Fellowship is designed for the next generation of scientists and engineers who excel in the application of fundamental science and engineering.

In 2021, SRNL welcomed two Eisenhower Fellows, Jonathon Baker and Nathaniel Hardin, to the laboratory team. These Fellows demonstrated their dedication to scientific discovery and its application furthering the Department of Energy's mission.

Dr. Hardin's Fellowship work focuses on iconic mass transport of non-conventional electrolytes for energy storage and carbon capture applications. In reflecting on his time as an Eisenhower Fellow at SRNL, Dr. Hardin has valued the ***opportunity to further his career as a scientist*** in the field of energy storage materials in a ***national laboratory setting*** and the exposure to the expansive research conducted by peers.

Dr. Baker's work focuses on the theoretical evaluation of point defect induced charge trapping mechanisms in CdZnTe and CdZnTeSe. Dr. Baker regards his position as an Eisenhower Fellow as offering additional ***freedom in choosing work that is important to him*** as a computational scientist, as well as additional responsibility of ***representing the Fellowship*** and setting a good example that can be emulated by future Fellows.

The work of SRNL's two Eisenhower Fellows for 2021 is detailed on the following pages.

Study of Ionic Mass Transport in Non-Conventional Electrolytes for Energy Storage and Carbon Capture Applications

Nathaniel Hardin

Project Highlight

The development and study of novel non-conventional electrolyte and eutectics to advance the field of energy storage for applications in vehicle electrification and grid storage.

Abstract

Electrolytes are the materials used to transport ions or redox active chemicals to facilitate an electrochemical process. Conventional electrolytes are the most common form of electrolyte used and consist of salts dissolved in a liquid solvent medium. While conventional electrolytes are generally inexpensive and work well with lithium-ion batteries, they have many shortfalls however, such as corrosion of the cell, flammability, toxicity, price, and incompatibility with other metals. This project investigates the fundamental properties in nonconventional electrolyte systems with an initial focus on eutectics being made. Using electrochemical methods (Cyclic Voltammetry (CV), Impedance, Conductance, etc.), we are studying the study of electrolyte systems containing ions used for thermal, chemical, or electrochemical energy storage such as Li^+, Mg^{2+}, Na^+, K^+, Al^{3+}, CO_3^{2-}, Cl^-, and O^{2-}. This research looks at how ion mobility effects the electrochemical characteristics and properties in green energy applications.

Project Team

Principal Investigator Nathaniel Hardin

Team Members

Patrick Ward

Zachary Duca

Objectives

- Design and build a cell and perform associated experiments
- Develop novel non-conventional electrolytes for analysis
- Initiate electrolyte characterization tests
- Electrochemically test electrolytes in an energy storage system such as batteries

Introduction

In the field of energy storage batteries have risen to the forefront due to multiple advances and applications. The forefront of these is lithium-ion batteries which have allowed for the development of modern electric vehicles and grid storage technologies. Lithium-ion battery research is however dominated by the use of conventional organic solvents which have numerous downsides. Because of the prevalence of conventional electrolytes, the field of non-conventional electrolyte research is behind conventional electrolytes in both number of papers and developed technology.

This project is focusing on the development and study of non-conventional electrolytes to address this shortfall. So far, this work has been able to develop a novel eutectic electrolyte for potential use in lithium-ion batteries. The developed electrolyte has shown satisfactory performance while also allowing for insights on the development of new electrolytes. The knowledge gained from this research can also be applied to non-lithium-based systems such as sodium, potassium, aluminum, magnesium, and calcium.

batteries, they have many shortfalls however, such as corrosion of the cell, flammability, toxicity, price, and incompatibility with other metals. This project investigates the fundamental properties in nonconventional electrolyte systems with an initial focus on eutectics being made. Using electrochemical methods (Cyclic Voltammetry (CV), Impedance, Conductance, etc.), we are studying the study of electrolyte systems containing ions used for thermal, chemical, or electrochemical energy storage such as Li^+, Mg^{2+}, Na^+, K^+, Al^{3+}, CO_3^{2-}, Cl^-, and O^{2-}. This research looks at how ion mobility effects the electrochemical characteristics and properties in green energy applications.

Approach

The approach used in this project highlights current knowledge in non-conventional eutectic electrolytes. Specifically, it allows for the study of molecular interactions hydrogen bond donors (in this case methyl carbamate) and acceptors with lithium salts and their ability to form a eutectic. The formulated eutectic is then studied using various electrochemical and spectroscopic characterization techniques to identify positives and shortfalls of the system. This approach allows translation of knowledge gained to other non-lithium-based systems and allows SRNL to develop in the field on non-conventional electrolytes. Specifically, electrochemical measurements such as CVs and galvanostatic cycling data provide us a tool to study the properties of the eutectic electrolyte in a battery. Furthermore, Impedance data allows us to directly measure how the change in eutectic conductance changes with regard to cycling and temperature.

Accomplishments

- Formulated a novel lithium eutectic based on TFSI (Bis(trifluoromethane)sulfonimide) and PF6 (hexafluorophosphate) salts with methyl carbamate in a ratio of 1:5 Li salt: Methyl carbamate wt:wt
- System cycles in full cell containing lithium titanate anode|eutectic electrolyte|lithium iron phosphate cathode
- Capacity retention at 0.5 C was 98% after 40 cycles and 95% after 50 cycles at room temperature
- Cycling efficiency is over 98%
- Conductance data shows good conductivity at room temperature
- Data and figures have been developed but we are refraining from adding them to this document while developing external publication and IP

Theoretical Evaluation of point defect induced charge trapping mechanisms in CdZnTe and CdZnTeSe

Jonathon N. Baker

Project Highlight

This project seeks to understand and further improve the CdZnTeSe material system for radiation detector applications, using cutting edge computational materials science. Improvement of this materials system will lead to advancements in technologies used for nuclear non-proliferation and medical imaging.

Project Team

Principal Investigator Jonathon N. Baker

Team Member Utpal Roy

Abstract

Cadmium zinc telluride selenide (CZTS) is a promising next-generation material for semiconductor radiation detector applications, with potential for enhanced room temperature performance and lower costs than current technologies. It is an improvement of the cadmium zinc telluride (CZT) material system, which has been under development for several decades. However, there is a lack of information on the fundamental atomic scale mechanisms behind this improvement.

This research seeks to use advanced computational techniques to develop that understanding, by performing quantum mechanical simulations of point defects and feeding that data into a thermodynamics model to obtain defect concentrations. Together with simulations of properties of interest for particular high-interest defects, this will enable a thorough and comprehensive understanding of the defect chemistry and defect derived properties, how they vary with processing, and how to improve performance by varying processing.

Objectives

- Generation and curation of high fidelity point defects databases for CdTe and ZnTe containing data on thermodynamic, electronic, optical, and vibrational properties of isolated and complexed point defects consisting of native species and impurities, including selenium
- Projection of CdTe and ZnTe databases into CdZnTe alloy compositions

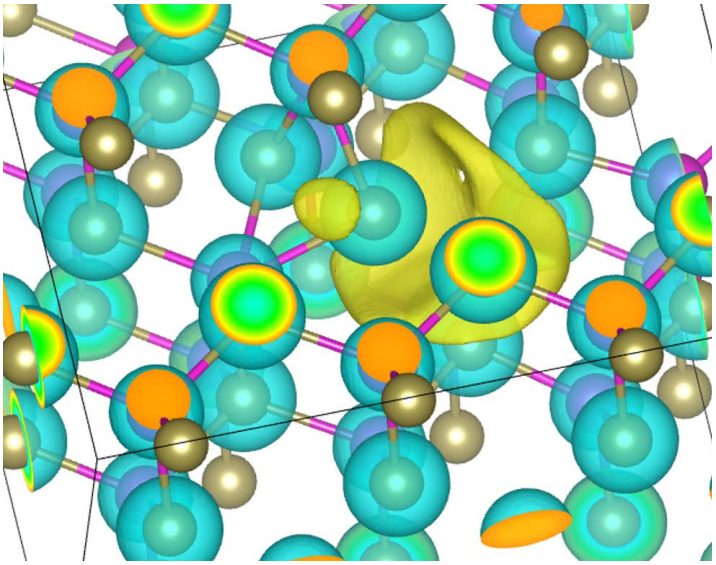

Figure 1: Potential field in and around displaced tellurium antisite defect in cadmium telluride (cadmium atoms shown in violet, and tellurium atoms are shown in tan)

- Development of thermochemical models to move past “cadmium rich” and “tellurium rich” chemical potential evaluation of point defect concentrations
- Analysis of point defect and carrier concentrations in CdTe, ZnTe, and CdZnTe alloys in terms of processing, composition, and doping level (esp. of Se)

Introduction

Techniques for accurately calculating the concentrations and ionization states of point defects in compound semiconductors have advanced rapidly in the past 10 years. However, these methods have yet to be applied in any kind of systematic way to materials of interest for radiation detection, due to difficulties in curating the large scale of hybrid exchange-correlation functional DFT (Density Functional Theory) data required to inform the necessary thermodynamics calculations. Additionally, the already extreme computational expense of performing these types of simulations for line compound materials is exponentially increased when considering alloys.

Simultaneously, substantial improvements have been made to the CZT material system by adding selenium, especially in terms of crystal quality, and these improvements and work to overcome fundamental hurdles facing CZT (e.g. substantial reduction of large amounts of sub-grain boundary networks and tellurium inclusions, and issues controlling alloy composition) have culminated in the development of CZTS. However, point defect derived trap states and their relation to processing remain, at best, poorly understood. This research seeks to systematically apply the advances in computational techniques for studying point defects to current state of the art methods for producing CZT and CZTS. This will fill the void of information on defect chemistry in CZTS while also allowing for very detailed study of particular defects of interest, and is expected to advance both defect science in CZT and CZTS, and computational science for the study of point defects.

To date, the project has developed the necessary thermochemical models and curated the large volume of point defect simulations needed to inform statistical mechanics calculations of point defect populations. The dataset is particularly large for the type of functional employed and will likely have much scientific utility even beyond the project it was generated for. Per the original project timeline, the project will shift much of its focus to analysis of this dataset and to simulation of impurities and vibrational properties in the next FY.

Approach

Hybrid exchange correlation functional density functional theory calculations (an advanced, high fidelity, and high computational expense method of treating the electron self-interaction in density functional theory) were performed for a large number of native and selenium-containing defects and defect complexes in ZnTe and CdTe, for use in projecting defect properties into lightly Se-doped CZT alloy. Alongside this effort, a thermodynamic model was derived for typical cases of CZT and CZTS growth. Together, these will be used for the next leg of the project to calculate defect chemistry and resultant properties, using statistical mechanics, and to inform impurity simulation selection and more advanced simulations targeting particular properties.

Accomplishments

- Hybrid exchange correlation functional density functional theory calculations have been performed for 163 defects across CdTe and ZnTe, with an additional 59 simulations for vibrational and spin-orbit-coupling perturbations. Current dataset size including ancillary simulations is approximately 1.1 TB. Simulations and curation of this dataset corresponds to tasks 1a, 1b, and 1c in the project's master Gantt chart, and to the first objective listed on page 1 of this report.
  - Completion of the simulations associated with Task 1a and milestone 1 proceeded slightly ahead of schedule, allowing Tasks 1b and 1c to be started early.
  - To the author's knowledge, the comprehensiveness of this dataset at the level of theory employed exceeds all other defect datasets for this materials family.
- Chemical potential models have been treated analytically for Bridgman growth and THM growth for CdTe and ZnTe, and are ready to be deployed numerically. The development of these models corresponds to task 2 in the project's master Gantt chart, and to the third objective listed on page 1 of this report.

FY21 Funded Projects

Fundamental ^{235}Uranium Nuclear Resonance Spectroscopy

Jonathan Christian

Project Highlight

Enriched uranium is ubiquitous in the nuclear industry, yet many of its quantum mechanical properties have never been observed using magnetic resonance. Using high frequency nuclear quadrupole spectroscopy, we seek to become the first research team to observe the quadruple resonance of the uranium-235 isotope.

Awards and Recognition

Parts of this project were presented at the 22nd International Society of Magnetic Resonance Conference via an invited presentation; the presentation was delivered in August 2021.

Some of the results from this project were published in the manuscript, Characterizing the solid hydrolysis product, $UF_4(H_2O)_{2.5}$, generated from neat water reactions with UF_4 at room temperature, Dalton Trans., 2021, 50, 2462-2471.

Intellectual Property Review

This report has been reviewed by SRNL Legal Counsel for intellectual property considerations and is approved to be publicly published in its current form.

Project Team

Principal Investigator Jonathan Christian

Team Members

A. Taylor Baldwin
Bryan Foley
Thomas Shehee
Michael Bronikowski
Matthew Wellons

External Collaborators

Christopher Klug (Naval Research Labs)
Joel Miller

Abstract

Uranium-235 is ubiquitous in the nuclear industry however, detailed characterization by magnetic resonance spectroscopy has remained largely elusive to-date. Conventional nuclear magnetic resonance techniques are ill-suited for characterizing ^{235}U due to the small gyromagnetic ratio and extremely large quadrupole moment of this spin $^{7}/_{2}$ isotope. Thus, we have designed and built a high-frequency nuclear quadrupole resonance spectrometer for measuring the quadrupole resonance of this important isotope.

A successful nuclear quadrupole resonance measurement of ^{235}U would be a significant accomplishment and could yield valuable physical parameters such as chemical shifts, local electric field gradients, and through-bond and through-space internuclear couplings, all of which are directly related to local structure. These terms can be used to understand structural details of poorly characterized uranium materials and can improve computational models of uranium for which accurate reference data is lacking.

Objectives

- Assemble high-frequency nuclear quadrupole resonance spectrometer using instrument components purchased in FY20.
- Perform functional tests of high-frequency nuclear quadrupole resonance spectrometer using well-characterized standards.
- Have SRNL staff gain competency in the assembly and operation of the high-frequency nuclear quadrupole resonance spectrometer.
- Execute solid-state 15N NMR measurements on 15N-enriched uranyl nitrate hexahydrate crystals.
- Prepare 235U-enriched uranyl nitrate hexahydrate crystals.
- Perform preliminary nuclear quadrupole resonance measurements on 235U-enriched samples.
- Prepare publications pertaining to the NMR of uranium in UF4.

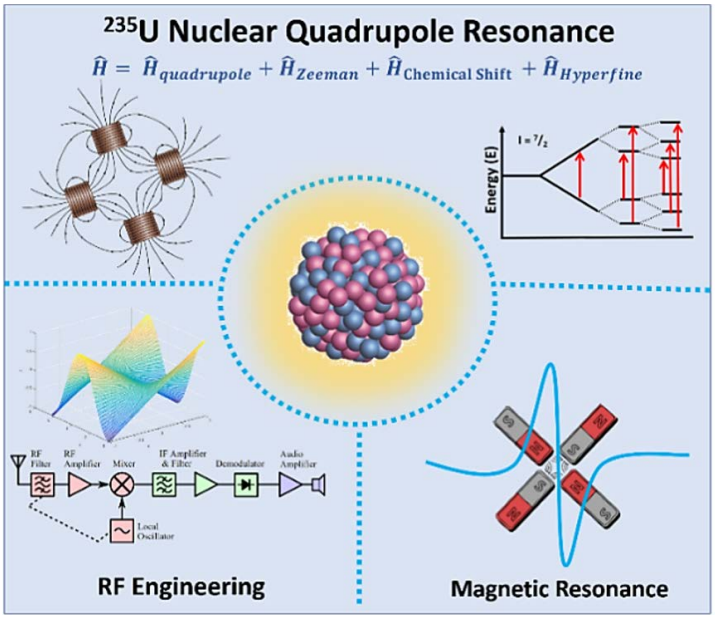

Introduction

Because of its non-zero spin, ^{235}U is potentially measurable via magnetic resonance spectroscopy (MRS). However, the gyromagnetic ratio of ^{235}U is estimated at 0.78 MHz/T, meaning the nuclear magnetic resonance (NMR) frequency, ν, of 235U due to Zeeman splitting in a magnetic field of 11.7 Tesla is 9.13 MHz, compared to 500 MHz for ^{1}H. Therefore, conventional NMR spectrometers are inapt at measuring this rare isotope. Furthermore, since signal-to-noise generally scales as $\nu^{5/2}$, detection of ^{235}U NMR at very low frequencies is challenging. The significance of these obstacles is evidenced by the scarcity of magnetic resonance literature pertaining to ^{235}U. The only published ^{235}U NMR reference is a two-and-a-half-page letter from 1983 involving 93.5% enriched liquid uranium hexafluoride heated to 380 K. The linewidth at 11.747 T was said to be 20 KHz, but no other relaxation information was given. This work has been rarely cited and most of those papers are theoretical.

Although the predicted NMR frequency of ^{235}U is extremely low and there appears to be numerous barriers in measuring and analyzing an NMR signal from this isotope, the nuclear quadrupole resonance (NQR) of ^{235}U is predicted to be near 1 GHz.[1] This is over two orders of magnitude larger than the NMR frequency, meaning that the quadrupole term is the dominant energy term in the ^{235}U spin Hamiltonian. Therefore, direct measurement of this term would be a significant scientific achievement and should give further insight into the magnetic properties of this important isotope.

Approach

The ambitious goal of being the first research team to measure NQR signals from ^{235}U has necessitated a detailed experimental approach. A high-level summary of our approach is as follows.

SRNL will develop robust synthesis methods for producing high quality single crystals of different uranium compounds, and together with NRL, will develop a homebuilt high-frequency NQR spectrometer for analyzing said crystals.

Following functional and benchmark testing of the homebuilt NQR spectrometer using chemical standards, depleted and enriched uranium-containing samples will be analyzed. Ultimately, the NQR spectrometer will be installed within SRNL's Category II Nuclear Facility where it will be utilized for additional NQR studies on enriched uranium and other radioactive isotopes that are amenable towards analysis by NQR spectroscopy.

Results/Discussion

The NQR spectrometer designed for this project is comprised of a 50 W high power GaN amplifier, multiples heat sinks, a 100 W high power LDMOS amplifier, multiple power supplies, and a compact, modular, NMR / NQR Tecmag Redstone console configurable with multiple transmitters, receivers, and gradient channels. With its numerous options, the Redstone can be configured for any magnetic resonance application in the frequency range from ~ 2 kHz to 3.5 GHz and does not require manual heterodyning of excitation signals. In FY21, this instrument was assembled at NRL, as shown in **Figure 1**.

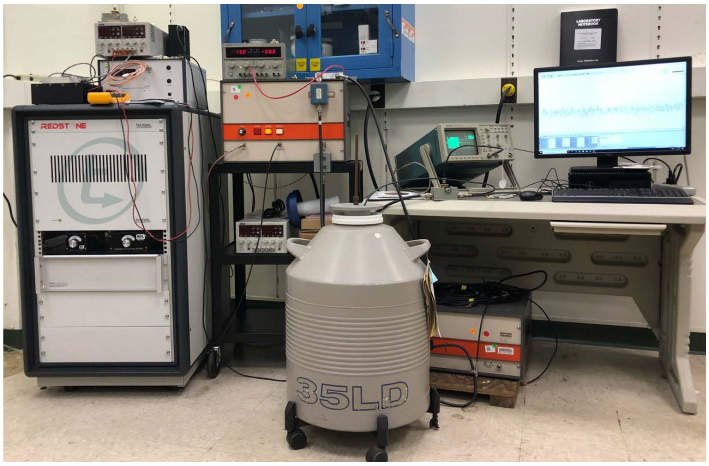

Figure 1: SRNL's new NQR spectrometer.

Functional and benchmark tests of the NQR spectrometer have proven successful up to 30 GHz. An example free-induction decay and Fourier transform NQR spectrum measured on the homebuilt NQR for ^{35}Cl in KClO3 is shown in **Figure 2**.

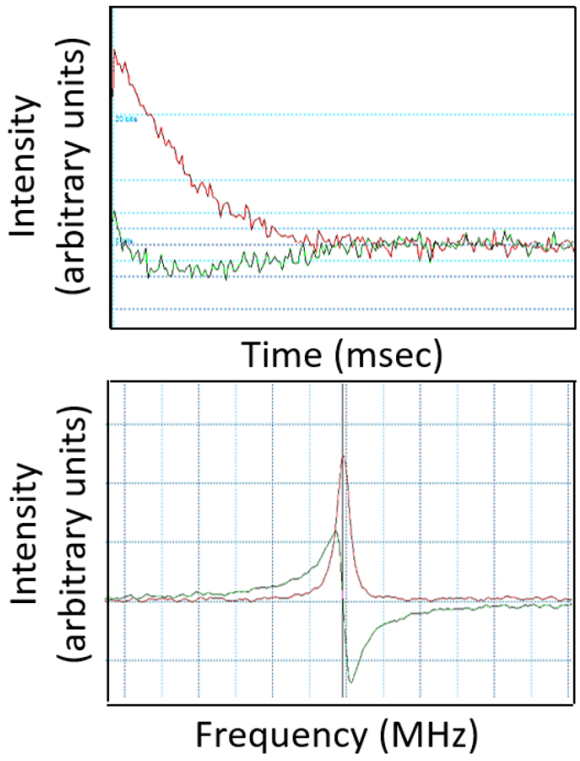

Figure 2: Top: Free induction decay of the 35Cl NQR signal at 28.1 MHz measured with SRNL's new NQR spectrometer. Bottom: Fourier transformed spectrum.

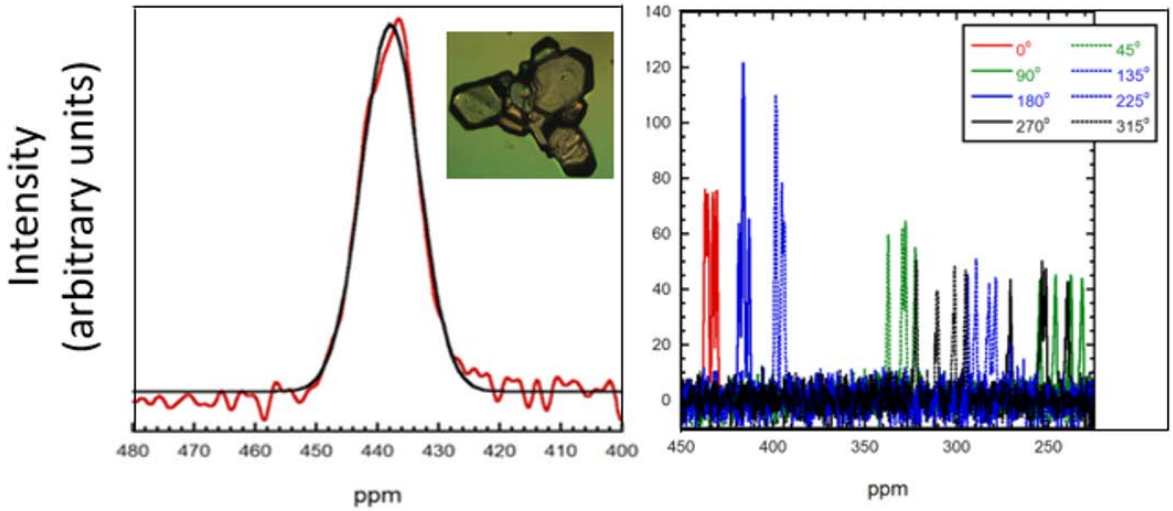

Figure 3: Left: 15N NMR spectrum for a hexagonal crystal of uranyl nitrate hexahydrate (red trace) fit to a Gaussian function (black trace) with FWHM = 11.0 ppm (~ 550 Hz at 11.7 T). Right. 15N NMR spectra measured at multiple crystal orientations using magic angle spinning. Spectra were acquired using a spin echo pulse sequence with a delay of 40 µsec between pulses and a wait time between scans of 128 s.

Extensive ^{15}N NMR measurements on ^{15}N-enriched uranyl nitrate hexahydrate (UNH) crystals have proven fruitful. As shown in **Figure 3**, a crystal of this compound exhibits a single spectral peak with a narrow linewidth (full width at half maximum, FWHM ≈ 550 Hz at 11.7 T). The longitudinal relaxation time, T_1 for this compound was found to be 128 sec and the transverse relaxation time, T_2 was relatively slow such that spin echo experiments used a delay between pulses, τ , of 40 µsec. The ^{15}N NMR spectrum of UNH was also found to be highly anisotropic. That is, the spectrum varies greatly depending on the crystal orientation within an external magnetic field.

The narrow linewidth, relatively long relaxation times, and highly anisotropic nature of ^{15}N in UNH are promising attributes for several reasons. First, spectral anisotropy is related to molecular anisotropy. Thus, the molecular structure of UNH is clearly anisotropic (as expected), which is an important prerequisite for compounds to exhibit a quadrupole moment, and thus be measured using NQR spectroscopy. Second, the narrow linewidth and relatively long relaxation times may allow NQR perturbations to be observed in ^{15}N NMR measurements of enriched uranium crystals (> 20% ^{235}U). If such perturbations are observed, quantum mechanical calculations can be used to estimate the nuclear quadrupole moment of ^{235}U, thus allowing NMR to provide indirect detection of ^{235}U and providing our research team with an estimate of the currently unknown quadrupole resonance frequency of ^{235}U. An estimate of the quadrupole resonance frequency will greatly facilitate future NQR measurements.

Additional NMR analyses of ^{19}F in UF_4 with ancillary vibrational spectroscopy measurements have proved fruitful in analyzing chemical and structural changes that occur for this important nuclear compound, as described in detail in our recent publication (Dalton Trans., 50, 2462-2471).

Accomplishments

- A novel high-frequency NQR spectrometer was designed and built.
- Functional and benchmark tests of the high-frequency NQR spectrometer have been performed up to 30 GHz.
- A manuscript describing chemical and structural details of UF4 as measured by 19F NMR was published in Dalton Transactions (Dalton Trans., 2021, 50, 2462-2471).
- A manuscript describing chemical and structural details of naturally-occurring UF4 hydrolysis products as measured by 19F NMR has been drafted and will be submitted for publication in early FY22.
- Extensive 15N NMR measurements of uranyl nitrate hexahydrate crystals have yielded interesting results that should support the goal of understanding how uranium enrichment affects NMR spectra.
- A manuscript describing 15N NMR measurements of uranyl nitrate hexahydrate has been drafted and will be completed following enriched uranium measurements.
- Published data were presented at 22nd International Society of Magnetic Resonance Conference
- Enriched uranium samples have been synthesized and will be shipped to NRL in late FY21/early FY22.
- Significant logistical arrangements have been made to allow SRNL to accommodate shipment and installation of the high-frequency NQR spectrometer in FY22.
  - Logistical considerations included, radiological concerns, electrical requirements, asphyxiation concerns for liquid cryogenic use, space requirements, etc.
-

FY21 Publications

Christian, J.H. et. al., Characterizing the solid hydrolysis product, UF4(H2O)2.5, generated from neat water reactions with UF4 at room temperature. Dalton Trans., 2021, 50, 2462-2471.

Contributing Postdoctoral Researchers

Bryan Foley Nicholas Groden

External Collaborators

Christopher Klug Joel Miller

Reference

Cho, H., Dependence of nuclear quadrupole resonance transitions on the electric field gradient asymmetry parameter for nuclides with half-integer spins. Atomic Data and Nuclear Data Tables 2016, 111-112, 29-40.

Acronyms

FWHM – Full Width at Half Maximum

NMR – Nuclear Magnetic Resonance

NRL – Naval Research Laboratory

NQR – Nuclear Quadrupole Resonance

UNH – Uranyl Nitrate Hexahydrate

Figure 4: LDRD researchers study enriched uranium materials inside a radiological glovebox within SRNL's Category II nuclear facility.

Deuterium Concentration Effects on Cell Cycle Progression

Wendy Kuhne

Project Highlight

This project is conducting basic science to investigate the role of Deuterium (D) concentrations on cell cycle regulation over time. Evaluating the role of D in human cells should lead to a better understanding of cell cycle progression on normal and cancer human cells and if there is a link to radiation resistance through genomic investigation.

Project Team

Principal Investigator Wendy Kuhne

Team Members
Candace Langan Lucas Angelette

Abstract

Deuterium (D) seems to play an important role in biology and is thought to be a missing piece in understanding cancer and radiation resistance. D is found in natural water at a concentration of ~150 parts per million (ppm), while D concentrations above 150 ppm are known to produce toxic effects in many organisms. There is evidence to suggest D levels significantly less than 150 ppm can cause delays in cell progression through the normal mitotic cell cycle. Some have theorized that the deuterium: hydrogen ratio (D:H) in cells may impact radiation resistance. Therefore, evaluating the role of D in human cells should lead to a better understanding of cell cycle progression and radiation resistance. To date, little has been revealed on the time-dependent effects of deuterium-depleted water (DDW – less than 150 ppm) on normal and cancer human cells or how the reduction of cell proliferation is associated with cell cycle regulation and consequence on gene expression profiles. Our studies will help further the mission of the Department of Energy to enhance the understanding of deuterium in fundamental biology by studying the cell cycle as a function of D concentration.

Objectives

- Perform kinetic studies of D levels with 5% CO_2 and temperature inside of the incubator over time
- Perform phenotypic investigations of normal and cancer cells with varying concentrations of Deuterium Water (D_2O) treatment over time. Measure morphology changes and proliferation/growth rate changes using microscopy and BD FACSMelody^{TM} cell sorter
- Perform molecular investigations of normal and cancer cells with varying concentrations of D_2O treatment over time- gene expression determination using RNA-seq, RT-qPCR and SDS-PAGE

Introduction

Investigation into the effect of deuterium depleted water (DDW), concentrations below the normal 150 ppm, on biological systems began less than 20 years ago.[1] Much of the published literature has focused on the effect of DDW on the phenotypic growth of normal/stem cells, tumor transplantation models, and tumor cell systems, with little emphasis on molecular mechanisms involved.[2] The few studies that attempt to investigate the effect of DDW on normal eukaryotic cells are either under hypoxic conditions, are poorly controlled and are ultimately largely uninformative.[3,4] The lack of information in this regard creates an opportunity to investigate and understand the mechanisms associated with why the (or a) cell cycle is delayed under DDW conditions in a controlled manner.

The role of D in biology is thought to be a missing piece in understanding cancer and cancer epidemics in western populations. Little has been revealed on the time-dependent effects of DDW on normal/cancer human cells or how the reduction of cell growth/proliferation is associated with cell cycle regulation/consequence on gene expression. Many different genes are involved in cell cycle regulation and activation of specific genes dictates response to cell proliferation.

The purpose of the project is to unravel the novel mechanisms involved with the effect of DDW, in differing concentrations, on normal and cancerous human cell proliferation.

Approach

Investigate phenotypic changes on human cells upon treatment of varying concentrations of DDW/D_2O in a time-dependent manner. We will culture normal/cancer human cells in varying concentrations of DDW/D_2O in cell growth media/control media, and measure D concentrations using a PICARO Isotope and Gas Concentration Analyzer. Microscopy/Imaging will be used to monitor cell morphology changes with exposure to DDW. Proliferation/growth rate will be determined using cell counting techniques.

We will investigate molecular changes in the transcriptome upon treatment of varying concentrations of DDW/D2O in a time-dependent manner. Cells will be collected at various time points for molecular analysis. RNA-sequencing (RNA-seq) will be performed to examine all transcripts/gene patterns that may be dysregulated upon DDW treatment. We will focus on suspected pathways including cell cycle, metabolism, cell death and DNA repair; genes/proteins of interest will be validated using RT-qPCR and SDS-PAGE protein detection.

Accomplishments

- Kinetics of Deuterium (D) exchange with ambient air and characterization of background deuterium levels in water and Dulbecco's Modified Eagle Medium (DMEM) cell media. No significant change in D concentration was measured over the course of three days in water **(Figure 1)** or in prepared cell culture media **(Figure 2**) at ambient conditions.
- Cell cultures were initiated with Biosafety Level 1 HEL 299 (human lung normal) and A549 (human lung cancer epithelial line.

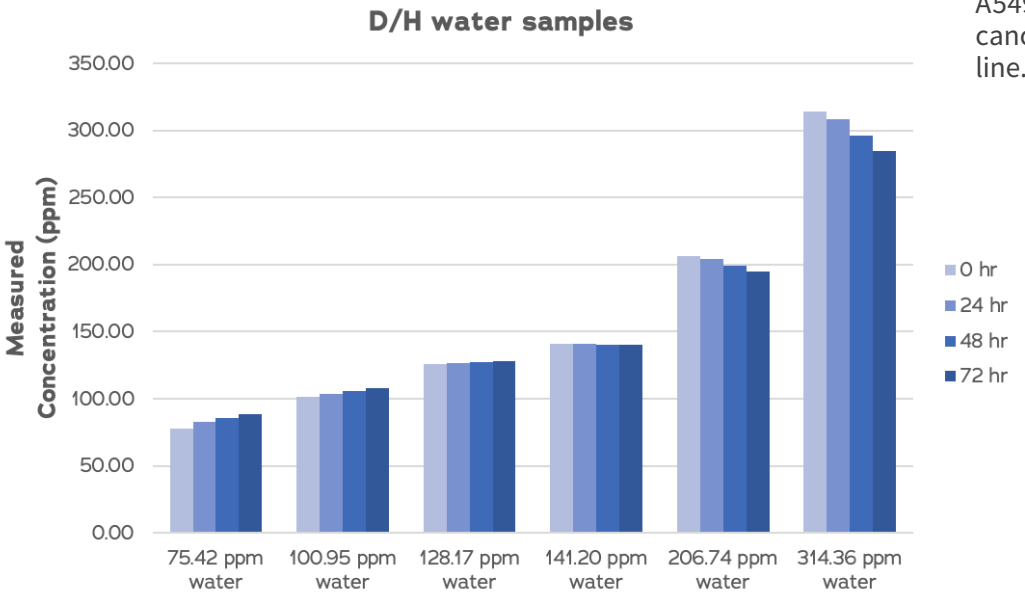

Figure 1: Deuterium concentration (ppm) measured in water only at ambient conditions for 72 hr.

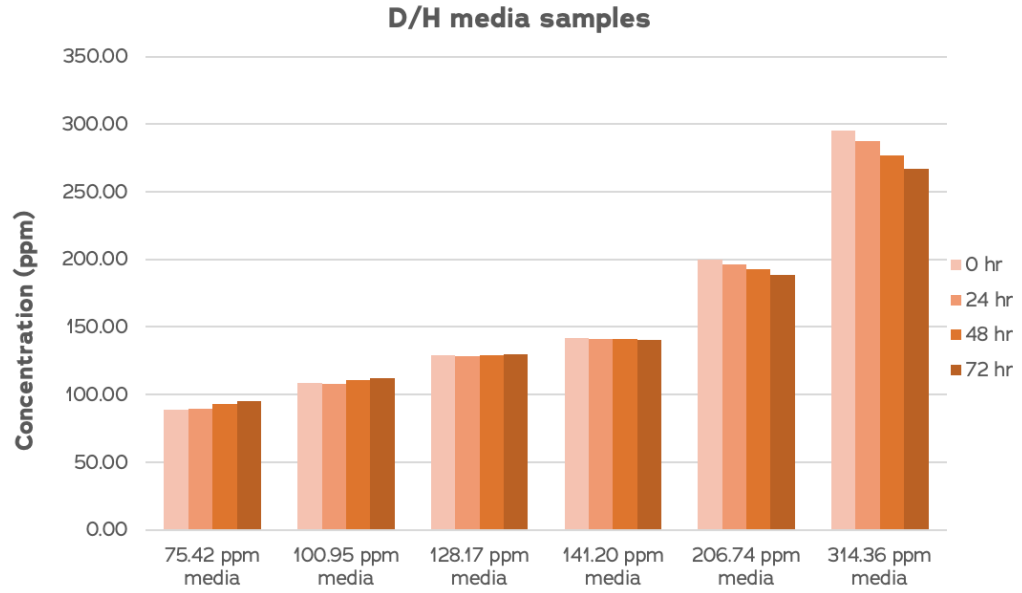

Figure 2: Deuterium concentration (ppm) measured in DMEM growth media at ambient conditions for 72 hr.

Contributing Postdoctoral Researcher

Candace Langan

References

1. Hohlefelder, L.S.; Stögbauer, T; Opitz, M.; Bayerl, T.M.; Rädler, J.O. Heavy water reduces GFP expression in prokaryotic cell-free assay at the translation level while stimulating its transcription. Biomed Res Int. 2013, 1-9. DOI:10.1155/2013/592745.
2. Basov, A.; Fedulova, L.; Baryshev, M.; Dzhimak, S. Deuterium-Depleted Water Influence on the Isotope 2H/1H Regulation in Body and Individual Adaptation. Nutrients. 2019. 11(8):1903. DOI:10.3390/nu11081903.
3. Zlatska, O.V.; Zubrov, D.O.; Vasyliev, R.G.; Syroeshkin, A.V.; Zlatskiy, I.A. Deuterium Effect on Proliferation and Clonogenic Potential of Human Dermal Fibroblasts In Vitro. Problems of Cryobiology and Cryomedicine. 2018.28(1):49-53. DOI:10.1155/2018/5454367.
4. Syroeshkin, A.V.; Antipova, N.V.; Zlatska, A.V.; Zlatskiy, I.A.; Skylska, M.D.; Grebennikova, T.V.; Goncharuk, V.V. The Effect of the Deuterium Depleted Water on the Biological Activity of the Eukaryotic Cells. J Trace Elements in Medicine and Biology, 2018. 50:629-633. DOI:10.1016/j.jtemb.2018 05.004.

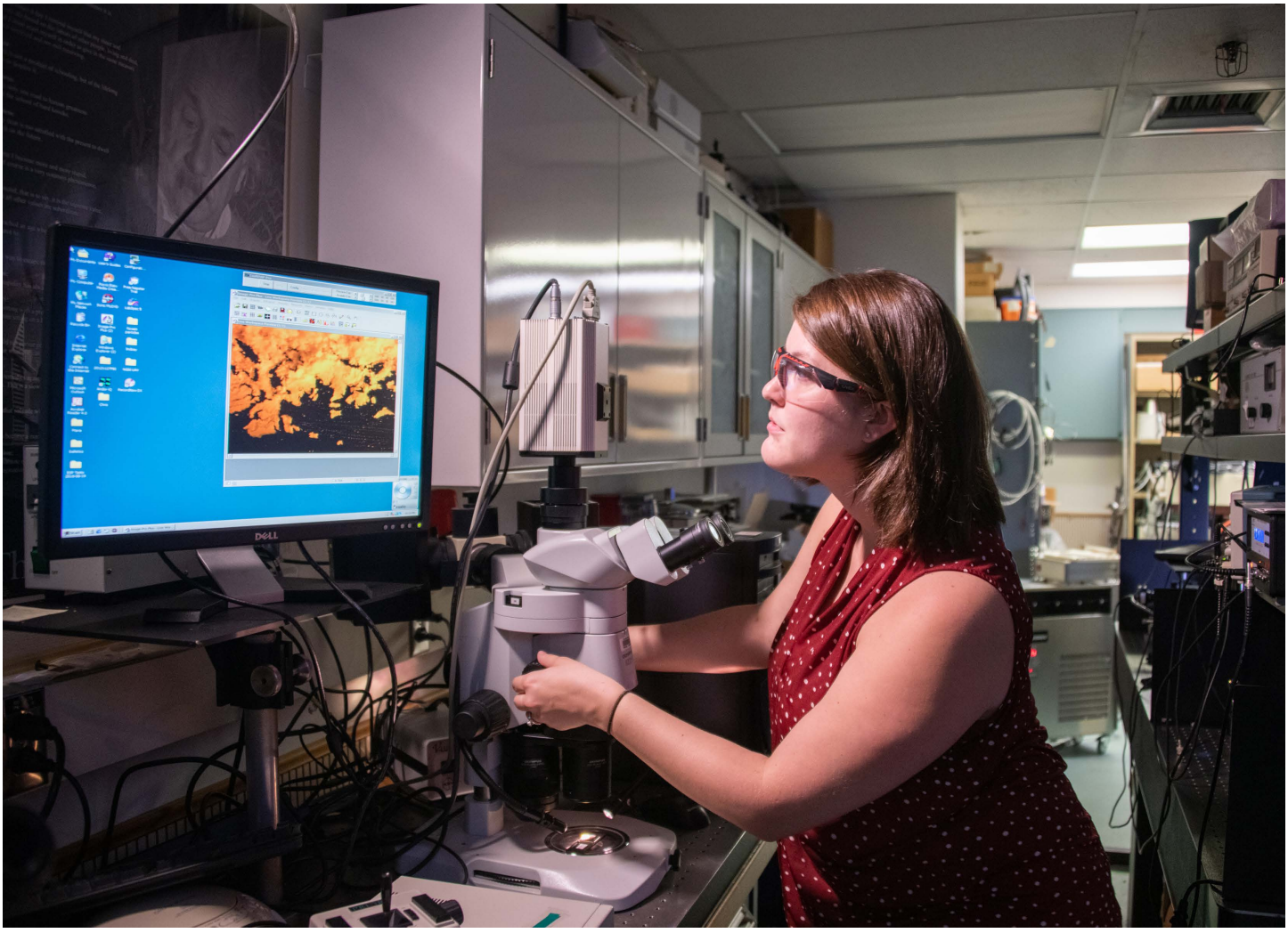

Laser-Based Means for Accelerating Nuclear Decay Rate

Robert Lascola

Project Highlight

This project aims to reproduce and explain reports of using tabletop pulsed lasers and gold nanoparticles to promote faster decay of radioactive materials. Verification of this observation could be the first step in finding a new method for addressing long-term storage of nuclear waste.

Project Team

Principal Investigator Robert Lascola

Team Members
Michael Thomas
David DiPrete
Simona Murph
Kalee Fenker

Abstract

This project aims to replicate and build upon a reported series of results whereby nuclear decay of unstable species has been accelerated under laser irradiation in the presence of resonantly excited plasmonic nanoparticles. Most theoretical investigations of this problem do not predict the enhancement to be significant. Further, alternate explanations for the observed decrease in signals associated with the supposedly destroyed species need to be examined. There are potentially substantial benefits from exploiting this effect to reduce the long-term radiological storage requirements of certain forms of nuclear waste. These benefits merit the confirmation or disproving of the effect.

Objectives

- Overall objective: investigate the accelerated α and β decay of radionuclides through exposure to the intense electric fields associated with laser-irradiated nanoparticles and nanopatterned surfaces
- Reproduce observations reported in the literature
- If observations are reproduced, establish quantitative relationships between experimental parameters and changes in the decay rates
- If observations are not reproduced, propose and investigate alternative explanations for the reported results

Introduction

This project aims to replicate and explain reported observations of the apparent acceleration of nuclear (α or β) decay of unstable species under laser irradiation in the presence of resonantly excited plasmonic nanoparticles. [1-2] Calculations disagree on the feasibility of altering nuclear processes through a non-resonant interaction of an atom with an intense external electric field. [3-7] Resonant excitement of plasmonic nanoparticles can lead to increases of electric field strength on the order of 10^5-10^6 near the nanoparticle surfaces. Laser pulses from commercially available, benchtop sources (such as a Nd:YAG laser) can thus be enhanced to 10^{18}-10^{19} W/cm^2, which is sufficient to excite relativistic energies in electrons. [8] In the reported work, fs, ps, and ns pulses directed into a solution of colloidal gold nanoparticles and dissolved UO_2Cl_2 altered the ^{238}U decay pathway, as detected by changes in the concentrations of daughter products ^{234}Th and ^{234}mPa.

The significance of these results is that the equipment and materials used to generate changes in nuclear decay rates are much more readily accessible than synchrotron sources or free-electron lasers which would access nuclear transitions directly. [9] The ability to accelerate decay rates would permit transformation of nuclear waste from a radiological and chemical problem at geologic time scales to a shorter-term chemical problem. Although significant engineering challenges would remain, not least of which being the determination of the form and materials for nanoparticles which can be used in massive quantities, the confirmation of these results would justify continued development in this field. Additionally, a more quantitative approach to irradiation parameters and the kinetics of decay and regrowth would inform and help resolve the discrepancy amongst the calculations.

In FY21, the Nd:YAG laser, optics, and cooling system were installed in a radiological laboratory to allow irradiation of samples (see **Figure 1**). Several uranyl solutions (nitrate or chloride salts in a matching mild acid) were tested to which Au nanoparticles were added. There is a narrow window of solution acidity and uranyl concentration for which both uranyl and the nanoparticles will remain soluble (see **Figure 2**). Laser irradiation of such samples did not result in a measurable change in the concentrations of the ^{234}Th and ^{234m}Pa daughter products, as measured by gamma spectroscopy using an in-well high purity Ge detector. Explanations for this negative result are explored which also provide insight to the previously reported results.

Approach

The approach was intended to maximize the likelihood of creating the reported decay effect, but also sought to gather evidence supporting alternate explanations for the observations. For example, the original reports generally featured the *in situ* formation of nanoparticles by ablation of a solid target suspended in a solution of radionuclides. Although the nanoparticles quickly coalesced and settled at the bottom of the container, new nanoparticles were formed by subsequent ablative pulses. In this work, *in situ* ablation was considered to be less logistically feasible than working with solvated nanoparticles.

Further, allowing the nanoparticles and radionuclides to exist in the same solution could allow the development of the solution, that is, foster the attraction of the radionuclides to the nanoparticle surface. This co-location is necessary for the radionuclides to experience the enhanced electric fields from the nanoparticle plasmons, which are essentially restricted to the surface.

Consideration was also given to collecting evidence that might support an alternate explanation for the original observations. In part, this was done by paying careful attention to the collection geometry for gamma emissions from the entire sample, in particular trying to include both sample supernate and precipitated solids. Other factors were considered, including the number of pulses needed to quantitatively interrogate the solution.

Figure 1: Setting up the laser irradiation experiment in a radiological laboratory.

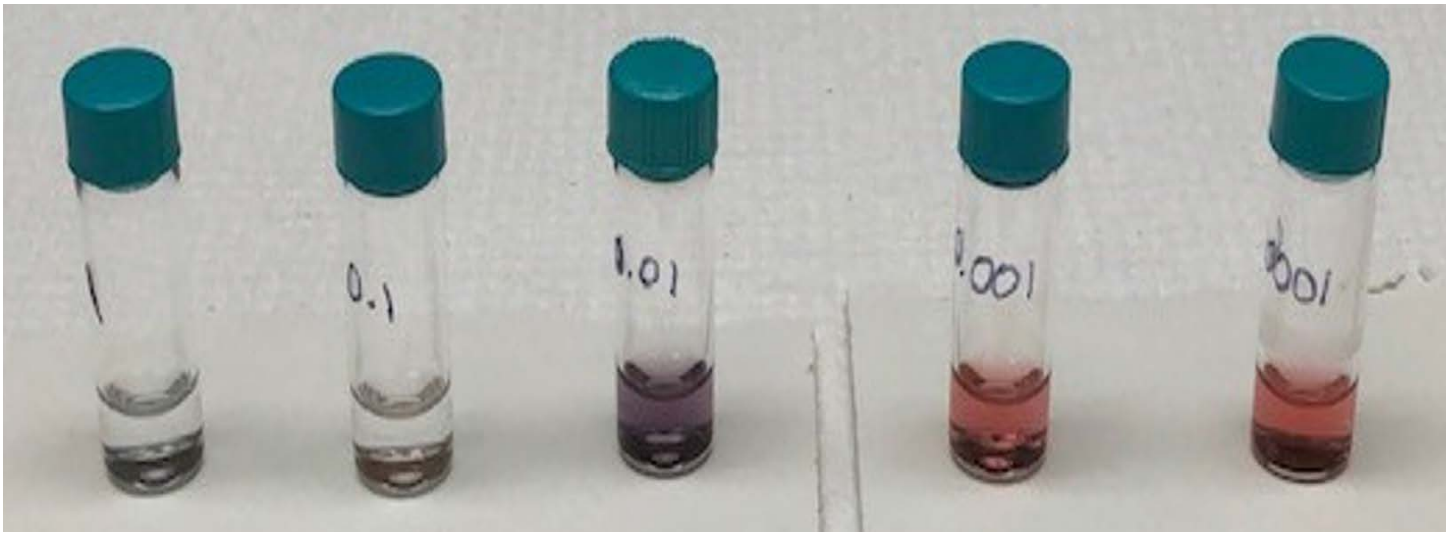

Figure 2: Stability of Au nanoparticles in various concentrations of HCl (1 M to 10^{-4} M, left to right).

Accomplishments

- Determined a set of solution conditions that simultaneously supported stable suspensions of Au nanoparticles and dissolution of uranium. This solution, at 0.01 M HCl and ~ 0.1 g/L U, was much lower (by 100x) in concentration of U than the previous work. Although there were many more U atoms than nanoparticles (by ~$2e^5$), this was still less of an excess than the previous work, and presumably would be more favorable for a quantitative transformation of the radionuclides.
- Laser-irradiated the stable solutions but did not observe a statistically significant change in the ratio of mother/daughter products.
- Noted that approximately 109 laser shots would be required to fully interrogate a sample volume of 4 mL. This is 2-3 orders of magnitude larger than used in any of the experiments previously reported and is not consistent with the reported large scale destruction of the daughter isotopes.
- Conducted preliminary experiments to determine if daughter products are selectively partitioning into precipitates.

Contributing Postdoctoral Researcher

Michael Thomas

Comprehensive Chemical Fingerprinting by Multidimensional GC and Supervised Machine Learning

Joseph Mannion

Project Highlight

The project successfully coupled cutting edge analytical instrumentation for trace atmospheric volatile organic compound detection with modern machine learning based data analysis strategies. This capability significantly advances our ability to characterize complex emission profiles within the atmosphere for national security applications.

Project Team

Principal Investigator Joe Mannion

Team Members
Heather Brant
Stephanie Gamble
Eric Hoar

External Collaborators
Sapna Sarupria (Clemson University)
Jiexin Shi

Abstract

This project leveraged advances in machine learning based data analysis techniques and untargeted analytical methods for organic analysis to progress nuclear nonproliferation technologies beyond current capabilities. The developed approaches can be used to detect and identify complex chemical fingerprints of facilities of interest. These techniques have been developed for fields such as metabolomics and genomics but have not been applied to nuclear nonproliferation applications. Adaptation of these techniques for volatile organic compound analysis has far reaching application within the scientific community including environmental chemistry, atmospheric physics, and climate sciences.

Objectives

- Develop multidimensional gas chromatography high resolution mass spectrometry analytical methods for the analysis of volatile organic compounds.
- Collect a training data set utilizing multidimensional gas chromatography for algorithm development.
- Develop machine learning based data analysis algorithms for complex VOC profiles using an open-source data set.

Introduction

Volatile organic compound (VOC) collection and analysis techniques have been under development at SRNL for more than two decades for national security applications. Traditionally these approaches have attempted to identify one to two “signature” species that are indicative of a given activity. The shortcoming of these efforts has been the fundamental limitations of a silver bullet approach with regards to organic signatures. VOC production and emissions are complex, highly dynamic, and subject to complicating matters such as holdup, chemical transformations, and complex backgrounds (up to 10,000 unique chemical species have been identified in a single air sample). Despite these challenges, VOC signatures are attractive as they can provide unique information.

The major goal of this project is to utilize machine learning based data analysis approaches to develop multi-species chemical signature “fingerprints” of processes relevant to nonproliferation interests. This untargeted approach will assess organic emissions as a comprehensive collection, rather than a “silver bullet” approach, to create more robust and informative chemical fingerprints of activities. The objective is to collect, analyze, and identify patterns present in measured volatile organic emissions from facilities of interest. The product of this work is data collection modalities, machine learning based data analysis algorithms, and a fingerprint database allowing for identification and assessment of activities.

A multipronged approach was taken for project efforts. The focus at SRNL was analytical method development for comprehensive VOC analysis utilizing the multidimensional gas chromatograph procured in FY19. This system is one of the most powerful commercially available instruments for VOC analysis and was found to afford ~4 orders of magnitude improved sensitivity (and 1 – 2 orders of magnitude peak capacity) over traditional GC/MS systems at SRNL. The focus at Clemson University was the development of machine learning based data analysis approaches utilizing the open-source EPA Speciate database. This database contains more than 3,000 pollution profiles from industrial, commercial, and residential emission sources. Traditional chemometric techniques were compared to the machine learning based approaches.

Approach

Multidimensional gas chromatography (MDGC) is an established technique for the analysis of highly complex samples (**Figure 1**). It is uniquely suited to applications involving complex matrices and hundreds to thousands of analyte species. Thousands of volatile organic compounds have been identified in the atmosphere that arise from both biogenic and anthropogenic sources. When MDGC is applied to complex samples and coupled with multichannel detectors, such as mass spectrometers, enormous amounts of data are generated (on the order of gigabytes for a single run). Traditional data analysis methods are not practical with such large data sets; therefore, modern data analysis techniques must be applied that take advantage of the higher order dimensionality of the data sets. These methods convert chemical data into information using algorithms. Machine learning based clustering and pattern recognition is utilized for this work.

The number of applications utilizing machine learning has vastly expanded in recent years; however, limitations, pitfalls, and hurdles exist in the implementation of machine learning techniques to some applications. Analysis of complex VOC emissions is an example of the curse of dimensionality. In essence, when the dimensionality of a problem increases (i.e. the number of chemicals present in a sample) the volume (i.e. data space) grows so quickly that the data becomes sparse. As the number of features (i.e. chemicals) increases, the data (i.e. number of samples) must grow exponentially to maintain accurate representation; for example, a system with 15 features may require millions of samples to accurately classify the system. Application of machine learning techniques for complex systems such as atmospheric VOC analysis containing thousands of features therefore requires implementation of approaches such as dimensionality reduction and feature engineering to overcome this curse of dimensionality. These techniques and various clustering approaches are explored in this work utilizing an adequately complex data set that represents real world data.

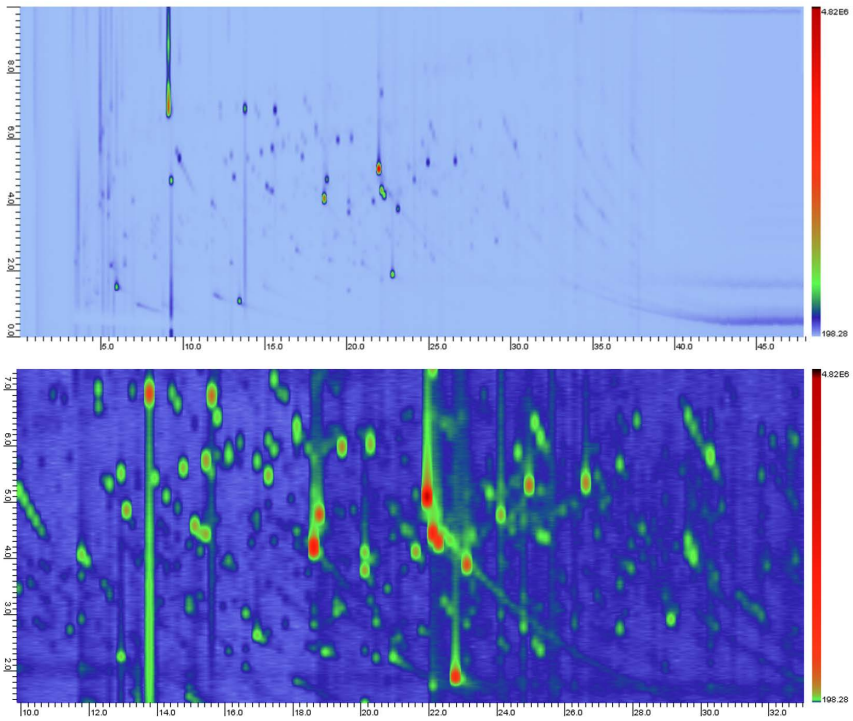

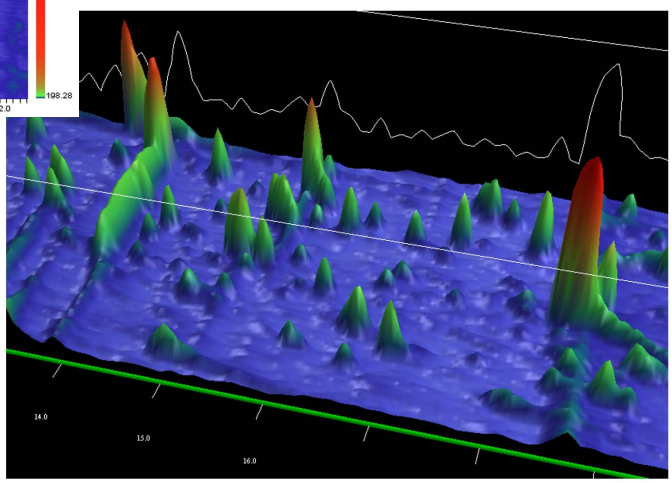

Figure 1: (Top left) An example multidimensional chromatogram of air collected at SRNL. (Bottom left) Increasing magnification of the air sample reveals thousands of trace level chemical species present in a single air sample represented by green ovals. (Below) 3D rendering of a trace levels compound detection.

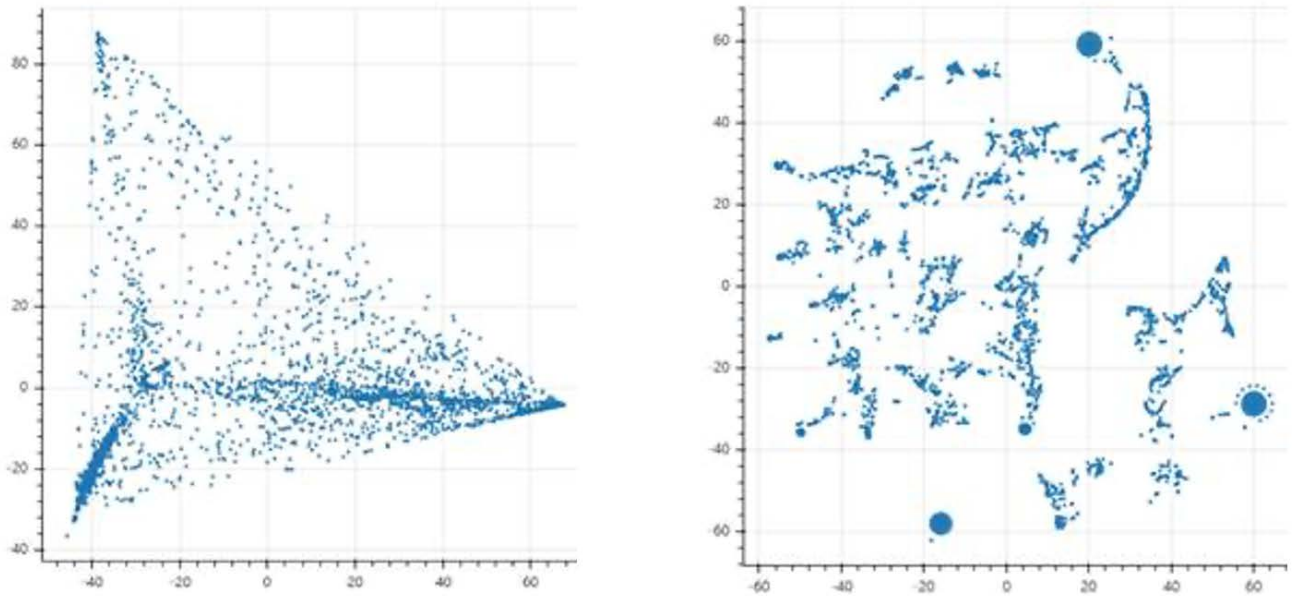

Figure 2: Data visualization of the EPA Speciate database after processing; each point represents a pollution profile contained in the database. (Left) 2-component 11 feature PCA data reduction representing classic chemometric approaches and (right) t-SNE non-linear machine learning based dimensionality reduction represented in 2 components.

Accomplishments

- Secured direct follow-on funding for FY22 at $500K; follow-on project is titled "GC x GC Analysis of Organic Signatures" and is projected to be funded through FY24 at a total project budget of $1,500K.
- Analytical methods developed under this LDRD project have been incorporated into the scope 3 existing projects at a total FY22 funding level of $2,700K.
- Analytical methods developed on new instrumentation improve sensitivity by 4 orders of magnitude over traditional GC/MS systems for species of interest. An example multidimensional chromatogram of air collected at SRNL is shown in **Figure 1**; thousands of species are detectable in a single air sample.
- Measurement accuracy was increased by a factor of 4 over previous analytical techniques.
- Developed machine learning based approaches for organic fingerprint detection utilizing the open-source EPA SPECIATE database. A comparison of machine learning based clustering vs. classic PCA is shown in **Figure 2**. An examples of unsupervised cluster identification is show in **Figure 3**.
- 60-page literature review on machine learning applications in GC/MS data analysis provided by Clemson University.

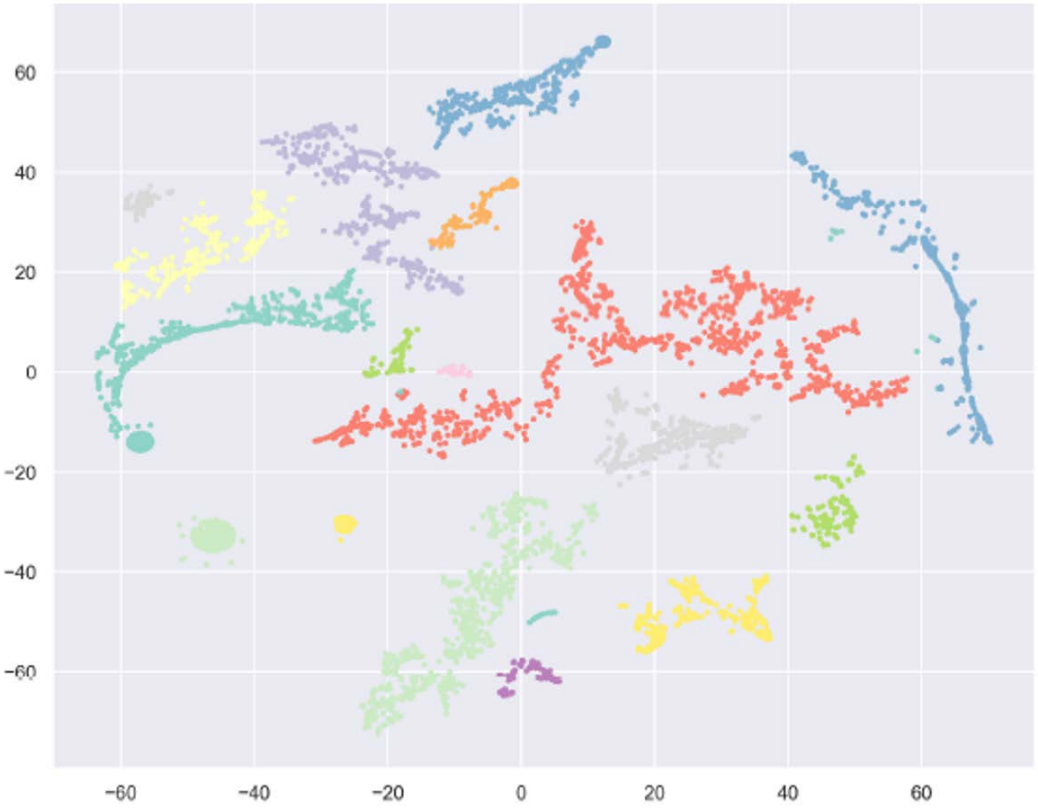

Figure 3: Data visualization of unsupervised cluster identification of the EPA Speciate database.

Contributing Postdoctoral Researchers

Stephanie Gamble

Eric Hoar

Contributing Student Researcher

Jiexin Shi (Clemson University)

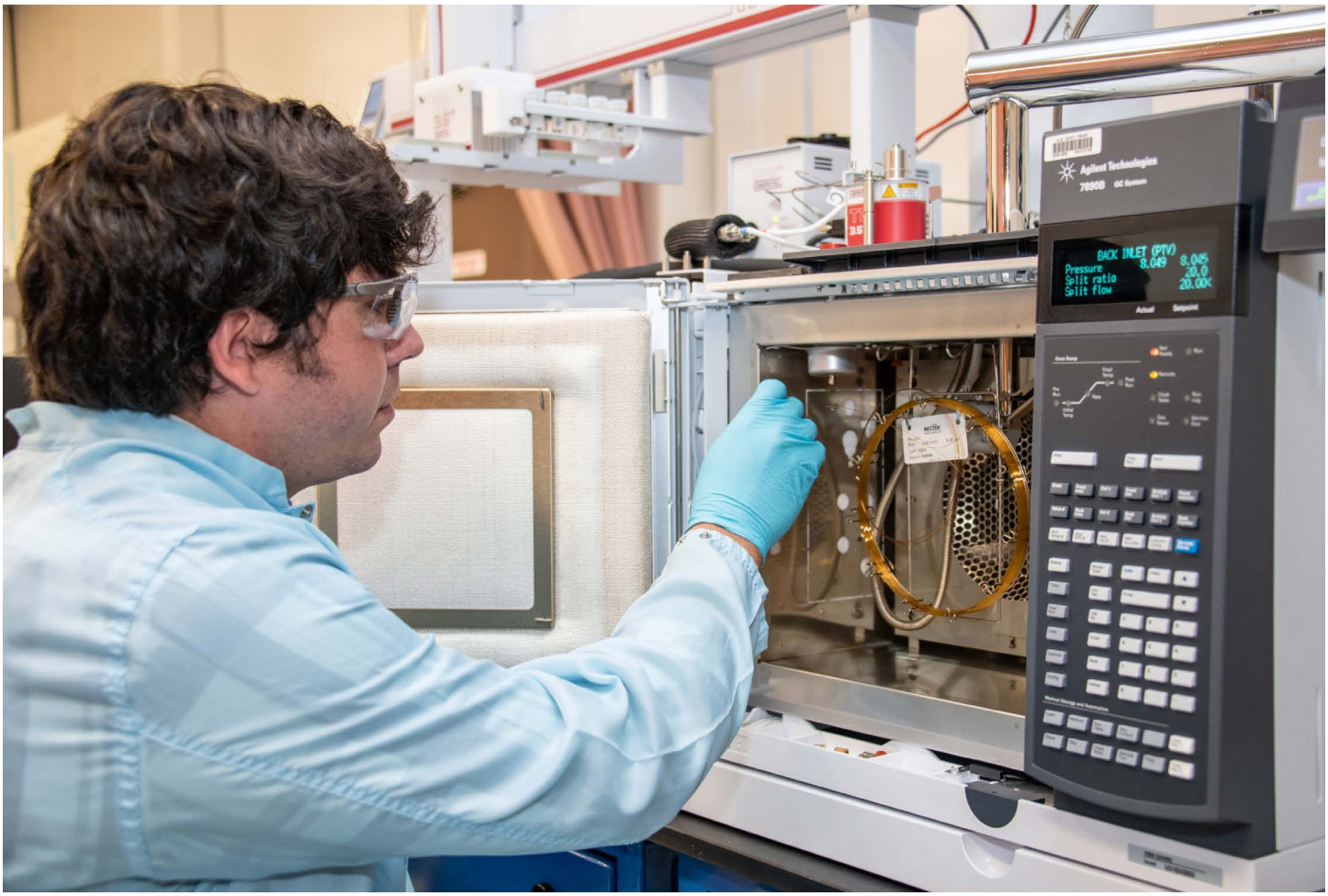

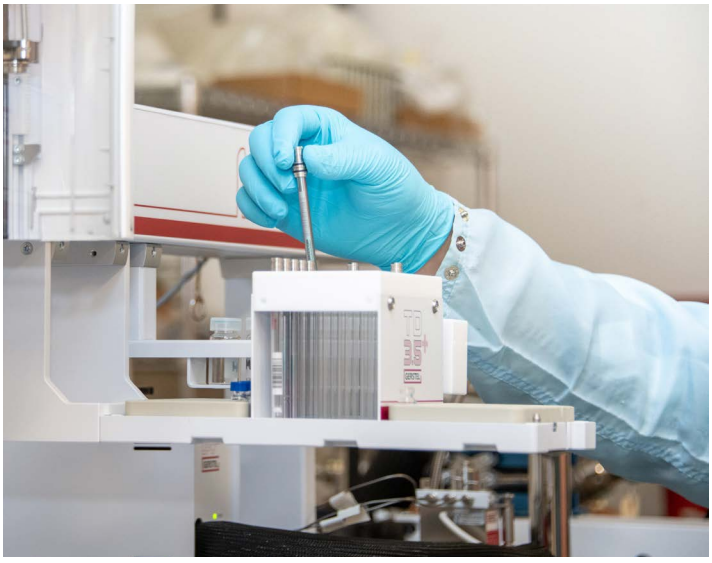

Effect of GPS Manipulation to Traditional and Next Generation Relay Protection

Klaehn Burkes

Project Highlight

This project's objective is to test the effect of GPS timing variations on relay protection algorithms to determine vulnerabilities and the associated hazards to the electric grid. This will focus on traveling wave protection which detects wave propagation down a line from a fault and can detect the location of the fault to the specific tower.

Project Team

Principal Investigator Klaehn Burkes

Team Members
Ian Webb
Sean Krautheim
Dillon Tauscher

External Collaborators
Johan Enslin
Moazzam Nazir (Clemson University)

Abstract

This project's objective is to test the effect of GPS timing variations on relay protection algorithms to determine vulnerabilities and the associated hazards to the electric grid. This will focus on time domain protection which utilizes traveling waves measured on the transmission lines to detect the fault within a tower span. This requires the use of GPS to sync the two substations and can be vulnerable to GPS manipulation. However, the effects of GPS manipulation are not a commonly known risk. Therefore, this LDRD will address the risks of GPS manipulation for on a new protective relay technology that has the potential to change protective relaying. For time domain protection a GPS resilient architecture was implemented and tested for time domain protective relays through a direct serial fiber connection between the two relays. This allows for one relay to be the master and provide synchronization outside of timestamp for traveling wave protection.

Objectives

- Set up SEL-T400L traveling wave protection relay within the SRNL-Critical Infrastructure, ICS and Cybersecurity (S-CIIC) lab.
- Program protective relays to perform time domain protection through controller hardware in the loop platform RSCAD.
- Time shift IRIG-B to perform time manipulation and then conduct faulting sequences on controller hardware in the loop test bed.
- Develop best practice for implementing traveling wave protection relay under GPS manipulation.

Introduction

Modern electric power systems are undergoing structural changes. Systems are upgrading supervisory control and data acquisition (SCADA) systems and replacing electromechanical protective relaying equipment with modern microprocessor-based relays. These advancements have allowed for more precise control through distributed and real time methods, though requiring more communication between intelligent electronic devices (IEDs) and remote terminal units (RTUs). These new devices are, at their core, programable logic controllers (PLCs) that resemble the communication protocols of industrial control systems (ICS). To complement these changes, the protocols and communication methods specific to the electric power system (traditionally Distribution Network Protocol (DNP3)) are being replaced with International Electrotechnical Commission (IEC) standard 61850. DNP3 has no timestamped data in its messaging protocol, meaning relay protection algorithms are not affected by GPS time stamps or data. Contrarily, IEC 61850 uses many different protocols that are based on fast fiber connections that utilize timing as a key part of the data transfer. These protocols, such as Manufacturing Message Specification (MMS), Generic Object-Oriented Substation Event (GOOSE), and Sample Measured Values (SMV), all run over Transmission Control Protocol/Internet Protocol (TCP/IP) networks utilizing high speed switching ethernet. TCP/IP connections enable IEC 61850 to obtain the necessary response times to achieve millisecond protective relaying controls. Therefore, the future of protective relaying is relying on accurate and synchronized timing to improve the electric power system reliability and stability.

An example of a protection scheme utilizing high-speed communication is traveling wave protection. This protection scheme monitors one end of a transmission line for different wave propagation from a fault. Another relay monitors wave propagation from a fault in another substation at the other end of the transmission line. These two can then determine where the fault is located up to the specific tower the fault occurs on. This calculation requires two substations to be synchronized on an accurate clocking signal, typically a GPS receiver. **Figure 1** represents this electrical system architecture.

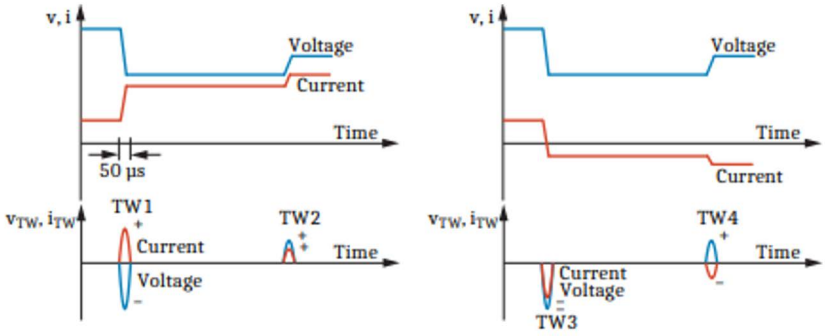

Figure 1: Traveling Wave Protection Operating Principle.

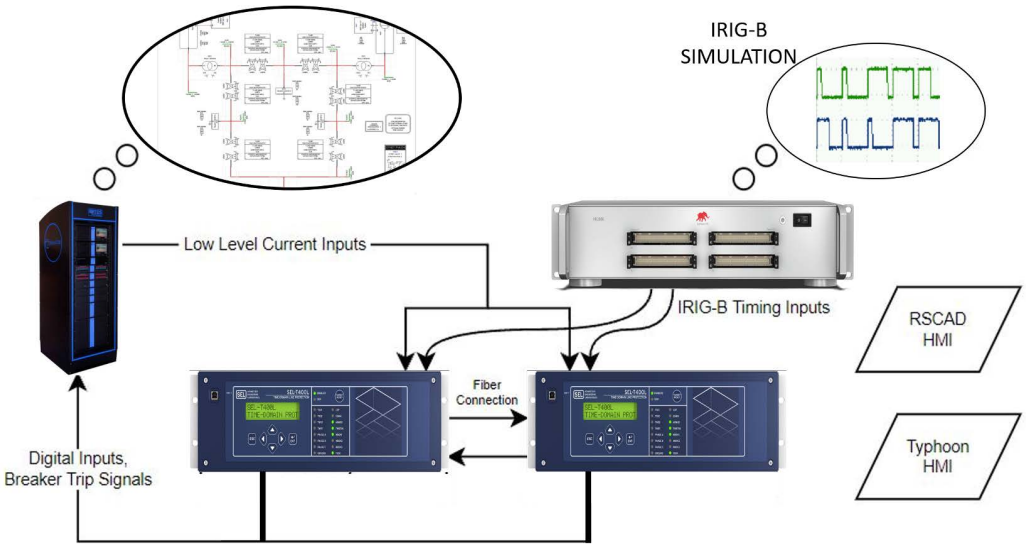

Figure 2: S-CIIC setup of relays, RTDS, and Typhoon.

This project's objective is to research the effects of GPS signal manipulation between two substations. Manipulation was performed by slowly walking off one substation's GPS signal and monitoring the protection algorithms to determine the failure mechanisms of these millisecond protective relaying functions. SRNL has already proven in previous work that the GPS receivers cannot detect small steps of GPS signal deviations; this implies that a GPS attack does not cause the receiver to revert to a holdover posture. Also, SRNL proved that line differential protection was not affected by GPS walk off due to the requirement to have one relay operate as a master clock. This project will allow for SRNL to become a leader in the field of GPS timing manipulation with previous knowledge of GPS receiver operation and the knowledge gained through determining the failure mechanisms of the millisecond protective relay functions of differential and time domain protection.

Approach

The approach for implementing and testing this is through setting up a controller hardware in the loop (CHIL) test bed for the protective relays. CHIL testing allows for controllable and repeatable testing of a variety of electronic power grid components, including protective relays. This allows for running many different power grid simulations and connecting the signals from within the simulation to get precise controlled results.

These simulations were produced via the software RSCAD, running on an RTDS stack (**Figure 2**). These systems allow precise emulation of an electrical power grid that can output current waveforms consistent with that emulation, including waveforms for fault currents. These outputs would be passed at a low level to the protective relay, which would interpret the signals to correspond to a "real" power system scenario via appropriate gain settings. The simulation used in this set of experiments consisted of varying lengths of transmission line between two simulated power generation plants, with the protective relays situated at either end of a 100 mile transmission line between the generation plants, as shown in **Figure 3**. RSCAD/RTDS additionally utilized digital inputs from the protective relays to take contactor inputs to control the virtual breakers within the simulation.

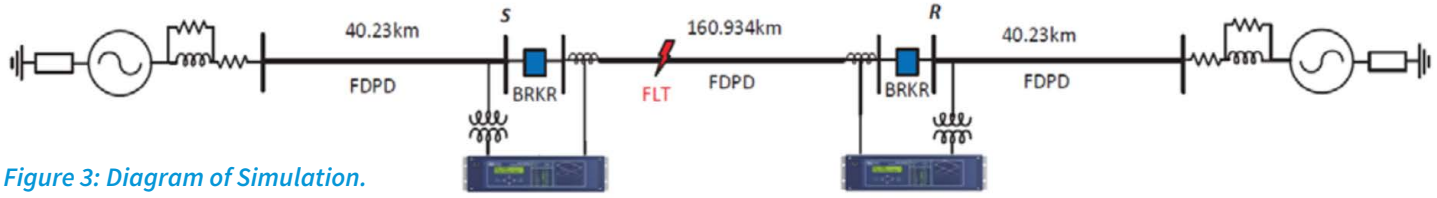

Figure 3: Diagram of Simulation.

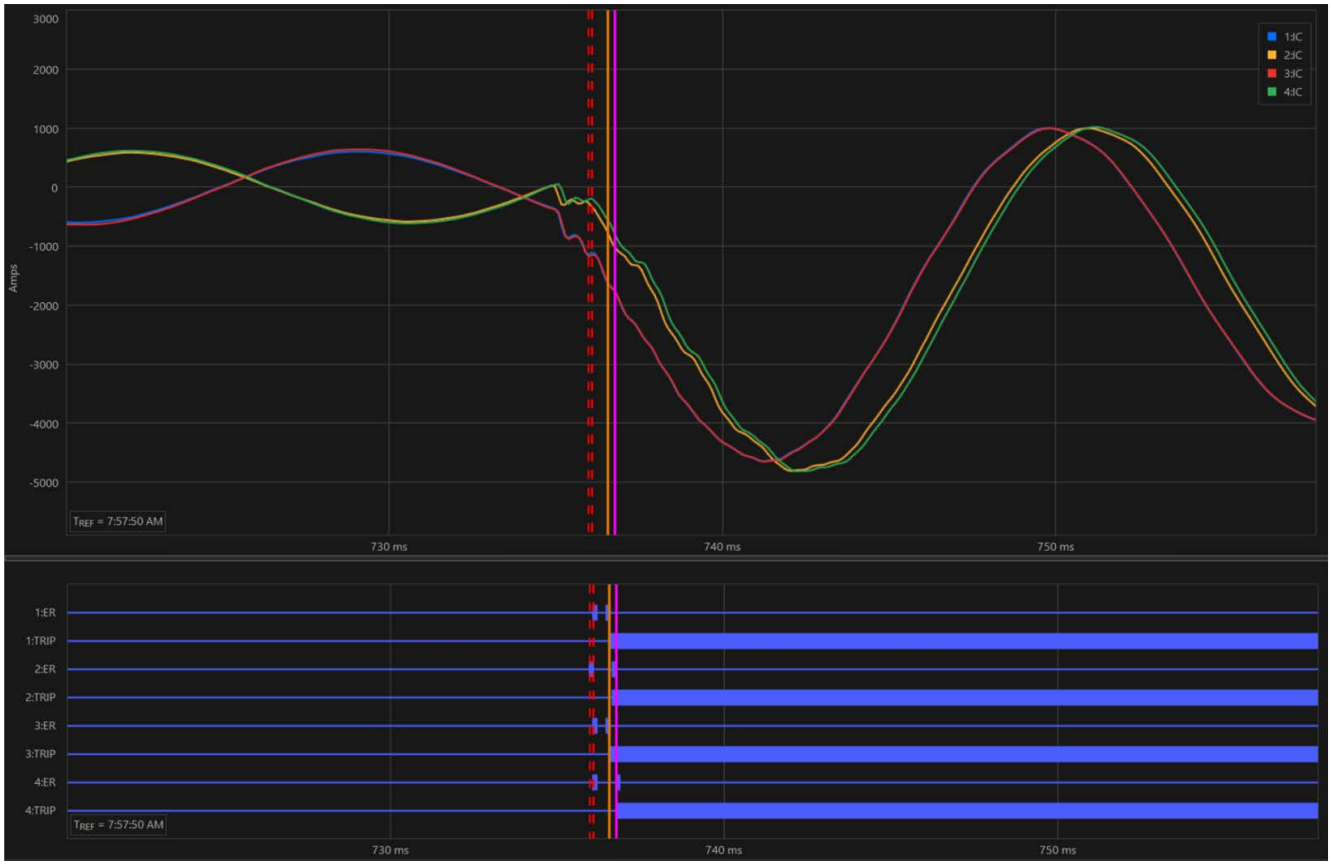

Figure 4: Fault Current at Sending and Receiving-End Relays with No Time Spoof and Time Spoof = +1ms (top), Relay TRIP Signal Assertions at Sending and Receiving End (bottom).

To implement a traveling wave protection scheme, including precise timing signals and appropriately spoofed GPS signals, the TyphoonHIL system simulated IRIG-B time code outputs to supply to the protective relays. TyphoonHIL then added time delay to one time code to simulate a GPS signal manipulation. This would internally cause one relay's high precision time measurement to be the delay was added in TyphoonHIL.

Figure 4 represents the actual test network established in the S-CIIC, consistent with this design.

Through combining the two technologies (RSCAD/RTDS and TyphoonHIL), every input and output to the protective relays were controlled by the operator to test the protective relay with values consistent with values commonly found during in-field deployment. The emulation scenario further allowed for flexible implementation and testing of multiple differential protection architectures to examining their vulnerabilities to GPS time walk off; specifically, those vulnerabilities directly related to the different IRIG-B inputs for the relays.

Accomplishments

- Implemented and tested a GPS resilient architecture for traveling wave protective relays through a direct serial fiber connection between the two relays.
- Established a relay experimental test bed to function test relays with controllable voltage and current outputs, timing signals, and breaker inputs.
- Demonstrated that traveling wave protective relay algorithm can be resilient to GPS manipulation.
- Traveling wave protection relay tripped faster than differential protection relay even under the presence of GPS manipulation.
- Developing Journal Publication on Results.

Contributing Student Researcher

Moazzam Nazir (Clemson University)

Component Development for Alkaline URFCs

Hector Colon-Mercado

Project Highlight

Alkaline electrochemical systems are the next generation of energy production and energy storage devices which do not require rare or precious metal catalysts when fully optimized. This project designed and demonstrated an optimized bifunctional oxygen electrode with ~50% round-trip efficiency using state-of-the-art platinum-iridium catalysts.

Project Team

Principal Investigator Héctor Colón-Mercado

Team Members
Aaron Lando Prabhu Ganesan

External Collaborators
William Mustain (University of South Carolina)

Abstract

Performance, cost, and durability of the catalyst materials are the key factors that govern commercialization of H2-based energy conversion devices such as unitized regenerative fuel cells (URFCs). Compared to existing battery systems, URFCs offer superior energy density and performance over prolonged operation. In addition, alkaline URFC systems, can utilize low-cost platinum group metal-free (PGM-free) catalysts, resulting in much lower overall system costs. This project seeks to address the major obstacles faced in URFC systems such as cost and efficiency and establish a URFC technical capability through the strategic partnership between UofSC and SRNL. The research focuses on the development of low-PGM and PGM-free based bifunctional oxygen catalysts and electrodes, as well as the development of a URFC testing capability at SRNL.

Objectives

- Establish ex-situ baseline performance of state-of-the-art bifunctional catalysts
- Establish in-situ discrete baseline performance of state-of-the-art bifunctional catalysts
- Low-PGM bifunctional catalyst development and ex-situ evaluation
- Design of URFC testing facility
- Facility construction/evaluation
- Cycle testing of electrodes

Introduction

The development of high-performance and low-cost bifunctional electrodes for oxygen evolution reaction (OER) and oxygen reduction reaction (ORR) is critical for enabling the use of electrochemical energy storage devices based on O2 chemistries such as metal–air batteries and URFCs. URFCs are superior to existing battery systems with respect to energy density and performance over prolonged operation, making them the preferred choice for applications such as stationary renewable energy storage for utility power, other large power applications (e.g. rail), and surveillance systems. URFCs are also seen as a key enabler of intermittent renewable energy technologies, as they are able to store and convert chemical energy to electrical energy depending on supply and demand.

URFCs are capable of operating in both power production (fuel cell, FC) and energy storage (electrolysis cell, EC) modes. The attractiveness of URFCs is that the theoretical energy density is approximately an order of magnitude higher than commercial lithium-ion batteries. However, as is typical with low TRL technologies, URFCs are currently too expensive to compete with existing energy storage technologies. A major contributor to URFCs high cost is their incorporation of platinum group metal (PGM) catalysts in the electrodes.

This reliance on PGMs is because they are currently the only catalysts that show both high activity and stability in the acidic environment of proton exchange membrane (PEM) based URFCs. Alkaline based URFCs circumvent the electrode material cost issue present in PEM systems, where PGM-free electrodes show good performance. By developing PGM-free catalysts designed for alkaline URFCs we can create higher efficiency and lower-cost systems.

Until recently, however, alkaline system performance has been negatively impacted by poor membrane and ionomer stability. These recent improvements to performance and stability seen in state-of-the-art alkaline anion exchange membranes (AEMs) has opened doors to exploring new low-cost catalyst technologies within alkaline URFCs, capable of competing with existing energy storage technologies in both system cost and performance.

Approach

Highly active and stable catalysts are needed to achieve high round trip thermodynamic efficiency (εRT>50%, **Figure 1**) and long system life for URFC systems. To meet these objectives, this project will focus on three main areas:

1. Increasing ε_{RT} through the development of stable catalysts with improved overall ORR and OER kinetics,
2. Electrode development capable of efficient operation at the conditions required in energy production and energy delivery modes, and
3. Establish a functional test facility capable of analyzing various operating energy cycles.

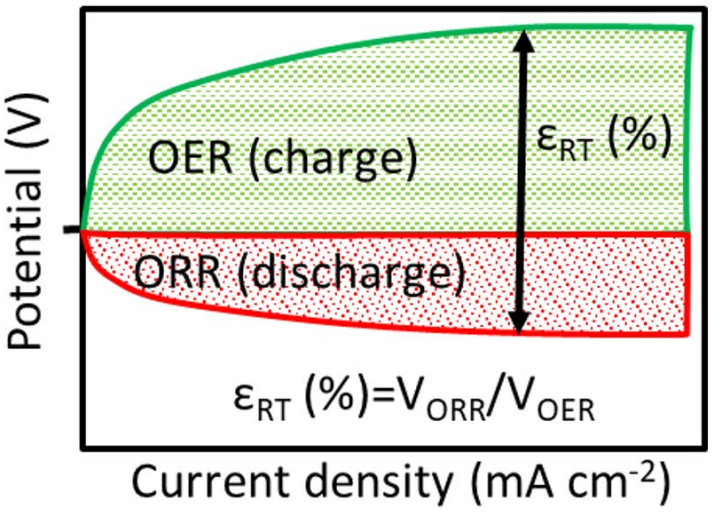

Figure 1: Representative performance curve of an URFC. Kinetic improvements are needed to minimize separation between the charge and discharge curves.

Accomplishments

- Optimized a membrane electrode assembly (MEA) fabrication process for direct catalyst coating using an ultrasonic sprayer to coat the electrodes with the desired catalysts at loadings ranging from 1.0 – 2.5 mg/cm2.
- Optimized bifunctional oxygen electrode design and operated 5 cm2 active area single cell URFC.
- Demonstrated ~50% round-trip efficiency while operating a single URFC in fuel cell and electrolyzer mode at i=0.5 A/cm2 (**Figure 2**).
- Demonstrated stable short-term URFC cycling studies for >5.0 hours (**Figure 3**).
- Used new additive to improve the URFC performance and durability.
-

Contributing Student Researcher

Noor Ul Hassan (UofSC)

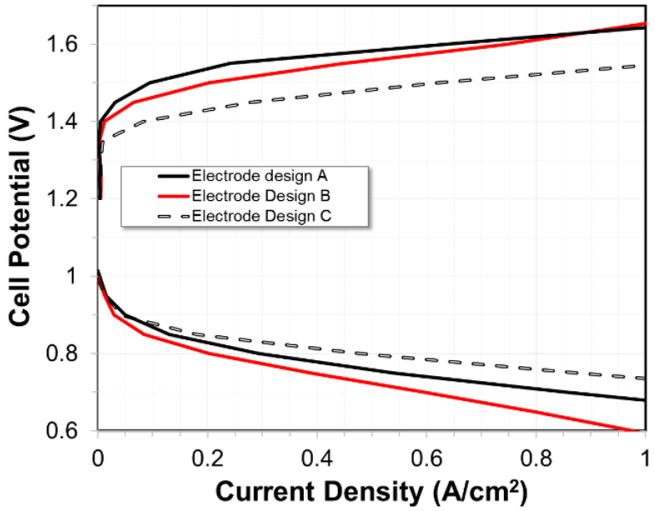

Figure 2: Performance of bifunctional oxygen electrode while operating under fuel cell and electrolyzer mode

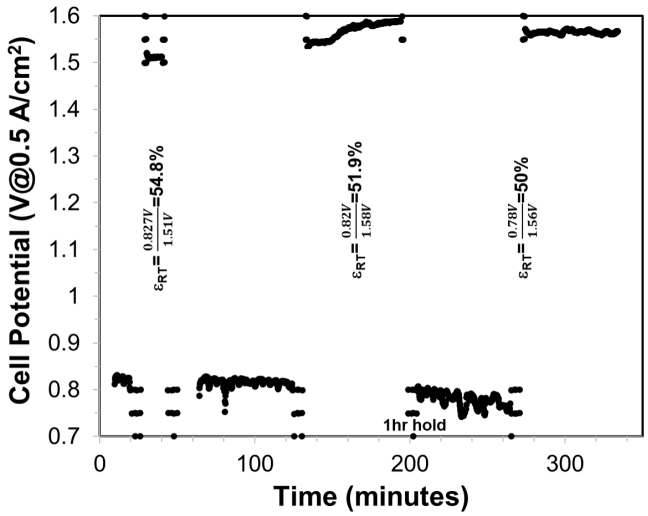

Figure 3: Short-term URFC durability test utilizing bifunctional oxygen electrode

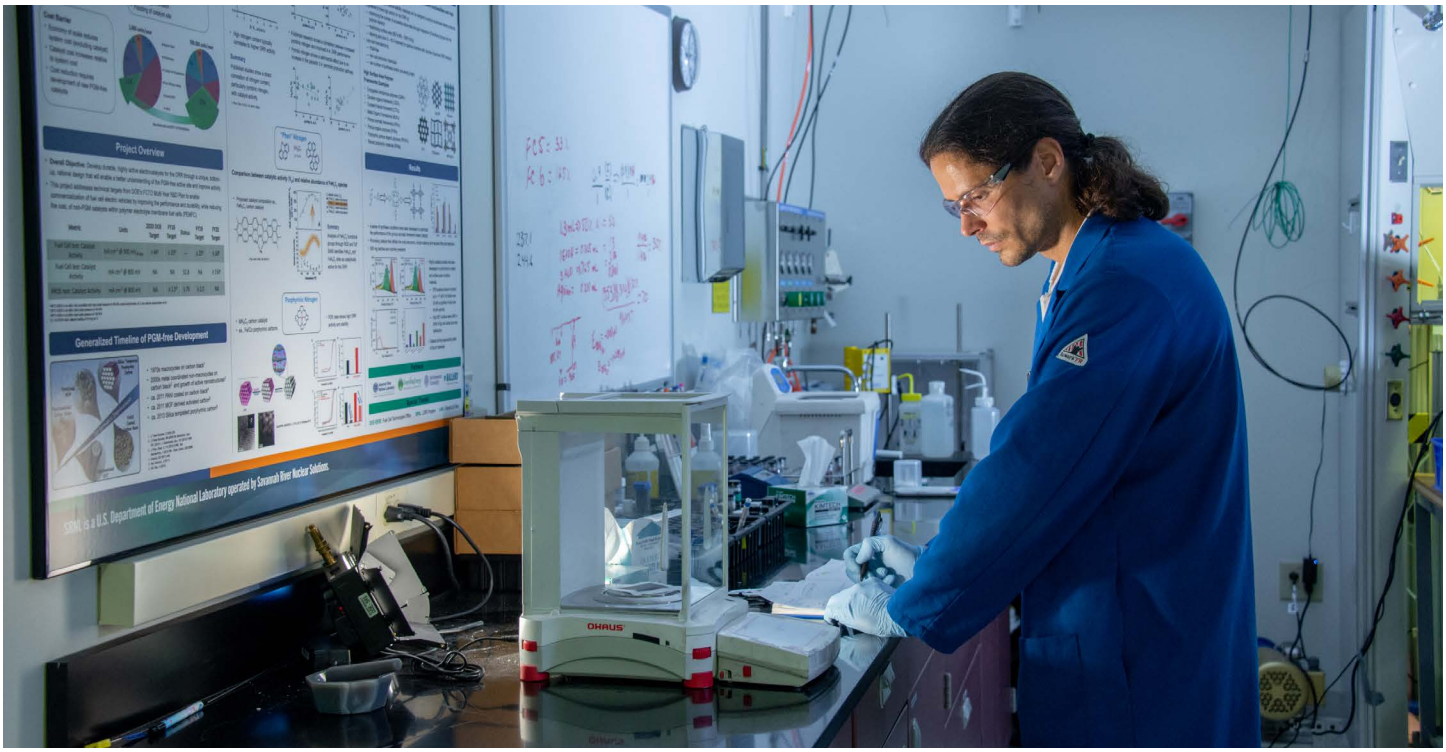

Solid State Ionics: Materials Development by Multiscale Modeling and Advanced Manufacturing Techniques

Lindsay Roy

Project Highlight

This project advances our fundamental understanding of solid-state ionic materials and enables new highly efficient processing techniques for energy conversion and storage device applications. Specifically, this research addresses compositional development through density functional theory and molecular dynamic simulations, explores the impact of microstructural modifications on optimized compositions, and demonstrates advanced manufacturing consisting of 3D laser processing for the deposition of thin film ion conductors in the form needed for a wide range of ceramic energy conversion and storage devices of interest to the Department of Energy.

Project Team

Principal Investigator Lindsay Roy

Team Members
Dale Hitchcock
Brenda Garcia-Diaz
Patrick Kuzbary
Christopher Dandeneau
Chandler Hawsey

External Collaborators
Kyle Brinkman
Lindsay Shuller-Nickles (Clemson University)

Abstract

Solid-state ionic materials are an important enabling technology for energy conversion and storage. Solid-state batteries would be a safer and higher energy density alternative to commercially available lithium ion batteries (LIB), however their implementation requires ion conduction in solids at room temperature to occur on the same level as the current generation of liquid electrolytes. Microstructural modifications have been demonstrated to play a major role on ion transport through the control of grain boundary interfaces, which traditionally serve as "blocking" layers. Ultimately, these materials will be fabricated in thin films form as electrolytes in order to minimize ohmic losses in electrochemical devices. This work uses advanced manufacturing techniques in combination with theoretical modeling to implement a science-based approach in the deposition of thin films ion conductors with controlled microstructures used in ceramic energy conversion and storage devices.

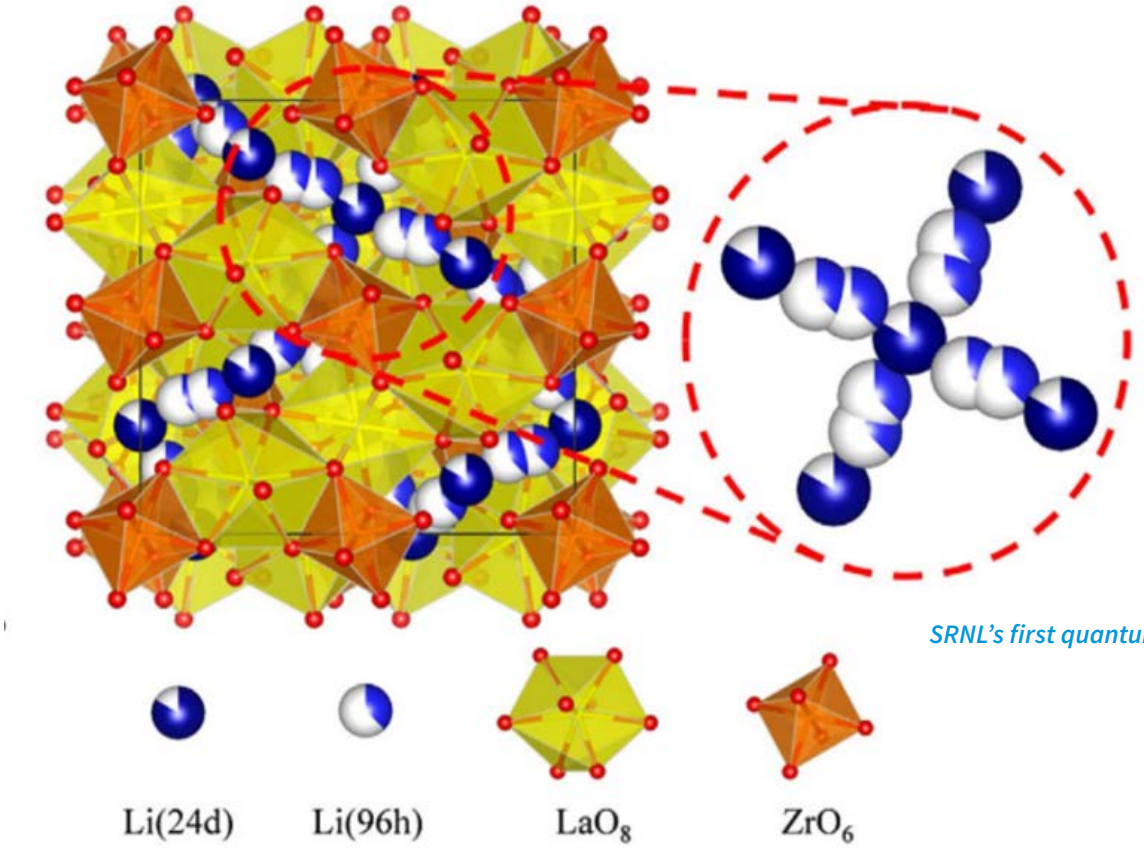

SRNL's first quantum image detected.

Objectives

- Microwave solution combustion synthesis (SCS) of pure cubic phase LLZO
- Electrochemical characterization of bulk and laser sintered LLZO
- Bulk defect incorporation and Li+ ion mobility calculations
- Defect migration and grain boundary energetics
- Solid state laser sintering of Ga-doped and Ta-doped LLZO
- Energy conversion device manufacturing

Introduction

Solid-state ionic materials are an important enabling technology for energy conversion and storage. While solid-state batteries would be a safer and higher energy density alternative to commercially available lithium ion batteries (LIBs), their implementation requires ion conduction in solids at room temperature to occur on the same level as the current generation of liquid electrolytes. Microstructural modifications have been demonstrated to play a major role in ion transport through the control of grain boundary interfaces, which traditionally serve as "blocking" layers. Ultimately, these materials will be fabricated in thin film form as electrolytes in order to minimize ohmic losses in electrochemical devices. This work uses advanced manufacturing techniques (e.g. 3D printing followed by laser processing) in combination with theoretical modeling to implement a science-based approach in the deposition of thin film ion conductors with controlled microstructures that are employed in ceramic energy conversion and storage devices.

Specific focus has been placed on the use of aliovalent dopants in Li-ion conducting $Li_7La_3Zr_2O_{12}$ (LLZO) with a garnet-like structure.[1] Although the thermodynamically stable tetragonal phase of LLZO exhibits relatively low Li^+ conductivity, dopants such as Ga^{3+} on Li sites or Ta^{5+} on Zr sites stabilize the cubic polymorph of LLZO thereby producing increases in both the Li vacancy concentration (for charge compensation) and ionic conductivity by two orders of magnitude.[2,3] However, the preparation of doped LLZO remains challenging because conductivity is dependent upon control of the dopant concentration *i* and conditions necessary to suppress the sublimation of volatile Li during sintering are dependent upon variables that are difficult to quantify or control.

To overcome these challenges, research has focused on tailoring the appropriate microstructure with fast manufacturing techniques and computational evaluations to enable significant progress toward understanding and controlling the microstructure of LLZO. Specifically, our results have shown that advanced quantum calculations can predict the precise dopant concentration necessary for rapid Li^+ migration, while fabrication techniques such as solid-state reactive sintering (SSRS) enable enhanced materials processing at lower temperatures.

Overall, this project addresses key scientific issues identified by the Department of Energy (DOE) – Basic Energy Science (BES), Fusion Energy Science (FES) and Energy Efficiency and Renewable Energy (EERE) program that limit the present understanding and implementation of solid-state ionic materials and devices in separations, energy conversion and storage applications. Key issues include the utilization of experimental and computational methods to elucidate phenomena related to ionic transport through the bulk of materials and across interfaces (e.g. grain boundaries, surfaces, and layers of functional devices). Since polycrystalline materials are likely to find widespread usage as low-cost and scalable energy conversion devices, an understanding and ability to tailor the microstructure of such compounds via fast manufacturing routes is essential to the development and implementation of new materials.

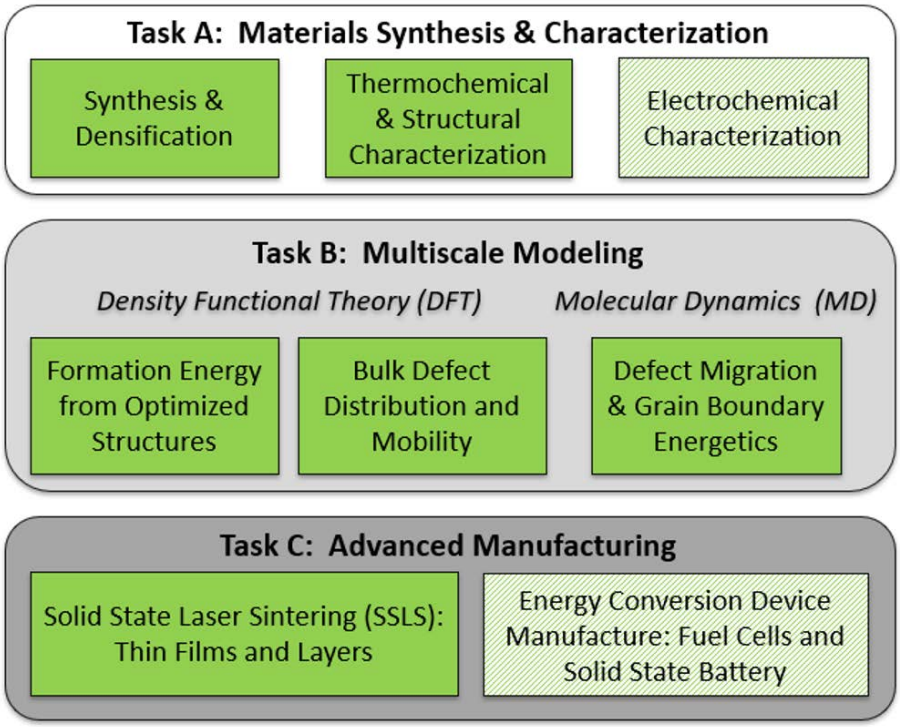

Figure 1: Pictorial representation of the approach used in this project.

Approach

This project incorporates a three-pronged approach as summarized in **Figure 1**. Task A focuses on novel synthetic and characterization methods such as solid-state reaction synthesis (SSRS) and solution combustion synthesis (SCS) for rapid and efficient materials production. Task B utilizes quantum mechanical calculations to help inform the experimental thrust by correlating the thermodynamic stability of doped LLZO with observables such as X-ray diffraction (XRD) and X-ray absorption spectroscopy data. Task C sets out to fabricate dense 3D thin films of doped LLZO followed by rapid laser sintering. Each box represents a subtask in the project and the items highlighted in green were completed during this project. Those in light green are in progress and will be pursued for follow-on funding.

Accomplishments

The project work was divided into three tasks: Progress in all areas along with the FY21 milestones for each task

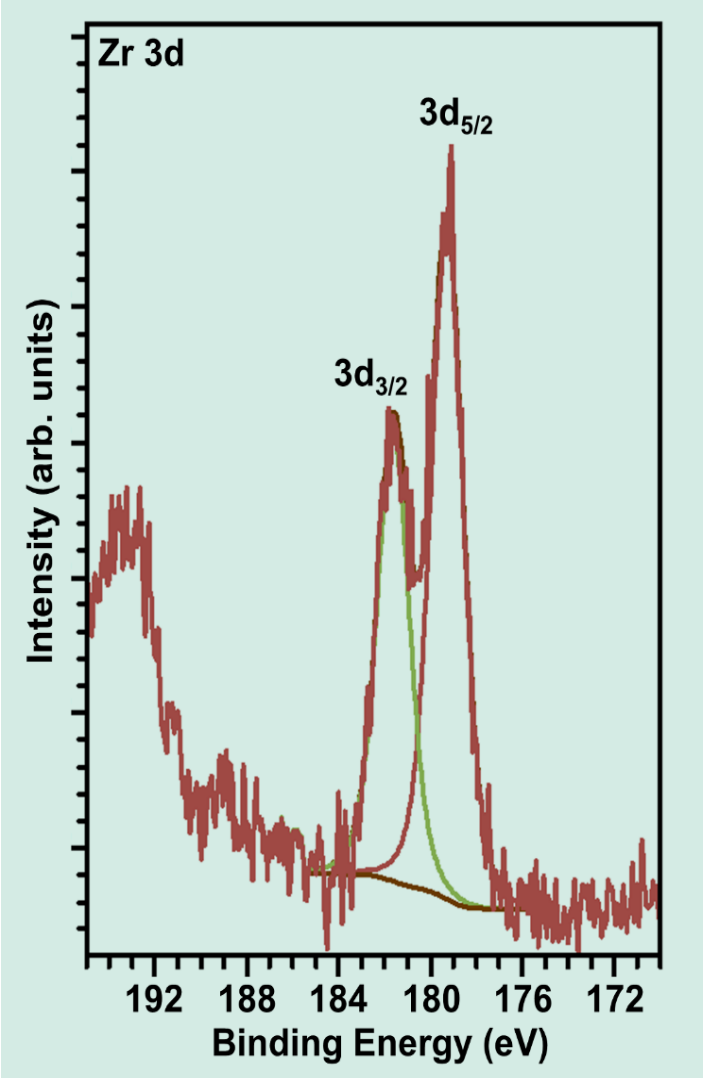

Figure 3: XPS spectrum of the Zr 3d peaks in undoped LLZO.

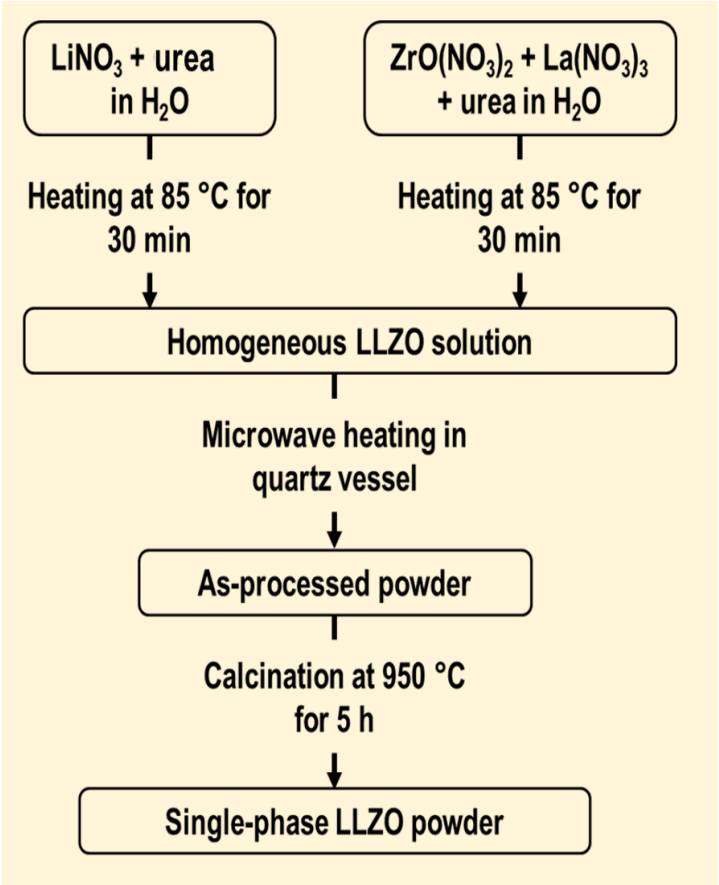

Figure 2: Diagram of the SCS process for undoped LLZO.

are outlined below. Results and accomplishments are presented under each milestone.

Task A: Materials Synthesis and Characterization

- M5: Microwave solution combustion synthesis (SCS) of pure cubic phase LLZO (Dec 2020)
  - The feasibility of fabricating single-phase cubic LLZO via microwave-assisted solution combustion synthesis (SCS) is investigated. SCS involves the initiation of a thermodynamically favorable, self-sustaining redox reaction between metal nitrates (oxidizers) and suitable fuels. The intermixing of molecular components in solution allows for excellent compositional control, while the simplicity of the process facilitates ease of scalability and the use of modular components.
  - Undoped, Ga-doped, and Ta-doped LLZO compositions were prepared via SCS.
  - Initial studies demonstrated the formation of undoped, single-phase tetragonal LLZO using $LiNO_3$, $ZrO(NO_3)_2$, and $La(NO_3)$ precursors with urea as a fuel (**Figure 2**). Subsequent X-ray photoelectron spectroscopy (XPS) analysis showed Zr occupying only one site in the LLZO lattice, thereby indicating an absence of trace secondary $La_2Zr_2O_7$ phases in the material (**Figure 3**).

– Ga-doped LLZO with composition of $Li_5.5Ga_{0.5}La_3Zr_2O_{12}$ was fabricated via SCS using $Ga(NO_3)_3$ as precursor. Calcination at 950 °C for 5 h yielded single-phase LLZO with a cubic garnet structure (**Figure 4**).

– Single-phase Ta-doped LLZO with composition of $Li_{6.5}La_3Zr_{1.5}Ta_{0.5}O_{12}$ was also fabricated via SCS and characterized by XRD. The preparation of Ta-doped LLZO is complicated by the lack of a Ta nitrate precursor. Here, Ta-oxalate solutions were prepared and NH_4NO_3 added to compensate for lack of an oxidizing component. Additionally, H_2O_2(30%) was utilized as a catalyst to break up hydrated tantalum oxide and facilitate dissolution/ complex formation with oxalic acid.

– Peer-reviewed manuscript in preparation to be submitted in November 2021. It will focus on the synthesis of single-phase undoped and Ga-doped LLZO via SCS.

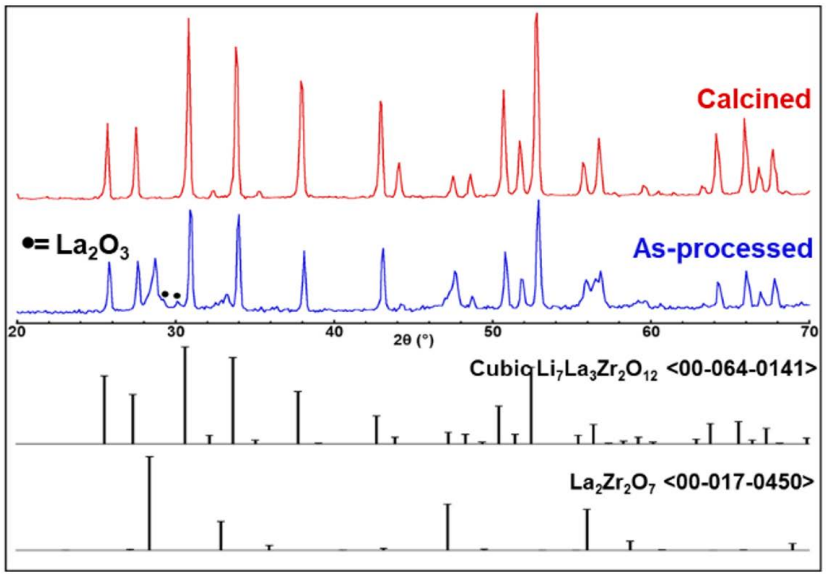

Figure 4: XRD patterns of as-processed and calcined (950°C/5 h) Ga-LLZO powders fabricated using SCS.

- M6: Electrochemical characterization of bulk and laser sintered LLZO (May 2021)

  – Ionic conductivity of SCS-derived Ga-doped LLZO was measured from room temperature to 370 K. The obtained ionic conductivity was low (1.8×10^{-6} S/cm), likely due to the low density of the sintered material. Future work is aimed at optimizing the sintering protocols for the SCS-derived powder.

Task B: Multiscale Modeling

- M4: Bulk defect incorporation and Li+ ion mobility calculations (Mar 2020)

  – In Ga-doped LLZO systems, the most stable configuration is when the interatomic distances between Ga dopants (*i.e.*, $Ga_{Li}^{\cdot\cdot} - Ga_{Li}^{\cdot\cdot}$ distances) and between Ga dopants and Li vacancies (*i.e.*, $V_{Li}^{\prime} - Ga_{Li}^{\cdot\cdot}$ distances) are minimized. Thus, defect clustering contributes to an energetic stabilization of the overall system until the solubility limit is reached. The U-shaped reaction energy (**Figure 5**) with respect to concentration emphasizes the complexity of the thermodynamic interplay that exists between endothermic (e.g. Li-loss, vacancy formation) and exothermic (e.g. vacancy ordering and aggregation) processes. In general, the formation of Li defects and Li defects clustering is an endothermic process considering the effect of increased organization in the system, particularly for clustering of same charged defects.

  – Submitted peer-reviewed manuscript in December 2020. Paper identified Coulomb energy and

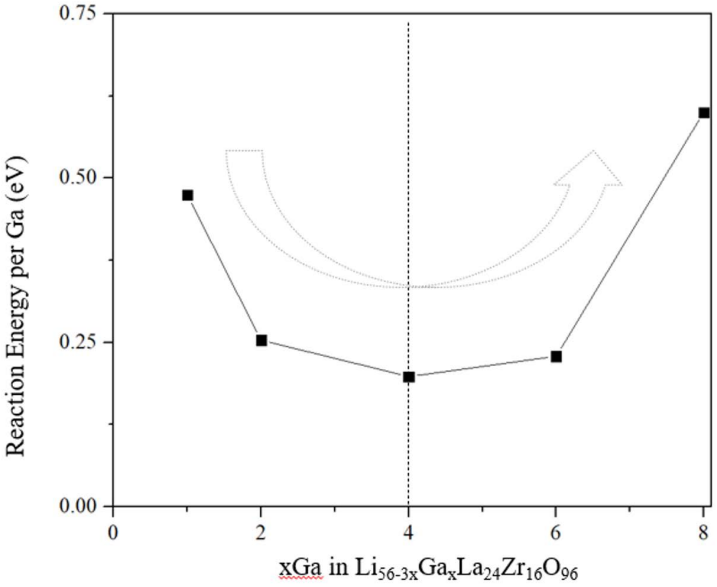

Figure 5: Stepwise reaction energy of Li56-3xGaxLa24Zr16O96 per Ga with respect to the xGa in LLZO. The reaction energy drops when xGa <=4, while it increased when xGa >=4.

DFT calculations were used to evaluate Li-site configuration. Energetic evaluation of Ga-doped LLZO ($Li_{7-3x}Ga_xLa_3Zr_2O_{12}$ where x=0, 0.125, 0.25, 0.5, 0.75, 1.0) was performed. Theoretical thermodynamic stability was used to investigate local coordination environments of Ga. Ga-concentrations, as well as crystal lattice parameters, were correlated with theoretical thermodynamic stability (under revision).

– MRS conference presentation: “Computational Insights of Ga-Doped LLZO with DFT Investigations”.

– ACS conference invited presentation: "Solid State Ionics: Materials Development by Multiscale Modeling and Advanced Manufacturing Techniques".

- M7: Defect migration and grain boundary energetics (Aug 2021 Go/No Go)
  - Preliminary calculations to understand Li-ion transport at the grain boundary examined two low-energy grain boundaries of Ta-doped LLZO (**Figure 6**). Molecular dynamics simulations found that Li transport is dependent upon structure and temperature. Transport in Σ3 remains relatively fast (near the bulk rate) while transport at the Σ5 boundary is roughly 3 order of magnitude slower.
  - Peer-reviewed manuscript in preparation to be submitted December 2021. Paper will also outline FY20 calculations on the computed energies and structural changes within the Ta-doped LLZO ranging from 25% to 75%. Systems doped around 50% Ta retain the symmetry needed for facile Li+ mobility; higher doped systems are lower in energy but break the necessary symmetry needed for Li+ mobility.

Task C: Advanced Manufacturing

- M8: Solid state laser sintering of Ga-doped and Ta-doped LLZO (Feb 2021 Go/No Go)
  - Two models were developed to predict the average crystallite size as a function of sintering temperature and time using different algorithms including Random Forest regression and fitting to a known grain growth kinetic equation. Due to the limited number of data points, all data were utilized in the training of each model. **Figure 7** shows a plot of average crystallite size vs sintering time where the dots correspond to experimental data points and the lines correspond to the Random Forest regression model fit. The average training error for this model was 1.54% with an R squared value of 0.955. **Figure 8** shows a plot of average crystallite size vs sintering time where the dots correspond to experimental data points and the lines correspond to the grain growth model fit. The average training error for this model was 9.25%, however, the figure shows that the model was unable to accurately describe the variability in the data. This can be seen from the fact that the model prediction lines are near straight whereas the data points show a logarithmic behavior.

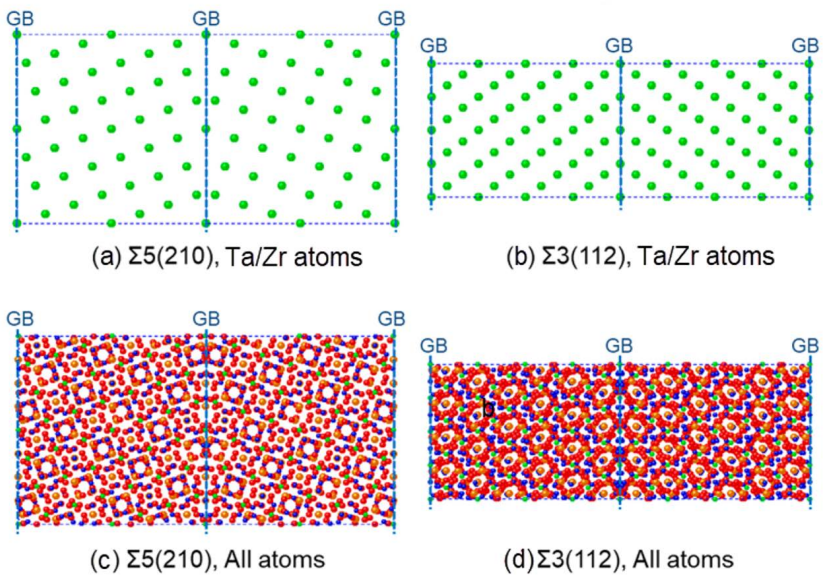

Figure 6: Unrelaxed structures of the two grain boundaries examined in Ta-doped LLZO.

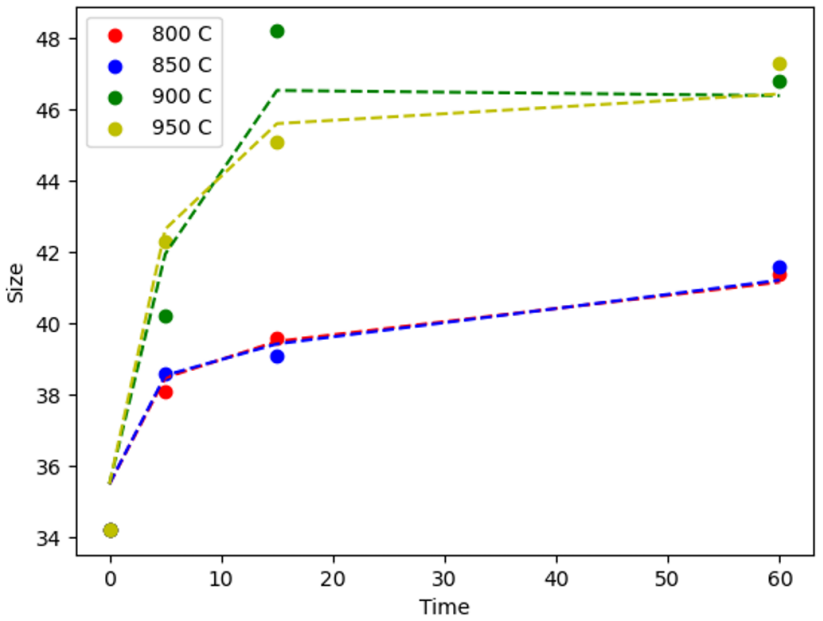

Figure 7: Plot of average crystallite size vs. sintering time showing experimentally measured data points (dots) and the preliminary results of model fit for the Random Forest regression model (dotted lines).

- The error analyses show that the Random Forest regression algorithm provides the best ability to model the sintering process for Ta-doped LLZO. This shows that the sintering process can be modeled using machine learning methods and future work in this area can expand upon these results.

- M9: Energy conversion device manufacturing (Aug 2021)
  - Work has started on the additive manufacturing based micro extrusion, modified micro extrusion by doctor blade smoothing, spray coating, and inkjet printing to allow the manufacturing of LLZO thin layers with thickness from 5-2000 µm. Combined with laser cutting, more precise complex shapes can also be fabricated. The laser processing can make the fully dense membrane, highly porous membrane from cost-effective raw materials of carbonates and oxides, etc. The proper sintering additives are the critical factor for achieving crack-free large-area parts by rapid laser reactive sintering.

Contributing Postdoctoral Researchers

Akihiro Ishii

Eric Hoar

Contributing Student Researchers

Changlong Li
(Clemson University)

Rahul Rajeev

References

1. Han, F.; Zhu, Y.; He, X.; Mo, Y.; Wang, C., Electrochemical Stability of Li10GeP2S12 and Li7La3Zr2O12 Solid Electrolytes. Advanced Energy Materials 2016, 6 (8), 1501590.
2. Wagner, R.; Redhammer, G. J.; Rettenwander, D.; Senyshyn, A.; Schmidt, W.; Wilkening, M.; Amthauer, G., Crystal Structure of Garnet-Related Li-Ion Conductor Li7–3xGaxLa3Zr2O12: Fast Li-Ion Conduction Caused by a Different Cubic Modification? Chemistry of Materials 2016, 28 (6), 1861-1871.
3. Gu, W.; Ezbiri, M.; Prasada Rao, R.; Avdeev, M.; Adams, S., Effects of penta- and trivalent dopants on structure and conductivity of Li7La3Zr2O12. Solid State Ionics 2015, 274, 100-105.

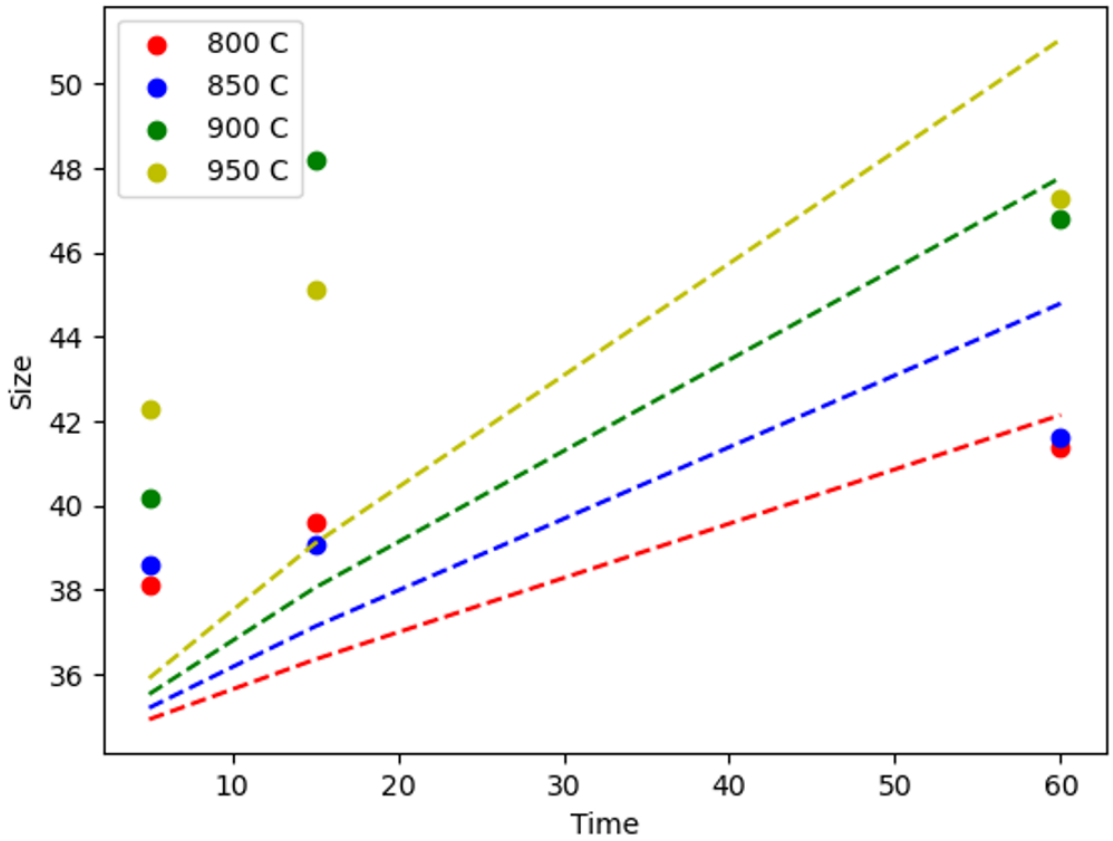

Figure 8: Plot of average crystallite size vs. sintering time showing experimentally measured data points (dots) and the preliminary results of model fit for the grain growth kinetics model (dotted lines).

Sea Breeze Influence on Aerosols and Convection in the Southeastern US

Stephen Noble

Project Highlight

Sea breezes in the southeastern United States can move inland covering a large area and occur more often than previously thought. They change atmospheric conditions that can affect clouds, rain, air quality, energy production, and climate.

Project Team

Principal Investigator Stephen Noble

Team Members
Brian Viner
David Werth
Jianhua Qian
Thomas White
Matt Nelson

External Collaborators
Len Pietrafesa
Paul Gayes
Shaowu Bao

Abstract

The goal of this research is to describe the inland penetrating sea breeze and interactions with atmospheric phenomena across multiple scales, thereby establishing a baseline of understanding. The land-ocean-atmosphere interface in the southeastern US drives regional sea breeze circulations that impact clouds, convection, and precipitation. We analyzed a variety of atmospheric observations to identify the characteristics and frequency of sea breezes. Sea breezes were identified all along the southeastern Atlantic coast (63% of days from March to September in 2019) at times impacting large areas of the southeastern US. They were found to penetrate inland to the Savannah River Site on about 27% of all days during the typical sea breeze season (March to October) from 2015 to 2020, often leaving a residual layer the following day. Future work focuses on modeling studies, analysis of additional data, and climate impacts on sea breezes.

Objectives

- Define characteristics of inland penetrating sea breezes
- Determine the frequency and spatial extent of sea breezes in the southeastern US
- Characterize particle size distributions associated with sea breeze intrusion at the Savannah River Site
- Determine chemical compositions of particles collected in precipitation associated with sea breeze aerosol
- Simulate the sea breeze using atmospheric model to understand the vertical properties of the sea breeze and perform sea breeze sensitivity tests
- Identify any climate connections to variations of inland penetrating sea breezes
- Assess the ability of large-scale earth system models to resolve sea breezes and their impacts

Introduction

The inland penetration of coastal sea breezes is a key atmospheric phenomenon in the southeastern US. Complex interactions between the atmosphere, land and ocean allow sea breezes to transport marine airmasses with generally higher moisture content, lower temperatures, and different aerosols inland. The southeastern US is an understudied region for convection, cloud formation, and precipitation which all have implications for a changing climate. These changes in atmospheric properties from the sea breeze can linger into the next day and may influence convective and cloud processes.

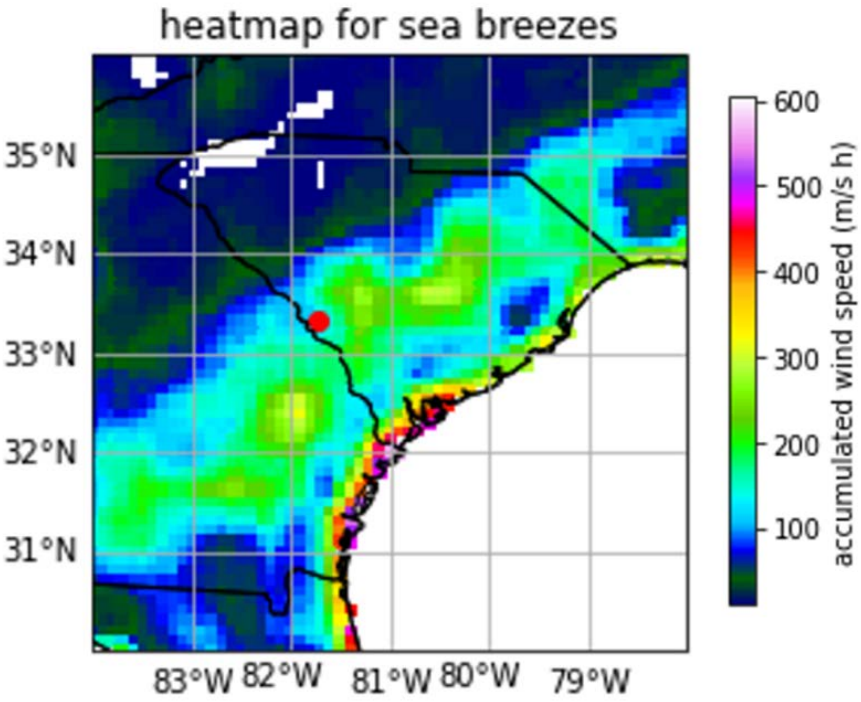

Heat map highlighting the extent of sea breezes in the southeastern US in 2019 (Bao et al., 2021).

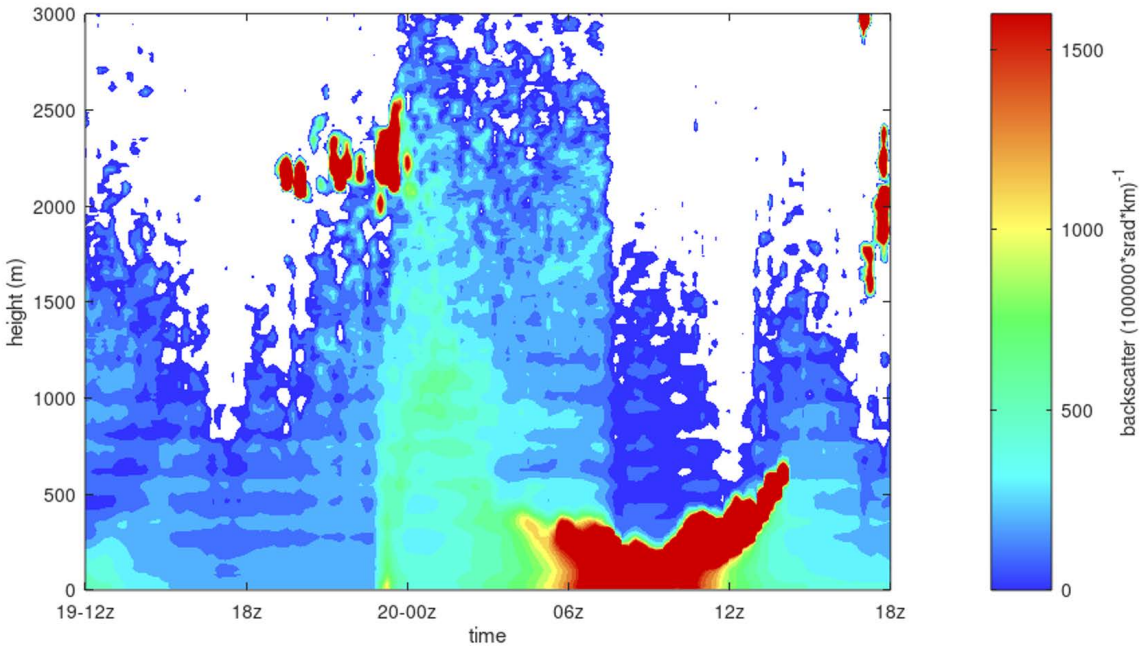

Figure 1: Ceilometer attenuated backscatter for the sea breeze case of May 19-20, 2019. Sea breeze is noted by changes in backscatter just before 00z which indicates changes in aerosol properties.

Due to the shallow nature and smaller scale of these circulations, earth system models may not correctly assess the importance of intruding sea breezes. Additionally, the sea breeze potentially impacts renewable energies, air and water quality, and radiative forcing of climate.

Our research demonstrates that sea breezes in the southeastern US can frequently penetrate inland more than 150 km. The residual sea breeze layer can remain in place into the next day with similar aerosol and increased humidity. These affect cloud formation and air quality on the day following the sea breeze (**Figure 1**). Inland penetration occurs more than 25% of the time during the active season (March to October) and cover large areas of the southeastern US beyond the coast. Thus, in the southeastern US, the sea breeze is important in determining the drivers of convection, cloud formation, and precipitation in the southeastern US. This research establishes a base line for future sea breeze research related to previously mentioned areas of impact.

Approach

We utilized a suite of observations and reanalysis data to identify sea breezes in the southeastern US region and those specifically penetrating inland to the Savannah River Site. The measurements highlighted defining characteristics of these sea breezes which further aided in their identification. Weather type analysis was performed for the southeastern US in an attempt to identify the large-scale patterns driving sea breeze formation. Observations were used as a validation to mesoscale modeling of the sea breeze. Our second-year research will utilize these models to determine the vertical characteristics of the sea breeze, processes that drive sea breeze formation, and links to the climate. An additional focus will be on the impact of the sea breeze on cloud formation, air quality, precipitation, and the carbon cycle.

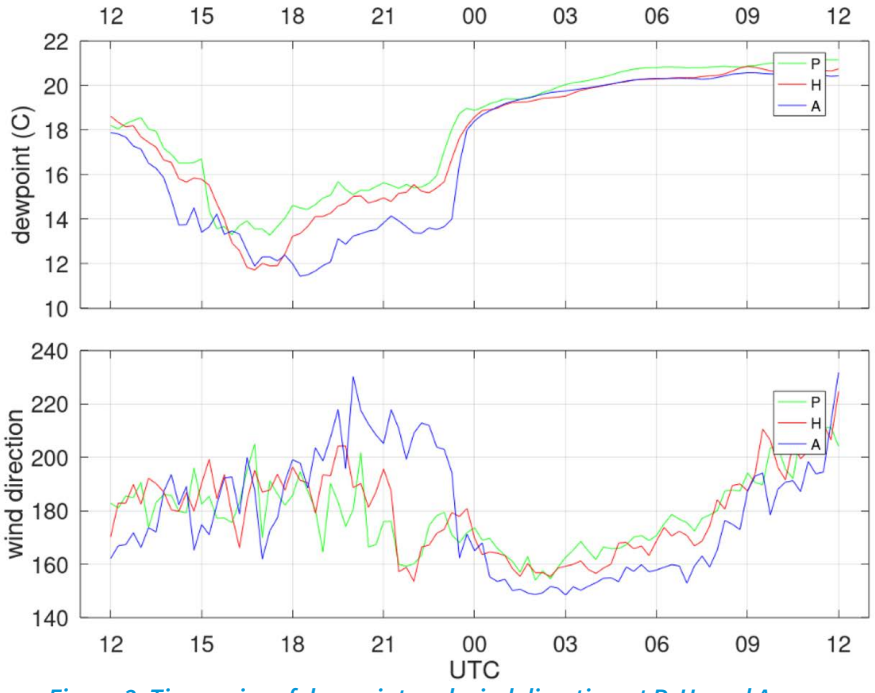

Figure 2: Timeseries of dewpoint and wind direction at P, H, and A area towers on May 19-20, 2019 highlighting characteristics of the sea breeze passage at SRS just before 00 UTC.

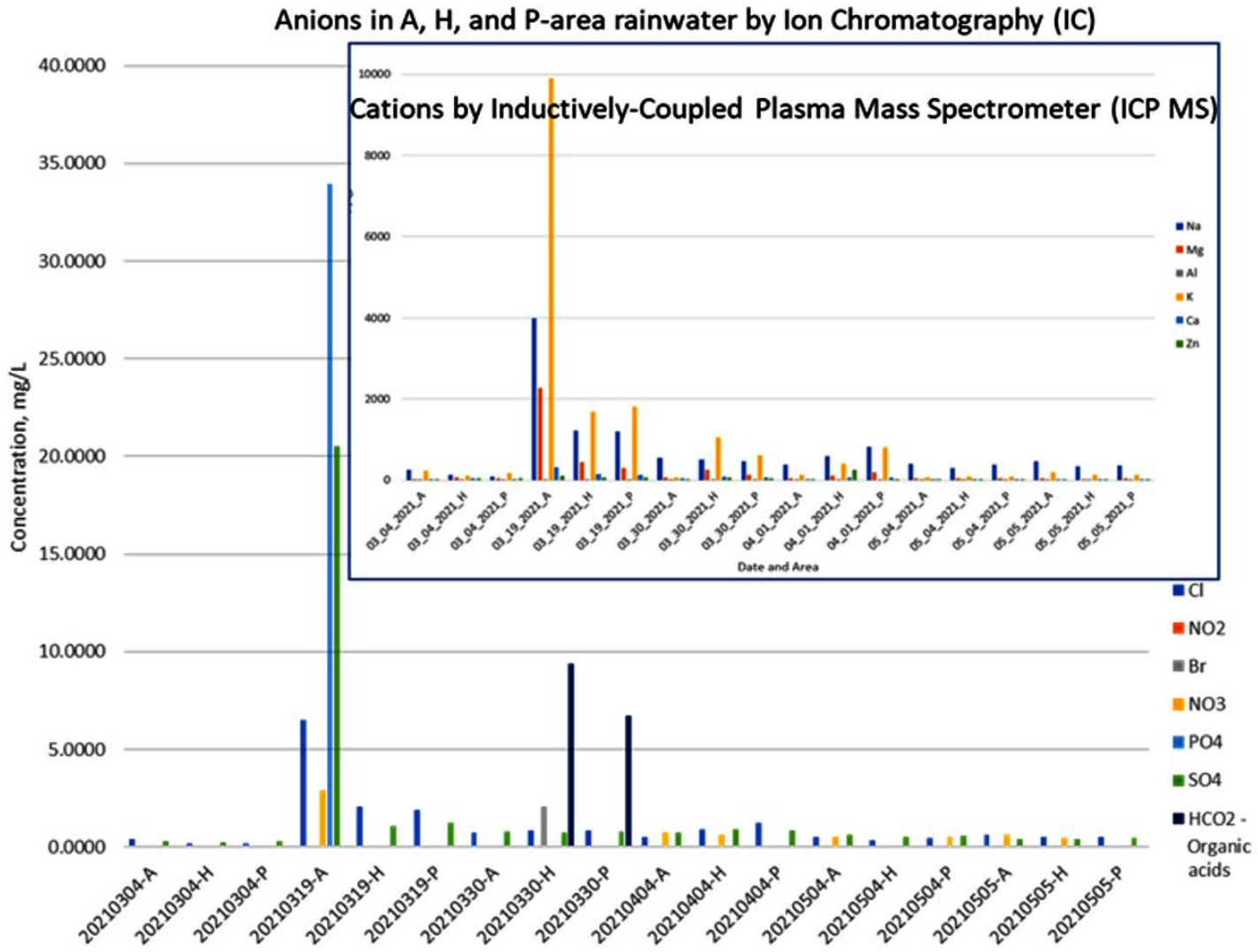

Figure 3: Initial results for precipitation chemical analysis. Note elevated concentrations of sodium, potassium, chloride and sulfate for the three locations on 3/19/21, which coincide to a sea breeze passage the day before.

Accomplishments

- Identified key meteorological characteristics (dewpoint rise, **Figure 2**; shift in wind direction, **Figure 2**; reduction of variability in wind direction; changes in aerosol backscatter, **Figure 1**; occasional wind speed increase; occasional temperature decrease) of inland penetrating sea breezes at the Savannah River Site.
- Identified 391 inland penetrating sea breezes that reached the Savannah River Site; 26.6% of days in the 2015-2020 sea breeze seasons (March-October) experienced a sea breeze.
- Identified and described 6 dominant weather types that occur in the southeastern United States during the sea breeze season using reanalysis data from 1979 to 2019.
- Installed an aerosol inlet system at the Central Climatology facility on the Savannah River Site for use with a Scanning Mobility Particle Sizer for identification of changes to aerosol properties with the sea breeze intrusion. This new capability can be used for additional aerosol research studies.
- Collected precipitation samples for most rain events during the 2021 sea breeze season for chemical analysis of dissolved aerosol that were collected by the drops. Early analysis indicates higher levels of sodium and chloride are related to sea breeze intrusion events (**Figure 3**).
- Developed a technique using fine scale reanalysis data to identify sea breeze cases in the southeastern US and identified 134 out of 214 days (63%) with sea breezes in 2019 (March-September) which is nearly consistent with other coastal locations (not inland) and methods.

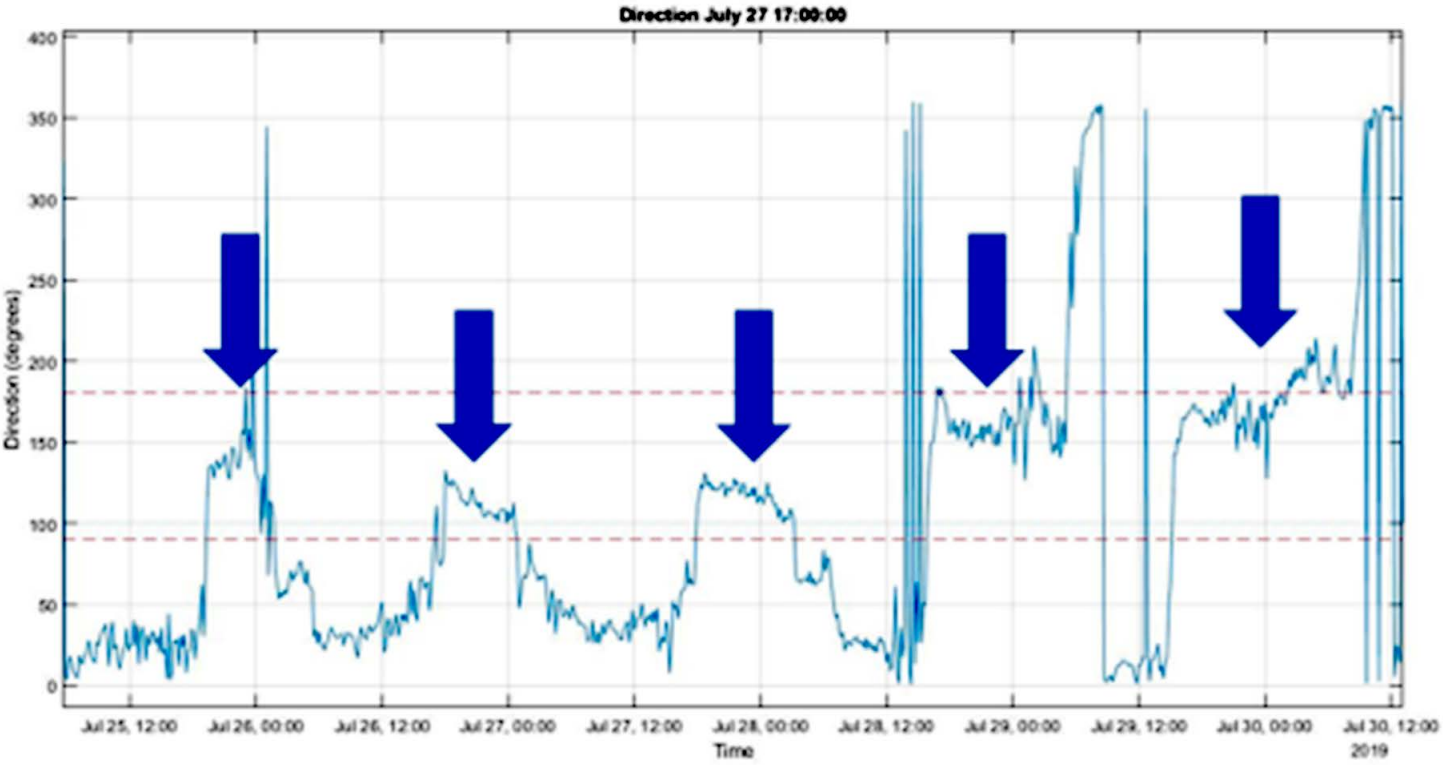

Figure 4: Examples of sea breeze passages in sodar data at North Myrtle Beach in late August to early September.

- Identified sea breeze cases using Sodars (**Figure 4**) and meteorological station data near the coast and inland to describe sea breeze characteristics from the coast moving inland and calculate the inland propagation speed of sea breeze fronts.
- Modeled sea breeze cases using two mesoscale models, compare results with meteorological data, and used model results to calculate particle dispersion and marine particle fractions.

FY21 Publications

- Viner, B.; Noble, S.; Qian, J.-H.; Werth, D.; Gayes, P; Pietrafesa, L.; Bao, S. Frequency and Characteristics of Inland Advecting Sea Breezes in the Southeast United States. Atmosphere 2021, 12 (8), 950. https://doi.org/10.3390/atmos12080950.
- Qian, J.-H.; Viner, B.; Noble, S.; Werth, D. Precipitation Characteristics of Warm Season Weather Types in the Southeastern United States of America. Atmosphere 2021, 12(8), 1001. https://doi.org/10.3390/atmos12081001.

Contributing Student Researchers

Grant Mitchell

Savannah Burdette

Understanding Photocarrier and Gas Dynamics to Rationally Design Heterostructured Nanocatalysts for Efficient Solar CO_2 Conversion

Anthony Thompson

Project Highlight

This project has established several new and unique capabilities that enable SRNL to synthesize unique nanomaterials and evaluate their performance as catalysts in chemical processes relevant to clean energy technologies, such as CO_2 photoconversion. The instrumentation developed in FY21 of this project allows understanding of electron transfer processes on extremely short timescales, which is relevant to photovoltaic cells and other applications in addition to photocatalysis.

Project Team

Principal Investigator Anthony Thompson

Team Members
Patrick Ward
Zachary Duca
Lauren Hanna
Simona Murph

External Collaborators
Yiping Zhao
Henning Meyer
Susanne Ullrich
Mona Asadinamin (University of Georgia)

Abstract

Recent research in CO_2 photocatalysis has largely focused on exploring new catalysts; however, details of how these materials work often remain unclear. Knowledge of these processes will allow one to rationally design highly efficient catalysts for solar CO_2 conversion. This project aims to develop new techniques and establish new capabilities in SRNL to enable the study of photocatalysts and other materials in extreme detail. In FY21, we developed two new *in situ* techniques that are unique to SRNL, allowing the study of reaction intermediates and adsorbed gases during photocatalysis. We also established new in-house capabilities for catalyst synthesis and transient absorption (TA) spectroscopy, which enables the study of very short-lived excited states on photocatalysts. These capabilities will be used extensively for this project and in other current projects relevant to clean energy technologies such as photovoltaic cells, providing a good return on investment in the coming years.

Objectives

- Synthesize new heterostructured nanomaterials for CO_2 photoconversion
- Establish Glancing Angle Deposition (GLAD) catalyst synthesis capabilities at SRNL
- Establish Transient Absorption (TA) capability at SRNL
- Develop novel *in situ* EPR technique for study of radical reaction intermediates and paramagnetic metal ions
- Develop novel *in situ* variable-temperature DRIFTS technique for study of adsorbed gases and intermediates

Introduction

CO_2 is a primary driver of global climate change and the ultimate product of fossil fuel combustion. As such, the development of commercially viable fuels from atmospheric CO_2 would help combat the climate issue both by actively removing CO_2 from the atmosphere and reducing its production from fossil fuel use. Although CO_2 conversion reactions such as the water-gas shift reaction and CO_2 methanation typically require high energy input in the form of heat, solar CO_2 conversion can occur at ambient temperature using primarily ultraviolet and visible light from the sun. Metal oxide semiconductor materials can catalyze solar CO_2 conversion by photon absorption, which excites an electron from the valence band to the conduction band, forming an electron-hole pair (charge carriers). Charge carriers can diffuse to the surface of the material to form excited states that increase reaction rate by attacking adsorbed CO_2 or reaction intermediates. However, the details of this process are unclear and highly dependent on catalyst and reaction conditions, and catalyst activities are still typically too low for commercial viability. Deep knowledge of these processes will help design the next generation of CO_2 conversion photocatalysts.

This project aims to elucidate the interaction between charge carriers and adsorbed gases and reaction intermediates in CO_2 photoconversion over semiconductor nanocatalysts. Novel materials and nanostructures are synthesized by Glancing Angle Deposition (GLAD) and tested in CO_2 photocatalysis using novel *in situ* techniques developed by SRNL including EPR and DRIFTS with tunable laser excitation. The ability to excite with high-intensity laser light of any desired wavelength allows for experiments to be run over a range of excitation wavelengths, unlike traditional *in situ* techniques using white light or broad UV light for excitation. This allows collection of data as a function of excitation wavelength for a single system, potentially giving better insight into charge transfer processes.

Approach

Two new techniques unique to SRNL were developed for this project. Diffuse reflectance infrared Fourier transform spectroscopy (DRIFTS) is a vibrational technique used to probe bonds on diffuse light-scattering surfaces such as powdered catalysts. This technique is especially sensitive towards CO_2, CO, and other possible reaction intermediates in CO_2 photoreduction.

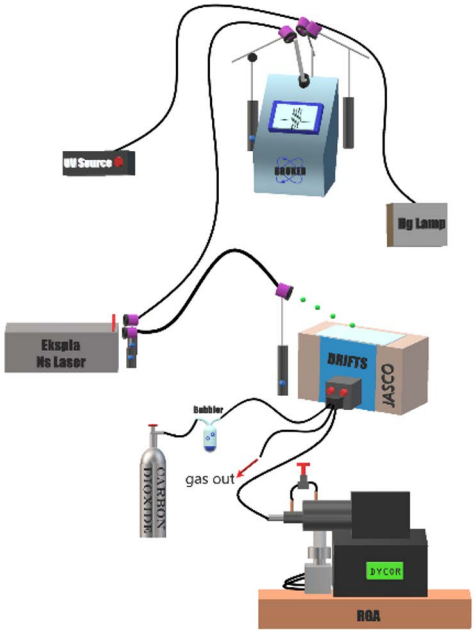

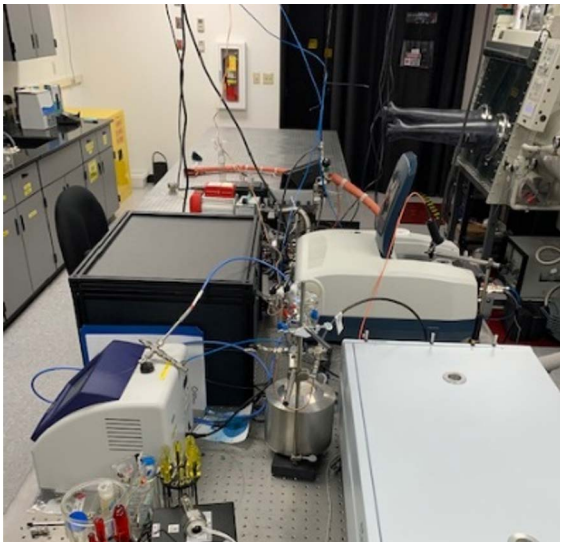

Figure 1: Diagram and photo of tunable laser DRIFTS/EPR setup with RGA product detection.

A tunable laser has been coupled with a DRIFTS *in situ* cell with variable temperature capability and online product detection to study adsorbed gases and metal sites during CO_2 photocatalysis (**Figure 1** and **Figure 2**). Electron paramagnetic resonance (EPR) or electron spin resonance (ESR) is a technique that measures unpaired electrons in a system. CO_2 photocatalysis reactions are generally accepted to begin with the formation of a CO_2 radical anion and potentially go through other radical intermediates in the reaction pathway. Although these radical species are short-lived, they can be trapped by forming an adduct with a secondary molecule called a spin trap (typically a nitrone compound), which forms a more stable radical that can be directly observed by EPR (**Figure 3**). An EPR flow cell was designed and constructed, and similar to the DRIFTS cell, has been coupled with a tunable laser and online product detection, allowing detailed study of radicals and other paramagnetic species such as metal sites during photocatalyst reactions (**Figure 1**).

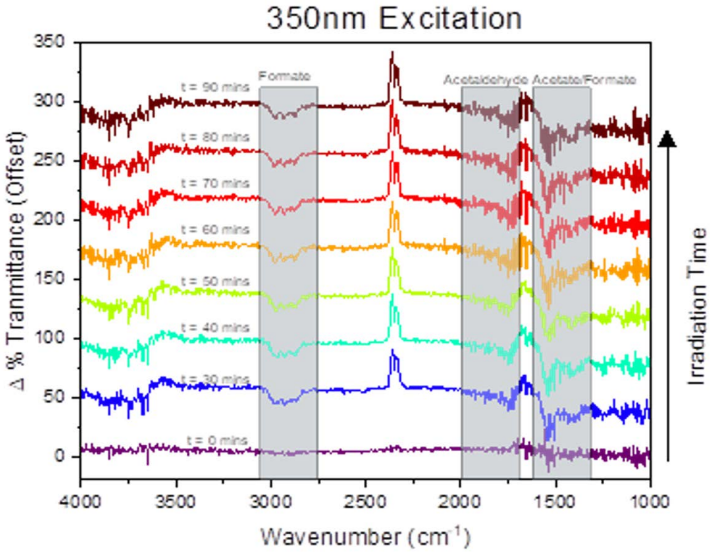

Figure 2: In situ DRIFTS difference spectra of TiO_2 nanocatalyst showing product formation in EtOH oxidation.

We have also established two new capabilities for catalyst synthesis and study of photoactive materials in-house. Glancing Angle Deposition (GLAD) is a physical vapor deposition technique in which materials are sputtered at an oblique angle to a rotating sample stage. The rotational speed and direction and the angle of sputtering are variable, which allows synthesis of unique heterostructured catalyst architectures. The oblique angle of the incoming vapor usually results in nanopillar architectures due to a shadowing effect. This technique is especially useful for photocatalyst synthesis as it can be performed with semiconductor oxides such as TiO_2, In_2O_3, and CuO. This system will be used extensively in the following years to develop unique materials for solar CO_2 conversion as well as other applications. **Figure 4** shows the GLAD deposition chamber during the first deposition with the new system as well as an SEM image of the resulting material. Transient Absorption (TA) spectroscopy is a pump-probe technique capable of characterizing electron transfer processes on extremely small timescales. A pump laser pulse is sent through a sample to create excited states, followed by a probe pulse of white light to measure the sample's absorption spectrum. The time elapsed between the two pulses is adjustable from zero to 8 ns using a moving mirror delay line, which allows the collection of an entire UV-Vis spectrum of the sample at any given delay time. The ground-state spectrum is typically subtracted from the excited-state to give a transient absorption spectrum.

An optical parametric amplifier (OPA) allows the pump wavelength to be adjusted over the UV-Vis-NIR spectrum. The ability to vary pump wavelength and delay time allow for a very large amount of data to be collected for a single sample, giving important insight into excited states and electron transfer processes in the sample.

Accomplishments

- Developed novel techniques for *in situ* photocatalyst characterization using IR and EPR spectroscopy with tunable laser excitation and online product detection (**Figure 1**)
  - Demonstrated proof-of-concept $CO_2^{\bullet -}$ radical anion detection by EPR (**Figure 3**)
- Synthesized and tested mixed-valent cobalt (II, III) oxide photocatalysts by solution method
- Synthesized and characterized TiO_2, In_2O_3, and CuO heterostructured catalysts by Glancing Angle Deposition (GLAD) through collaboration with University of Georgia
- Established in-house Glancing Angle Deposition (GLAD) capability for synthesizing unique catalyst architectures
- Established femtosecond pump-probe spectroscopy capability for characterizing photocatalysts and other photoactive materials

Contributing Postdoctoral Researchers

Lauren Hanna

Zach Duca

Contributing Student Researcher

Mona Asadinamin (University of Georgia)

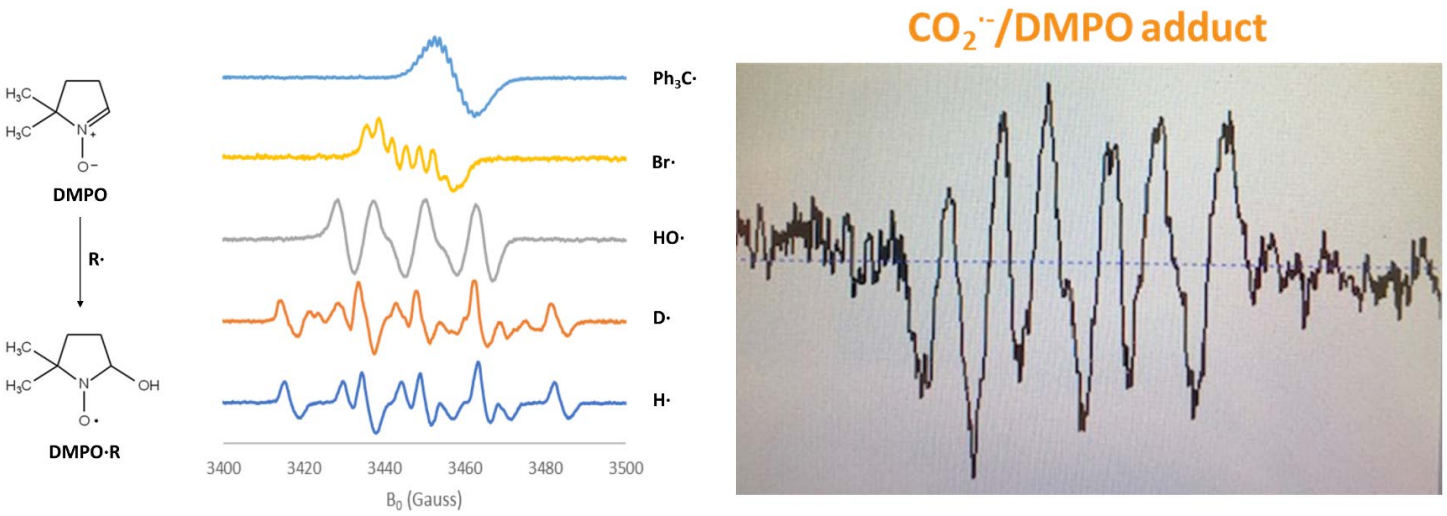

Figure 3: In situ EPR spectra showing spin trapping capabilities and proof-of-concept detection of various radicals, including the $CO_2^{\bullet -}$ radical anion relevant to CO_2 photoreduction.

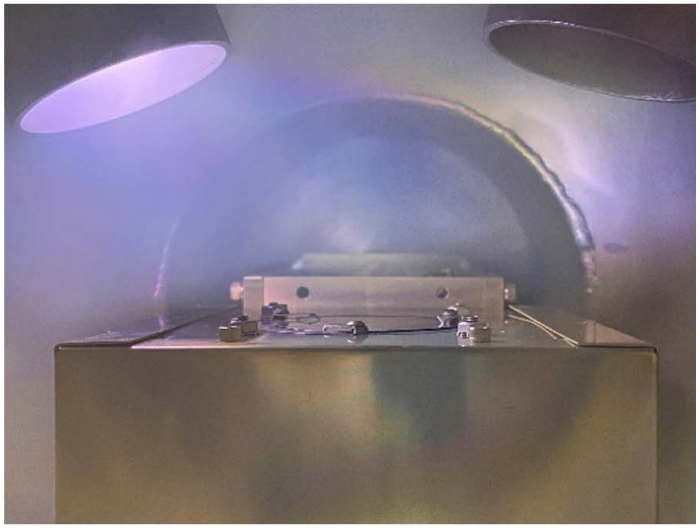

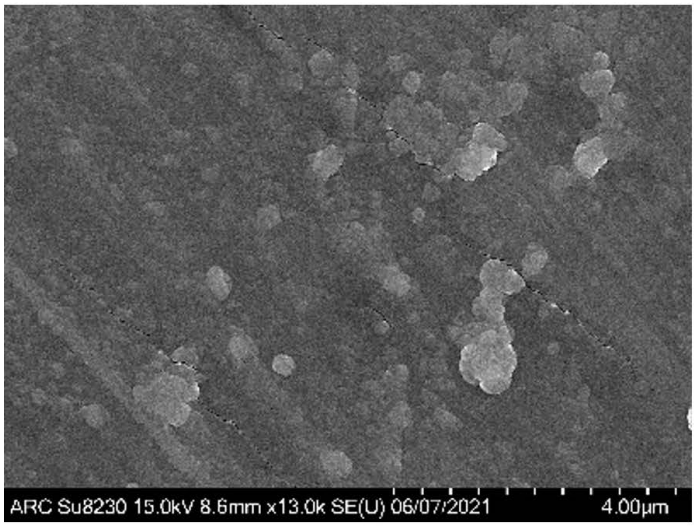

Figure 4: Deposition chamber of newly-developed GLAD system during first deposition; SEM image from first deposition of TiO_2 .

Biomining Rare Earth Elements (REEs) through Bioextraction

Robin Brigmon

Project Highlight

Critical elements play a vital role in consumer electronics including computers, cell phones, medical equipment, as well as military hardware that are critical to the country's economic and national security. Strategies are needed to reduce our dependency on critical element imports. This project is developing approaches for biomining critical elements from geological materials.

Project Team

Principal Investigator Robin Brigmon

Team Members
Charles Turick
Daniel Kaplan
Anna Knox
Alex Kugler
Jason Westrick
Andrew Fu
Elizabeth Ottesen
Sirivatch Shimpalee
John Seaman
Jackson Devault
Hunter Teel

Abstract

The US government has identified 17 critical elements, including most rare earth elements (REEs), which are used extensively in consumer electronics as well as military and national security hardware. We are developing techniques for biomining these elements, the process of using microorganisms to extract critical elements from water, ores, and mine waste to fill these needs. Bioextraction is focusing on: 1) building on our first-year successes of identifying microbes that generate exudates that enhance the extraction of multivalent cations, 2) evaluating available phosphate solubilizing microbes to dissolve apatite and monazite, and 3) and biosurfactant producing microbes. Bioaccumulation efforts involves testing microbes that: 1) naturally release complex exudates that contain organic chelating agents, and 2) naturally accumulate or hyperaccumulate (wt-% levels) metals. Results from year one includes proof of concept that biosurfactant producing microorganisms can release REEs from select ores and that release of REEs is increased by the addition of glucose.

Molecular results for microorganism profiling proved a population shift after addition of microorganisms. The study will culminate in a proof-of-concept demonstration, manuscripts, and the data needed for scaled-up biomining of REEs.

Objectives

- Develop a technology for bioextracting of REEs from minerals known to be high in REEs
- Develop a technology for the bioaccumulation of REEs
- Demonstrate electrochemical monitoring of microbial activity could be applied for biogeochemical interactions
- Conduct a proof-of-concept demonstration of the most effective biomining processes
- Create an industrial partnership

Introduction

While rare earth elements (REE) are a critical US resource, there is currently no domestic infrastructure to process mine REEs into individual elements. REEs are widely dispersed throughout the environment making extraction and isolation a costly endeavor. For example, Cerium (Ce) is the 26th most abundant element in the upper crust making it more abundant than various commonly mined metals such as lead, cobalt, molybdenum, uranium, and all the precious metals. There are abundant domestic REE resources available, however due to the wide dispersion and complex industrial mining processes, new methods must be developed to make these options viable.

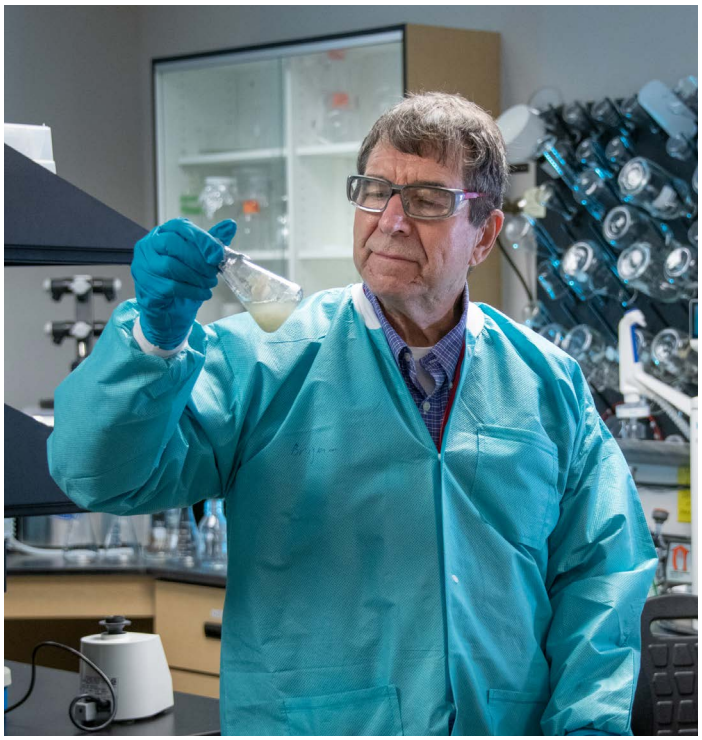

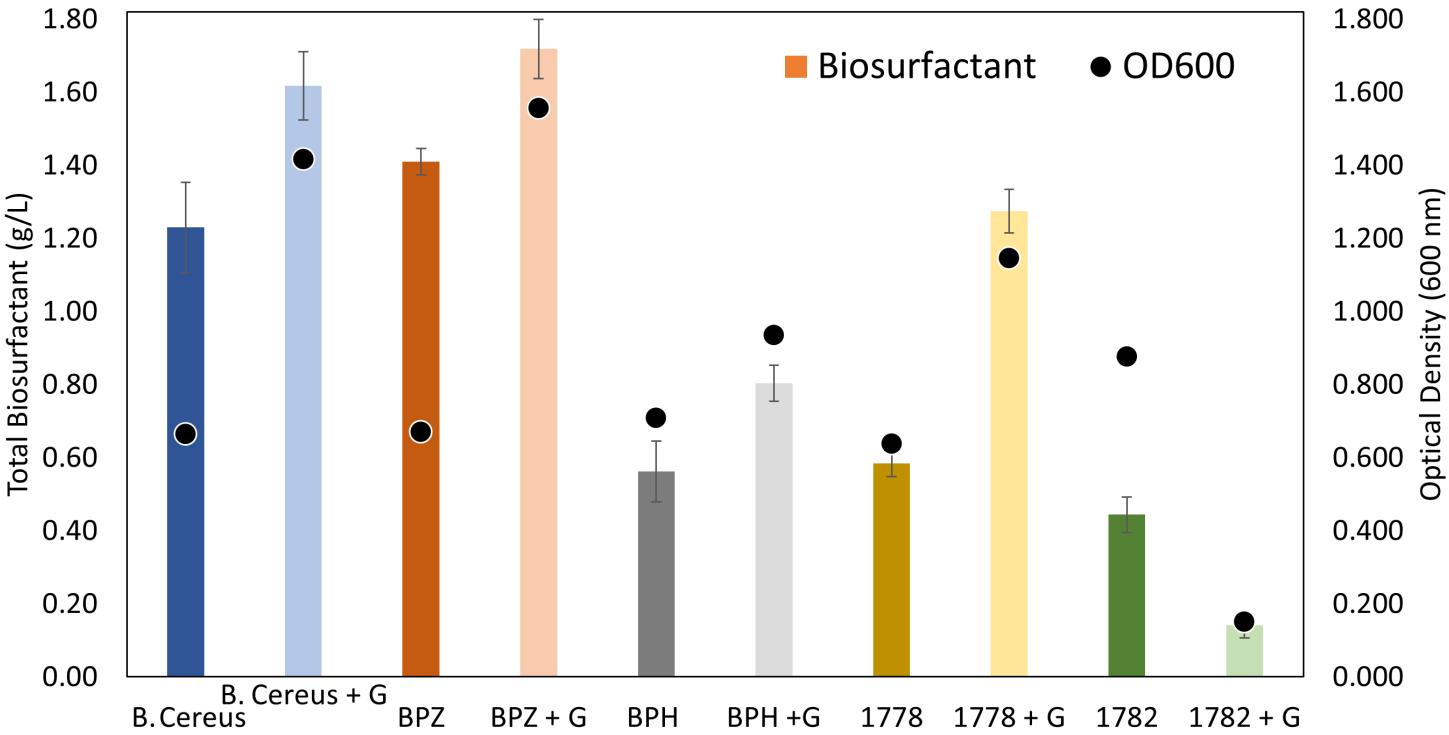

Figure 1: Environmentally resilient microorganisms being screened for biosurfactant production for use in biomining applications. Bacillus cereus has been tested previously but BPZ (Alcaligenes piechaudii) and BPH (Sphingomonas SP. S37) are part of the SRNL BioTiger consortia and proven to grow in extreme environments. Both 1778 and 1782 are mutants of BPH).

In order to develop biomining methods for enhanced extraction and reconcentration, we are applying physical, chemical, and microbiological methods. First, appropriate mining materials were selected for testing as biomining candidates. Second, culture conditions were identified using known biosurfactant producing microorganisms and/or bioprecipitating organisms. Third, we conducted initial screening tests, to quickly identify the most effective microbes and then do more involved testing to define the limits of the optimal biological, chemical, and mineral conditions for bioextraction and bioaccumulation.

These latter, more in-depth, studies included microbiological laboratory techniques, microscopy, spectroscopy, genomic, and electrochemical techniques to optimize process efficiency and yields using the most promising organism/organisms. **Figure 1** shows biosurfactant production being screened for select cultures to be applied in biomining efforts.

While it has been observed that microbes can interact with metals including REEs, the mechanisms with respect to extraction are not well understood. As part of our efforts to develop and optimize biomining, we applied molecular techniques to: 1) improve our understanding of bioaugmentation mechanisms, 2) identify shifts in microbiological populations as a function of biomining efforts, and 3) optimize the process to achieve an economically viable alternative to conventional metal and REE extraction processes. Experiments are being conducted with raw materials acquired from the one of the largest REE mines in the country, Mountain Pass Mine (CA), and apatite from the Florida phosphate industry. These materials are being ground to ~1 mm to simulate the feed used in present mining operations for inorganic leaching (e.g. sulfuric acid). **Figure 2** demonstrates molecular level changes observed in biomining extractions. This information can be used to optimize the process in future extractions.

Methods are currently being developed to recover critical elements from key environments, bioremediation efforts, and additional biomining processes. Biosurfactant, surfactants of microbial origin, producing microbial consortia were found to release REEs from selected mine ores (**Figure 3**). Current efforts include modifying the media to increase biosurfactant production and correlate with REE extraction. In year 2, we plan to apply organic acid producing microorganisms to further increase REE release.

Approach

The resulting information from this work identified common genetic characteristics of microbes that are correlated to bioprecipitation and/or bioaccumulation, examination of the composition of microbial communities in REE enriched environments, as well as of consortia showing promise, and key microbes correlated with improved biomining performance. This approach includes not only observing and tracking changes in which microbes interacted with REEs, but also using community transcriptomics to observe changes in microbial gene expression over time in our lab microcosms.

Figure 2: Changes in the bacterial profile based on experimental surfactant treatment show domination of several genus's, while rare genus appear such as Abditibacterium, an extremophile known for living in nutrient poor envrionments. These molecular techniques can be used to help demonstrate the stability and metabolic capacity of the biomining technology.

By tracking microbial behavior both *in situ* and ex situ with REE rich materials we can develop successful biomining protocols. Through a current transcriptional analysis of active cultures, we are identifying mechanisms of action and potential inhibitors.

Our biomining approach for release of critical element is illustrated in **Figure 4**. We are leveraging key microbial products including enzymes, organic acids, ligands, reductases, and polysaccharides that can facilitate release of critical elements ex situ. Thus, biomining can be accomplished in a controlled manner by regulating culture conditions including speciation, nutrients, temperature, time, and respiration rate. Electrochemical methods were being tested to monitor microorganism in controlled biogeochemical interactions (**Figure 5**).

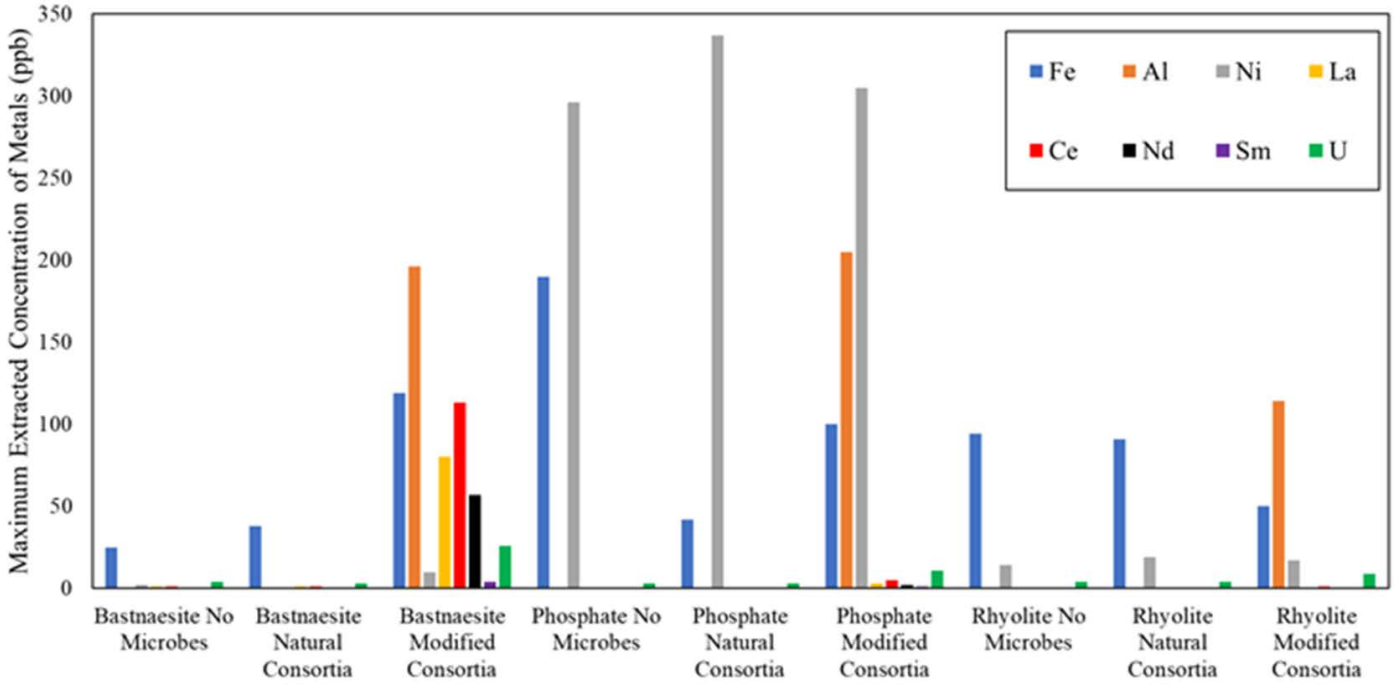

Figure 3: Maximum concentration of bioextracted metal ions (ppb) including REEs from mine ores. Modified microbial consortia were added to make biosurfactants enabling REE release of interest including Cerium (Ce), Lanthanum (La) Neodymium (Nd), and Samarium (Sm) as shown.

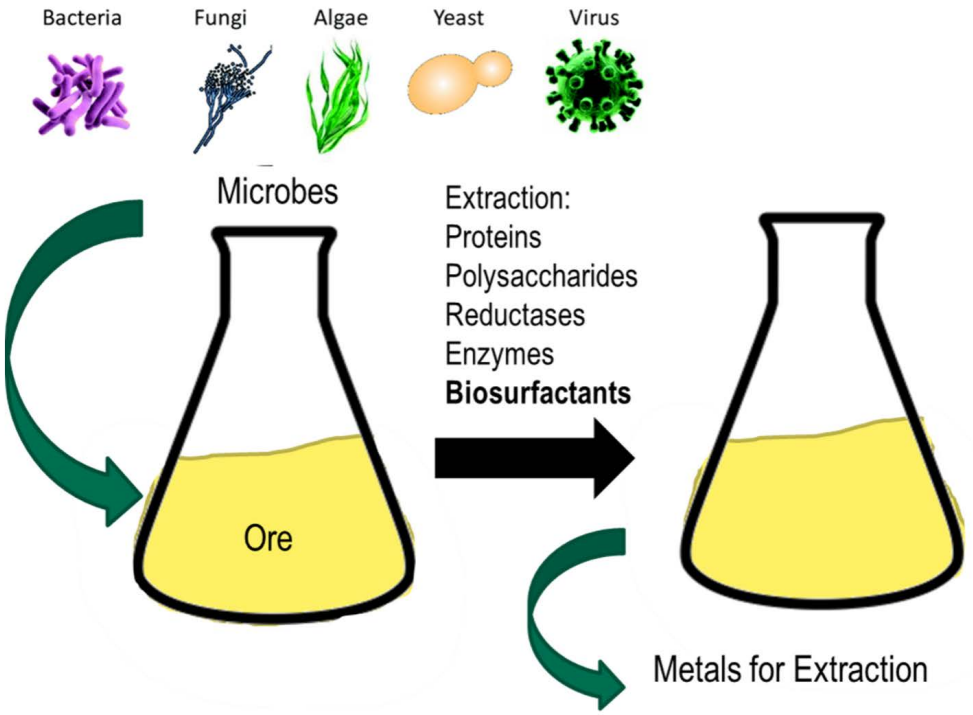

Figure 4: Approach using natural microorganisms and byproducts for critical element release. This method allows screening of varying cultures, environmental conditions, and media to optimize biomining.

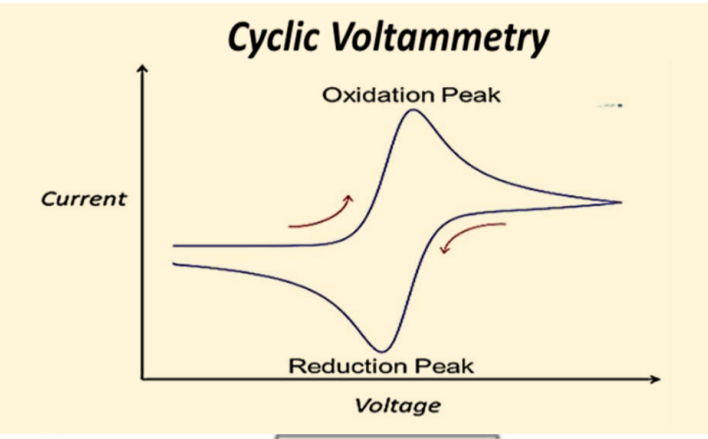

Figure 5: Electrochemical methods were proven to be a means of studying and monitoring microorganisms in metal shuttling by cofactors including riboflavin. These techniques allow real-time testing of microbial activities.

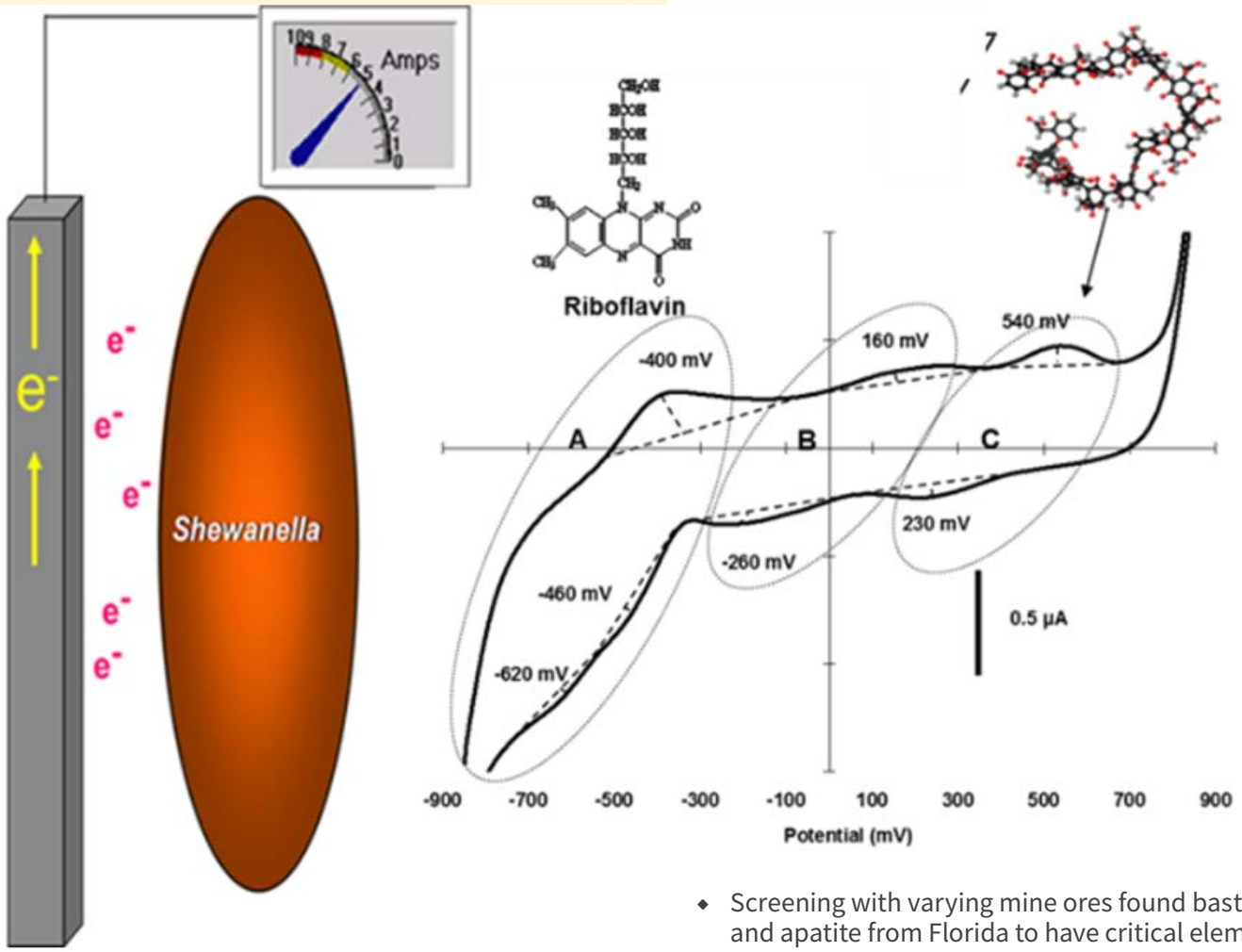

Accomplishments

- Proof of principle was achieved demonstrating that REEs could be bioextracted with biosurfactant producing microorganisms.
- Screening with varying mine ores found bastnasite and apatite from Florida to have critical element potential.
- Molecular analysis showed that the added microorganisms for bioextraction were resilient in the mining environment.
- Screening with varying mine ores found bastnasite and apatite from Florida to have critical element potential.
- Discovered that biosurfactant release of REEs could be enhanced by the additional glucose as measured experimentally.
- A Non-disclosure Agreement (NDA) has been established with the mining company Mosaic, Inc (https://www.mosaicco.com), for technical data and mining-sample exchanges.
- Electrochemically monitoring microbial activity & biogeochemical interactions to provide an indirect assessment of biomining.

Contributing Postdoctoral Researchers

Alex Kugler
Andrew Fu
Jason Westrick

Contributing Student Researchers

Jackson Devault
Hunter Teel

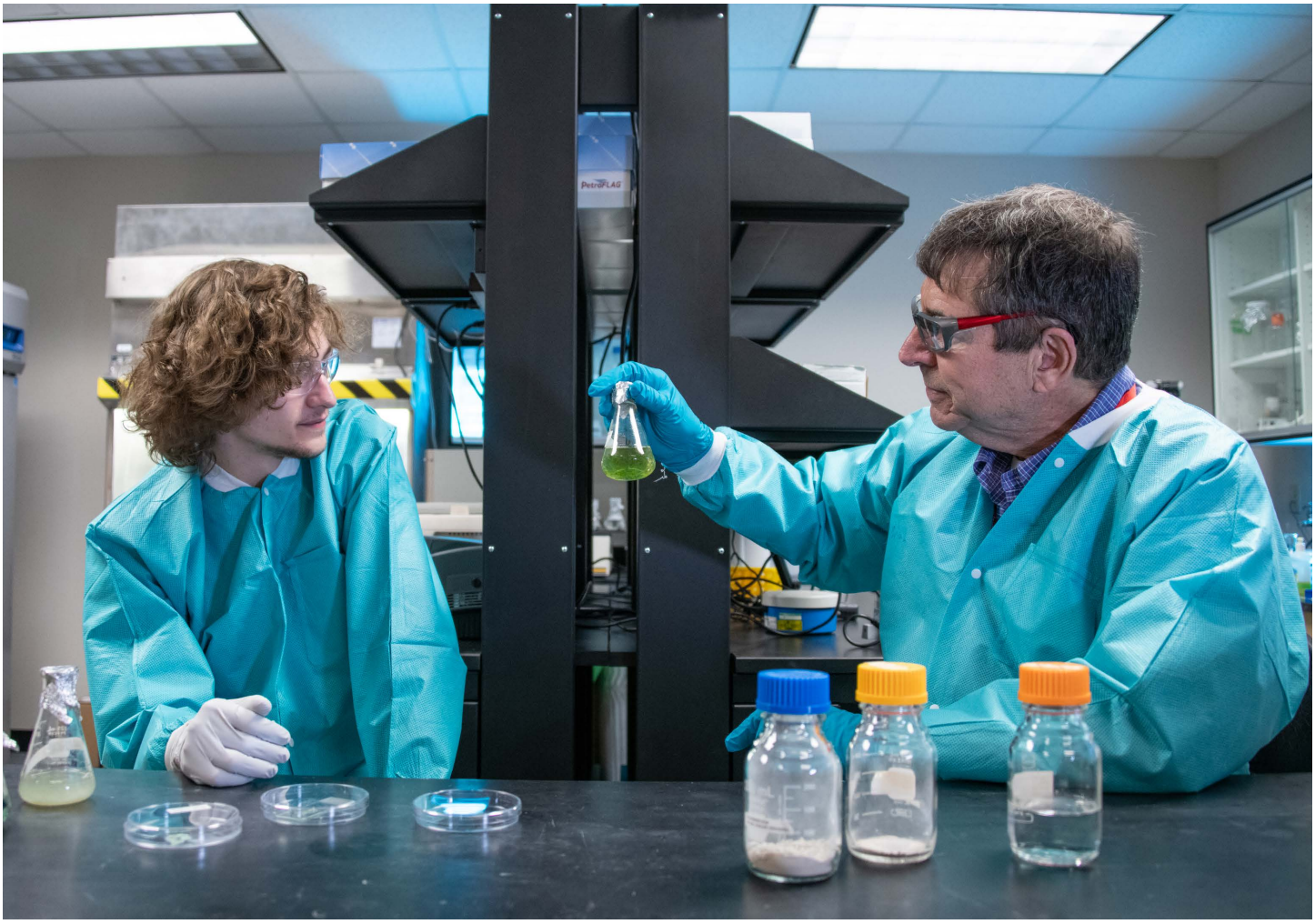

Unraveling the Mysteries of "Magic" Ionization: A Basic Science Approach to Understand Ionization Mechanisms without Heat, Electrons, Photons, and High Voltage

Danielle Mannion

Project Highlight

Matrix-Assisted Ionization (MAI) is a new and highly promising mass spectrometry technique for rapid analysis of inorganic analytes; however, the chemistry and physics underlying this ionization mechanism are largely unknown. This effort seeks to understand the fundamental ionization phenomena of MAI by characterizing both ionization matrix materials themselves and analyte chemistry ionization trends.

Abstract

Ambient mass spectrometry is a new method for the rapid detection and characterization of trace inorganic analytes with minimal sample preparation. Matrix-Assisted Ionization (MAI) is one of the most recently discovered ambient mass spectrometry techniques, wherein ions are produces without the application of heat, photons, electrons, or high voltage as required for conventional mass spectrometry. Although SRNL was the first to demonstrate that this technique could be used to ionize inorganic compounds in aqueous solutions, the underlying ionization phenomena remains uncharacterized. This effort seeks to examine fundamental aspects of MAI via a combination of mass spectrometry, microscopy, and x-ray diffraction experiments. Within the first project year the effort has already identified several key ionization factors that influence the generation, intensity, and species of the matrix-assisted ions. Future efforts will seek to refine these ionization phenomena, leading to sensitivity and accuracy gains and informing future development of fieldable mass spectrometry methods.

Project Team

Principal Investigator
Danielle Mannion

Team Members
Haley Lawton
Kyle Samperton
Matthew Wellons
Joseph Mannion

External Collaborators
Chuck McEwen (MSTM Solutions)
Sarah Trimpin (MSTM Solutions and Wayne State University)

Objectives

- Refine MAI instrument operational parameters and sample introduction methodology.
- Investigate the origin of matrix-derived ions and their role in the ionization process.
- Characterize a model chemical matrix via microscopy, mass spectrometry, and x-ray diffraction.
- Examine correlations of lanthanide trends with ionization through mass spectrometry experiments.

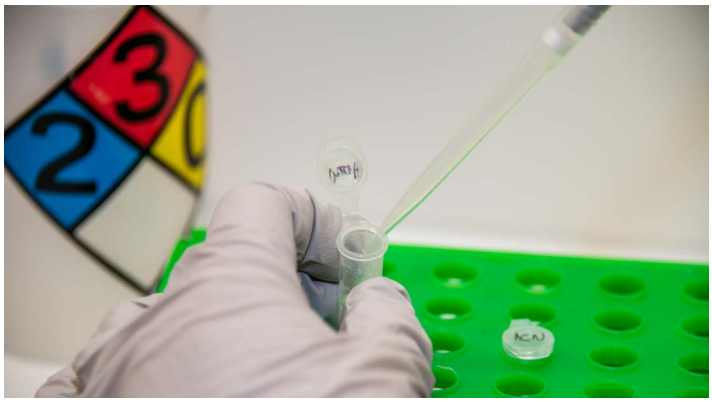

"Magic" Ionization

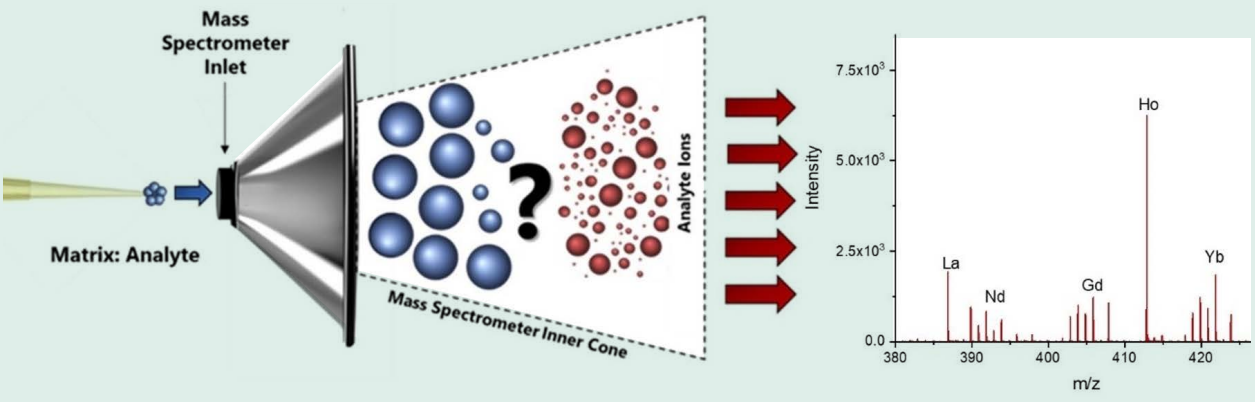

Unravelling the Mysteries of "Magic" Ionization: A Basic Science Approach to Understand Ionization Mechanisms without Heat, Electrons, Photons, and High Voltage

Introduction

Matrix-Assisted Ionization (MAI) is one of the newest, potentially highly advantageous, but least characterized ambient mass spectrometry techniques. Initially referred to as "magic" ionization, MAI was serendipitously discovered during unrelated Matrix Assisted Laser Desorption/Ionization (MALDI) experiments[1-2]. It was observed that addition of specific matrix chemicals to organic samples produced whole-molecule organic ions when the mixture was placed under vacuum. Interestingly, ion production occurs without the application of heat, photons, electrons, or high voltage necessary in other mass spectrometry methods. Despite its relatively recent discovery and current lack of mechanistic understanding, MAI has demonstrated picogram to femtogram detection limits for an array or organic analytes using no sample preparation beyond the addition of solvent and chemical matrix[3-9]. MAI studies of large molecule ionization have produced the theory that ionization occurs from a sublimation-driven triboluminescence process, though this mechanism is itself neither proven nor well understood[10-13]. A scoping study previously conducted with an applied technology SRNL LDRD effort demonstrated unexpected but informative results for MAI ionization mechanisms of inorganic analytes[14]. When uranium was analyzed using MAI, it was discovered that some uranium-bearing ion complexes contained molecules appearing to originate from the chemical matrix itself. It was hypothesized that these "matrix-derived ions" are formed *in situ* during the ionization event and subsequently recombine with gas phase inorganic analytes. These initial results suggest that the ionization process for inorganics is fundamentally different from those reported in the literature for organics.

In this work, the impact of matrix and analyte physical and chemical properties on ionization was investigated through experimentation. First, MAI instrument parameters and sample introduction modalities were refined. Parameters and methods that lead to the highest ion abundance and repeatability were utilized in subsequent experiments. Second, the matrix 3-nitrobenzonitrile (3-NBN) was analyzed as a model matrix via microscopy, mass spectrometry, and X-ray diffraction. It was discovered that matrix-derived ions are only observed when analyzing 3-NBN with MAI, and these ions are subjected to fragmentation within a few centimeters after being introduced to the instrument orifice. Data from these fragmentation experiments are shown in **Figure 1**. Furthermore, preliminary crystal structure data was acquired for this model matrix and is shown in **Figure 2**.

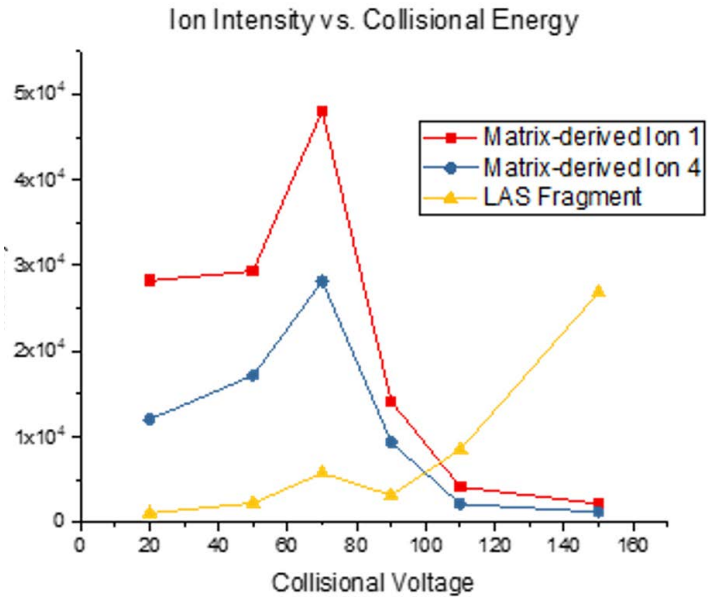

Figure 1: The relationship of ion intensity as collisional voltage increases. With increasing collision energy, the matrix-derived ions disappear and fragment ion of linear alkylbenzene sulfonate (LAS) increases.

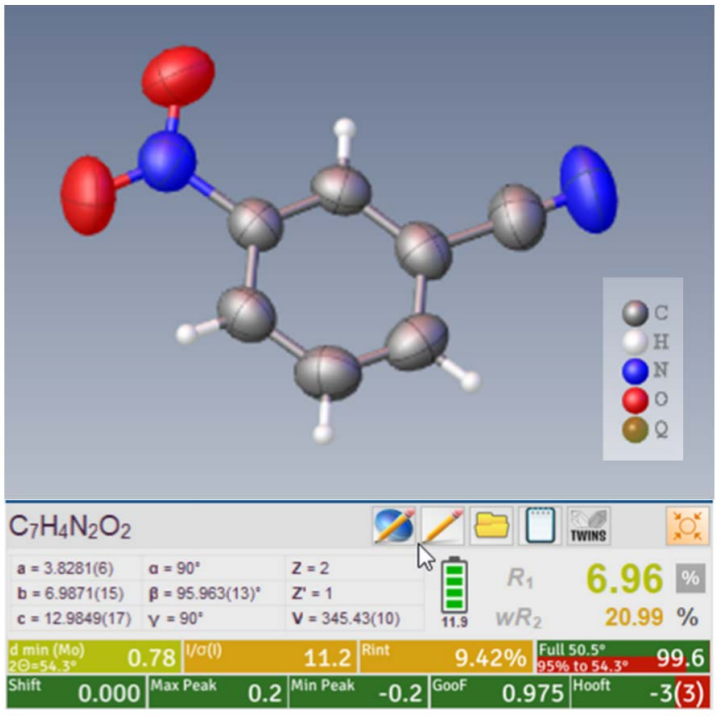

Figure 2: Preliminary crystal structure of 3-NBN acquired by SCXRD.

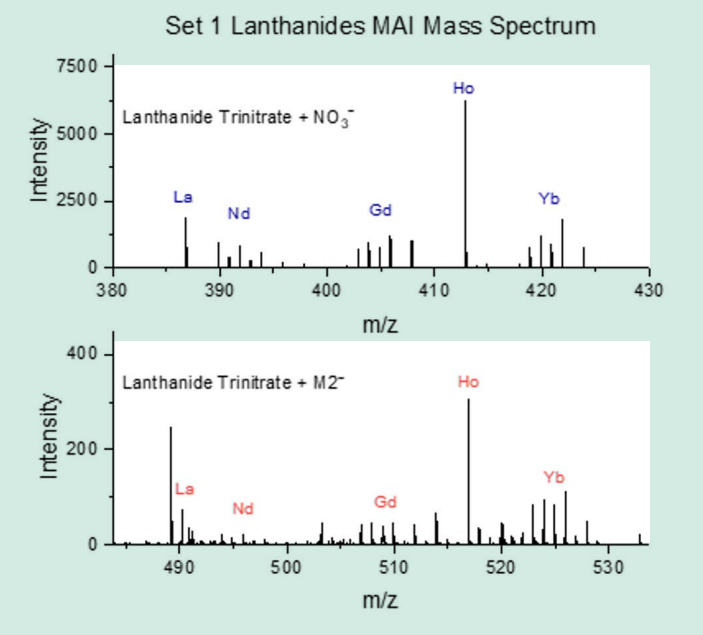

Third, the lanthanide series of elements was analyzed using MAI to investigate the impact of analyte properties on ion formation. This is the first demonstration of lanthanide analysis with MAI, and all lanthanides were detected as ion complexes containing matrix-derived ions (**Figure 3**). A trend was discovered between lanthanide ionic radius and matrix ion complex formation, as shown in **Figure 4**. A subsequent analysis of lanthanide samples both with and without 3-NBN failed to produce these complexes using Electrospray Ionization (ESI). A schematic of this experiment and resulting spectra is show in **Figure 5**.

Figure 3: (Left) MAI mass spectra of mixed lanthanides showing the nitrate adduct (top) and matrix-derived adduct (bottom).

Figure 4: (Below) Mass spectra of single-isotope lanthanides in complex with a matrix-derived ion (left) and a plot showing the relationship between the intensity of these ion species and ionic radius (right). This relationship suggests that lanthanide shrinkage directly correlates with the formation or stability of this ion complex.

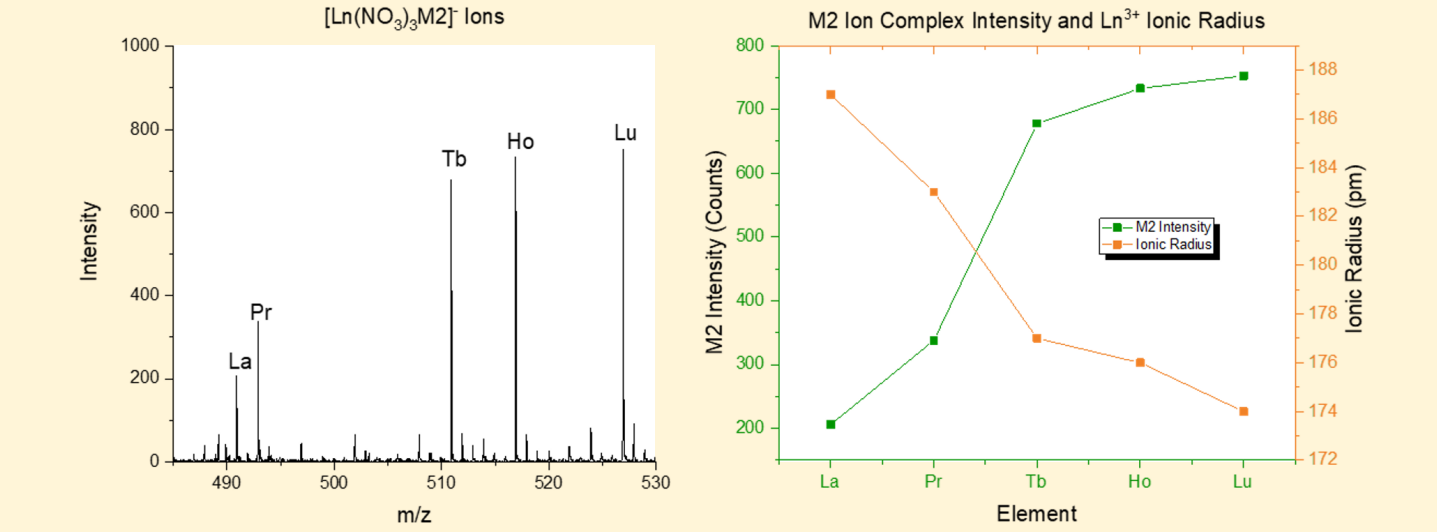

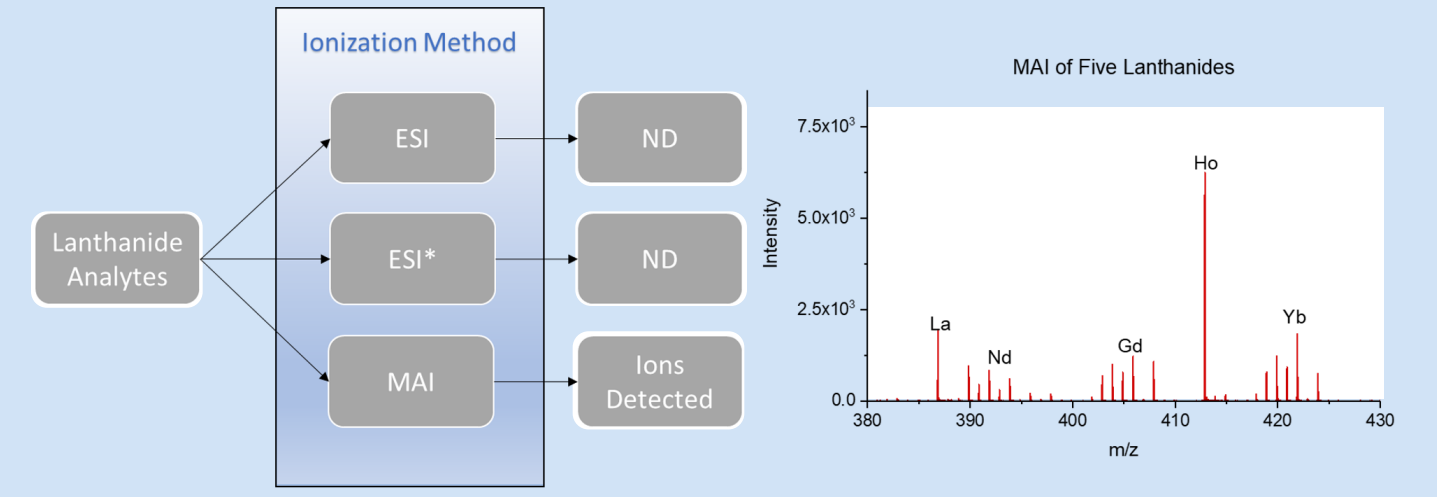

Figure 5: Comparison of analyte ion signals acquired between three different ionization experiments. ESI of a lanthanide test solution with (ESI) and without 3-NBN generated no detectable lanthanide species containing matrix-derived ions. MAI experiments did resolve these species.*

Work conducted during this first year of the project has led to insight about the MAI inorganic ionization mechanism. Key findings are summarized as follows:

- 3-NBN matrix-derived ions are formed within a few centimeters after being introduced to the instrument orifice and are created from the MAI process.
- Some of these matrix-derived ions are detected in ion complexes with lanthanides using MAI. There is no evidence that these complexes form in solution.
- The relative abundance of non-matrix containing lanthanide ion species is similar between MAI and ESI (**Figure 6**).

These findings suggest that the ability of a matrix to form matrix-derived ions when exposed to vacuum plays an important role in the inorganic ionization process. Additionally, it appears that analyte factors that influence ionization by ESI similarly affect the MAI ionization process. Future work will aim at further elucidating these processes to develop a general model of MAI ionization. Advancing the fundamental science of this breakthrough technique is highly transferable to end users seeking fieldable mass spectrometry methods for radionuclide analysis and may become an invaluable tool for rapid sample screening and triage in safeguards/nonproliferation applications.

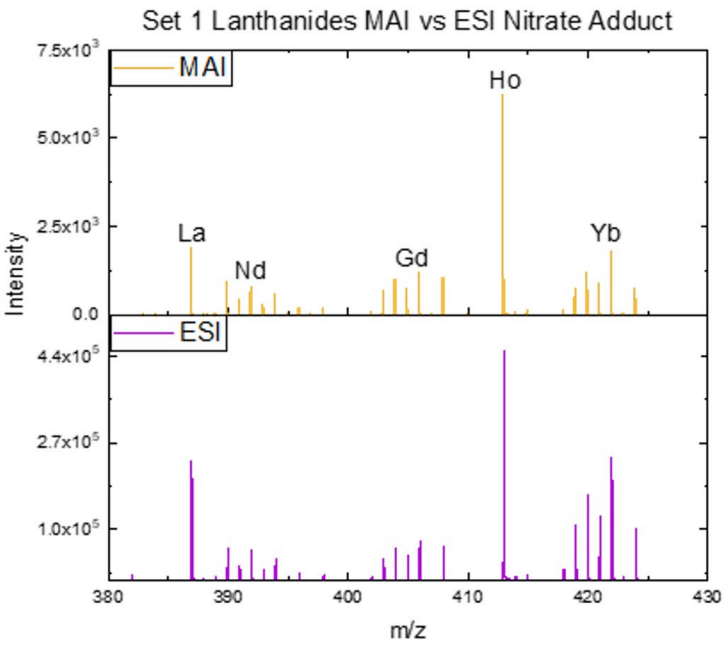

Figure 6: Comparison of mass spectra acquired for mixed lanthanides using ESI with (EIS) and without 3-NBN and MAI. The ions shown are the lanthanide tetranitrate complexes. Relative abundances between the elements are similar between the two ionization methods.*

$$\frac{N_+}{N_0} \propto E_{MS}\ [M_F]\ DF\ [A_F]$$

E_{MS} is Mass Spectrometer Ion Transmission Efficiency
M_F is the Matrix Factor
DF is the Driving Force
A_F is the Analyte Factor

Equation 1: Concept of the MAI formalization equation, with key investigative factors that are the focus of this work in brackets.

Approach

The objective of this project was to investigate the MAI inorganic ionization mechanism through systematic experimentation and to develop a testable theory for the inorganic ionization process. A key part of developing an ionization theory is to develop and understand the factors of an MAI formalization equation as shown in **Equation 1**. Defining the relationship and impact of these variables on ionization efficiency is fundamental to comprehending this ionization mechanism. The main investigative avenues of this project are to characterize the influence of matrix and analyte properties on MAI ionization. Understanding these impacts will enable subsequent definition of the matrix factor and the analyte factor of the formalization equation. Initial instrument optimization was performed to determine the parameters and sample introduction methods that resulting in high reproducibility and ion sensitivity. Additionally, to standardize and expedite data analysis, development began on an RStudio data processing suite.

To investigate the matrix factor, the chemical matrix 3-NBN was studied as a model matrix. This chemical was examined via mass spectrometry analysis using three ionization methods to determine the origin of matrix-derived ions. In-source collision induced dissociation (CID) was also performed on these matrix-derived ions to determine where in the instrument they are formed.

To enable targeted fragmentation studies to definitively identify these ions an Agilent Ultivo triple quadrupole mass spectrometer was procured for future research. Powder X-ray diffraction (pXRD) and single-crystal X-ray diffraction (SCXRD) was performed on 3-NBN to determine crystal structure and intermolecular contacts. Various methods of crystallization were investigated to produce crystals of adequate dimension for SCXRD, a summary of which is depicted in **Table 1**. To investigate the analyte factor, the lanthanide series of elements was selected for spectrometric analysis due to their well characterized physical and chemical trends. MAI analysis was performed on solutions of single element and multi-element lanthanide nitrates to determine if lanthanide shrinkage impacts ionization efficiency. ESI analysis was also performed to compare the ion species formation and ion abundance between the two methods. Lastly, to interrogate the formation of matrix-derived ion containing complexes, solutions of lanthanides saturated with 3-NBN were analyzed with ESI.

Accomplishments

- Demonstrated that 3-NBN matrix-derived ions are formed within the first few centimeters of the instrument and are created from the MAI process.
- Resolved the preliminary crystal structure of 3-NBN using SCXRD, a previously unknown structure.
- Discovered that two matrix-derived ions are detected in ion complexes with lanthanides using MAI. There is no evidence that these complexes form in solution.
- Determined that the relative abundance of non-matrix containing lanthanide ion species is similar between MAI and ESI.

FY21 Presentations

- Matrix-assisted Ionization mass spectrometry for the detection and characterization of uranium species. The Great Scientific Exchange (SciX) 2021 Conference, Providence, RI September 26-October 1, 2021. Invited Oral Presentation.
- Matrix-assisted ionization and quantitative analysis of uranium isotopic composition and assay by AccuTOF time-of-flight mass spectrometry. 69th ASMS (ASMS) Conference on Mass Spectrometry and Allied Topics, Philadelphia, PA October 31-November 4, 2021. Abstract. Oral Presentation.

Contributing Postdoctoral Researchers

Elizabeth Pettit Abigail Walford

References

1. Trimpin, S.; Inutan, E. D., Matrix assisted ionization in vacuum, a sensitive and widely applicable ionization method for mass spectrometry. Journal of The American Society for Mass Spectrometry 2013, 24 (5), 722-732.
2. Trimpin, S., " Magic" ionization mass spectrometry. Journal of the American Society for Mass Spectrometry 2016, 27 (1), 4-21.
3. Inutan, E. D.; Trimpin, S., Matrix assisted ionization vacuum (MAIV), a new ionization method for biological materials analysis using mass spectrometry. Molecular & Cellular Proteomics 2013, 12 (3), 792-796.
4. Trimpin, S.; Inutan, E. D., New ionization method for analysis on atmospheric pressure ionization mass spectrometers requiring only vacuum and matrix assistance. Analytical chemistry 2013, 85 (4), 2005-2009.
5. Woodall, D. W.; Wang, B.; Inutan, E. D.; Narayan, S. B.; Trimpin, S., High-throughput characterization of small and large molecules using only a matrix and the vacuum of a mass spectrometer. Analytical chemistry 2015, 87 (9), 4667-4674.
6. Chakrabarty, S.; DeLeeuw, J. L.; Woodall, D. W.; Jooss, K.; Narayan, S. B.; Trimpin, S., Reproducibility and quantification of illicit drugs using matrix-assisted ionization (MAI) mass spectrometry. Analytical chemistry 2015, 87 (16), 8301-8306.
7. Trimpin, S.; Thawoos, S.; Foley, C. D.; Woodall, D. W.; Li, J.; Inutan, E. D.; Stemmer, P. M., Rapid high mass resolution mass spectrometry using matrix-assisted ionization. Methods 2016, 104, 63-68.

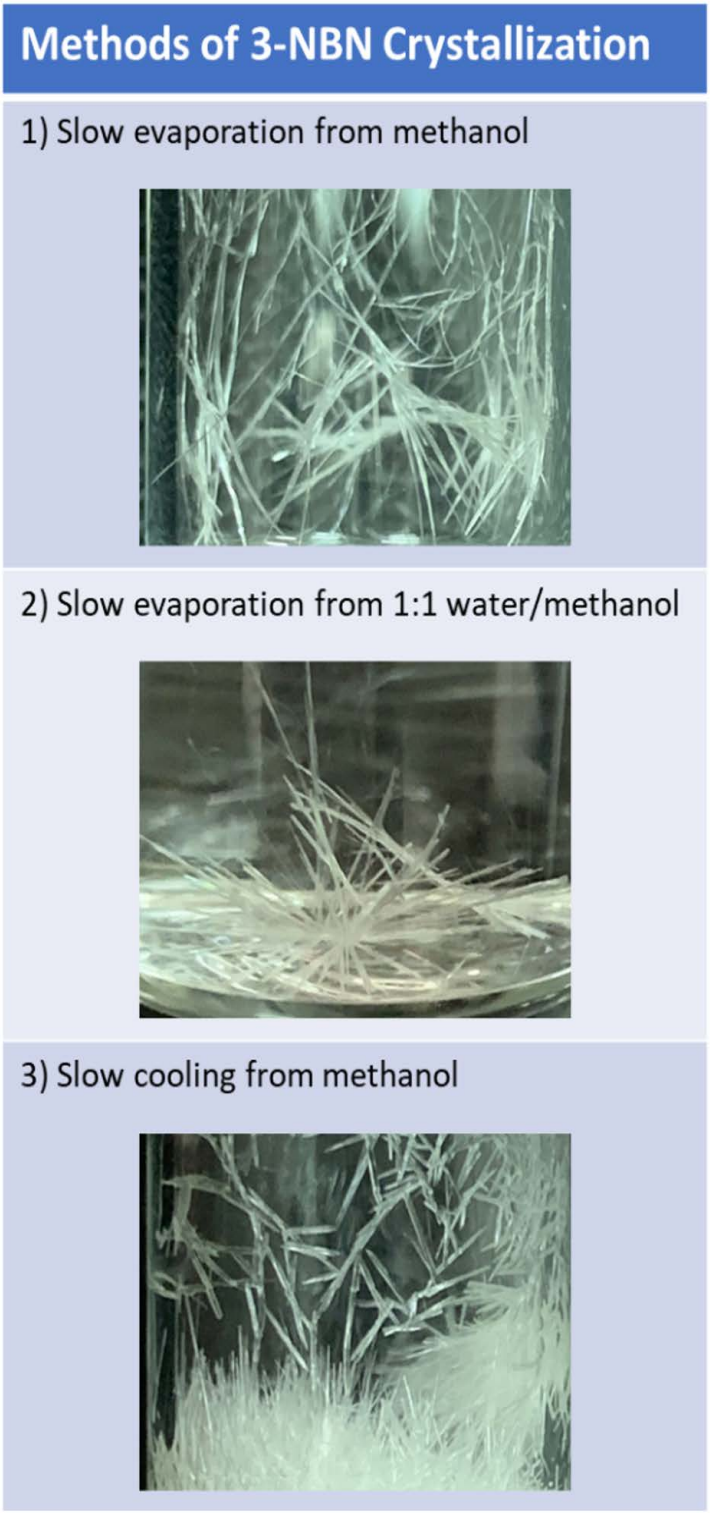

Table 1: Methods of 3-NBN crystallization and resulting crystal morphology.

8. Hoang, K.; Pophristic, M.; Horan, A. J.; Johnston, M. V.; McEwen, C. N., High sensitivity analysis of nanoliter volumes of volatile and nonvolatile compounds using matrix assisted ionization (MAI) mass spectrometry. Journal of The American Society for Mass Spectrometry 2016, 27 (10), 1590-1596.

9. Cody, R. B., Ambient Profiling of Phenolic Content in Tea Infusions by Matrix-Assisted Ionization in Vacuum. Journal of The American Society for Mass Spectrometry 2018, 29 (8), 1594-1600.
10. Trimpin, S.; Lutomski, C. A.; El-Baba, T. J.; Woodall, D. W.; Foley, C. D.; Manly, C. D.; Wang, B.; Liu, C.-W.; Harless, B. M.; Kumar, R., Magic matrices for ionization in mass spectrometry. International Journal of Mass Spectrometry 2015, 377, 532-545.
11. Trimpin, S.; Lu, I.-C.; Rauschenbach, S.; Hoang, K.; Wang, B.; Chubatyi, N. D.; Zhang, W.-J.; Inutan, E. D.; Pophristic, M.; Sidorenko, A., Spontaneous charge separation and sublimation processes are ubiquitous in nature and in ionization processes in mass spectrometry. Journal of The American Society for Mass Spectrometry 2018, 29 (2), 304-315.
12. Banstola, B.; Murray, K. K., Sublimation Electrification of Organic Compounds. Journal of the American Society for Mass Spectrometry 2020, 31 (4), 888-893.
13. Lee, C.; Inutan, E. D.; Chen, J. L.; Mukeku, M. M.; Weidner, S. M.; Trimpin, S.; Ni, C. K., Toward understanding the ionization mechanism of matrix-assisted ionization using mass spectrometry experiment and theory. Rapid Communications in Mass Spectrometry 2019.
14. Mannion, D. R.; Mannion, J. M.; Kuhne, W. W.; Wellons, M. S., Matrix-Assisted Ionization of Molecular Uranium Species. Journal of the American Society for Mass Spectrometry 2020, 32 (1), 8-13.

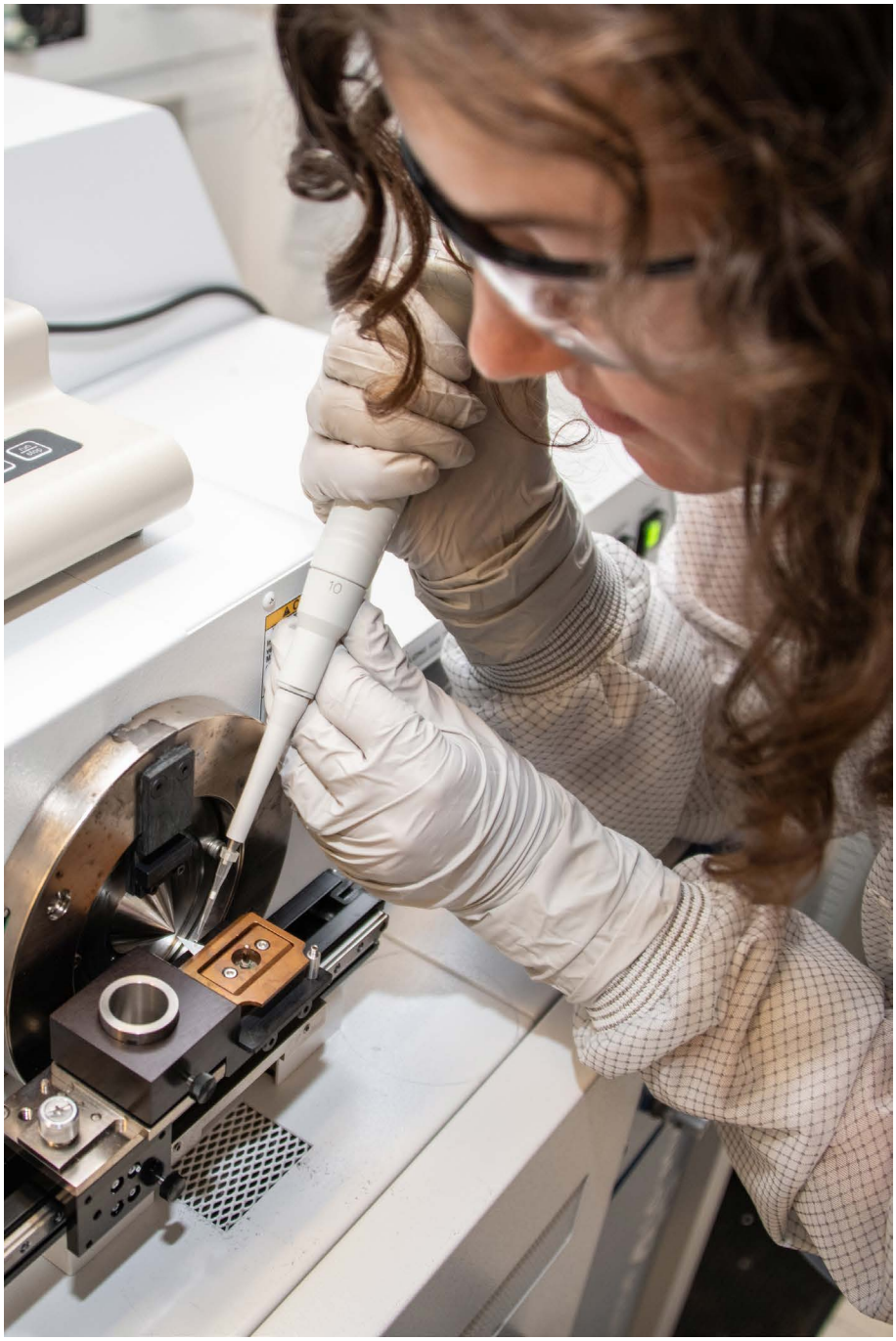

The Application of Machine Learning Techniques to Meteorological Forecasting

David Werth

Project Highlight

A labeled data set comprising the two predictands (fog and the sea breeze) and related meteorological predictors has been developed, and several machine learning algorithms have been trained to find relationships between the predictors and the subsequent occurrence of the predict and events.

Abstract

Fog and inland-penetrating sea-breezes occur often at SRS and have a strong impact on site operations. Site personnel therefore require accurate forecasts of these events, but both are difficult to forecast using traditional techniques. Our goal is to apply machine learning (ML) techniques to the problem of forecasting fog and the sea breeze at the Savannah River Site. We apply several such techniques - decision trees, regression, and a series of classification/regression techniques – and train them using the large datasets collected by our group at SRS and from external organizations that maintain databases of regional meteorological variables. The proposed methods have been developed and have shown varying degrees of skill in predicting fog when compared to existing forecasting tools. We will further advance the use of these algorithms for weather forecasting, taking them towards becoming wide-spread forecasting tools.

Project Team

Principal Investigator David Werth

Team Members
Thomas Danielson
Elizabeth LaBone
Stephanie Gamble
Eric Hoar
Stephen Noble
Brian Viner

External Collaborators
Ajay Kumar Gogineni
Brian Mayer
Naren Ramakrishnan (Sanghani Center for Artificial Intelligence and Data Analytics)

Objectives

- Collect fog and sea breeze data from onsite sources, and label all data with its respective category
- Develop Random Forest algorithm
- Develop Ordinal Regression algorithm
- Develop Neural Network algorithm

Introduction

Our objective is to apply multiple machine learning (ML) algorithms to the problem of forecasting fog and the sea breeze at the Savannah River Site. This task comprises collecting and organizing data from onsite and offsite sources, labeling periods during which these events occurred, training the algorithms to recognize the conditions that preceded their occurrence, then testing them using new data to verify that the forecasts are accurate. For both applications, the ML techniques are to identify patterns and correlations from this labeled data, allowing classification of future predictors to the proper category (e.g. fog or no fog will occur tomorrow). The methods we have selected have been proven useful for a variety of applications, and by developing multiple methods, we ultimately plan to assess how an ensemble of predictions can be used to estimate the uncertainty of the forecasts.

For fog, we put together a large, labeled dataset of predictors and associated readings from the site visibility sensors, which can be used as a continuous predictand or instead be used to develop a binary predictand – as the visibility readings fall below certain thresholds, we can assume that fog exists at various intensities. The selected algorithms were each applied to the dataset and demonstrated skill at predicting fog on the subsequent day. Currently, the existing Model Output Statistics (MOS) model yields a visibility forecast, and serves as the baseline forecast upon which the ML must improve. Several (though not all) of the methods have significantly improved on this forecast, highlighting their benefit.

Fog and the sea breeze are affected by small-scale variations in temperature, moisture, etc., that are poorly reproduced by existing computer weather models that do not resolve such features, so this project has the potential to improve the forecasting of these complex weather phenomena. The ML algorithms are executed using existing software, and the developed modeling system could be i) applied at any location with sufficient training datasets, or ii) applied to predict other weather phenomena with a clearly defined predictand and data to do the training.

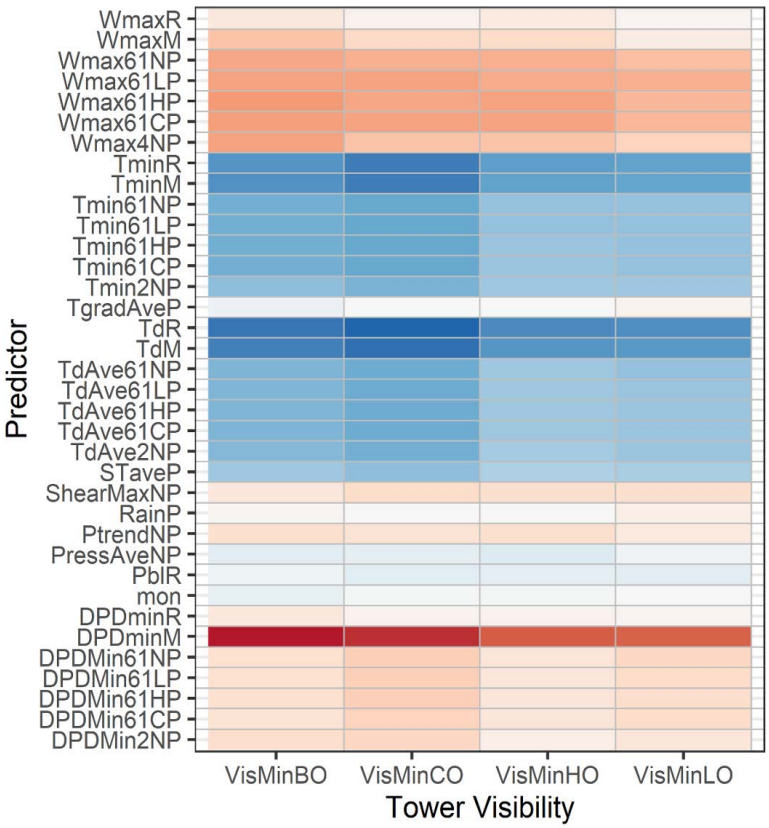

Figure 1: Correlation matrix showing the Pearson correlation coefficients between the observed predictor variables (left column) and the next-day observed morning minimum visibility at the four site towers (bottom row - B, C, H, and L).

Approach

The predictors comprised i) observations from site instruments and ii) predictions from existing weather models. Data was collected from our site towers (including visibility data, a proxy for fog formation), from radar maps (to identify sea breezes), and from archived weather forecasts of temperature, dewpoint, etc. for SRS from two weather models. These were composited into a single dataset for each day by averaging or selecting minima or maxima (e.g. the observed morning low temperature and the forecasted average dewpoint for the next day from an existing weather forecast model), creating a set of inputs and desired outputs (e.g. the next day's minimum visibility onsite between 0600UTC and 1200UTC) for the machine learning algorithms to train on. To identify the inputs that best serve as precursors to fog, the team developed a Pearson correlation matrix (**Figure 1**), which indicates that several model and observed variables correlate with the site visibility values on the subsequent day. The best correlated predictors include the morning minimum of dewpoint depression from the MOS model (DPDminM), the average morning dewpoint from the RAMS (TdR) and the MOS (TdM) weather models, and the morning low temperatures from those same models (TminR, TminM).

Several methods – the random forest, logistic regression, and a series of classification/regression models - were applied to the data assuming both a continuous predictand (the measured visibility value) or a binary predictand (setting a visibility threshold for 'fog' or 'no fog'), using various methods for sampling the data (to account for the differing number of foggy and non-foggy days) and selecting the most useful input variables. Equitable threat scores (ETS, for which higher values indicate more accurate forecasts) and other similar metrics are used to validate the forecasts.

Accomplishments

- When using a random forest with a binary predictand, the best classification model has only a 6% precision (True Positives) (True Positives + False Positives) when predicting fog, due to a high number of false positives. We are continuing efforts seek to improve the performance metrics of the model.
- When we instead use a random forest algorithm to forecast the actual values of visibility, the model results indicate an ability to accurately train on known data but with limited ability to predict future visibilities (**Figure 2**).
- The number of foggy days is much lower than the number of clear days, which can frustrate attempts to train an ML algorithm to predict fog. To compensate for this, the logistic regressions were trained using sampling methods to balance the number of days with and without fog, either by i) under sampling, ii) over sampling, or iii) creating synthetic data. These performed better than a logistic regression trained with the unmodified data. The highest ETS values for two data sets were 0.29 for a data set using data from the current MOS forecast model as predictors. This is a large improvement on the existing MOS ETS of 0.19.
- As a precursor to the neural net techniques, we applied a series of other classification/regression techniques that did very well (exceeding the 0.19 MOS ETS) for predicting continuous visibility or when a binary predictand was used (**Table 1**).

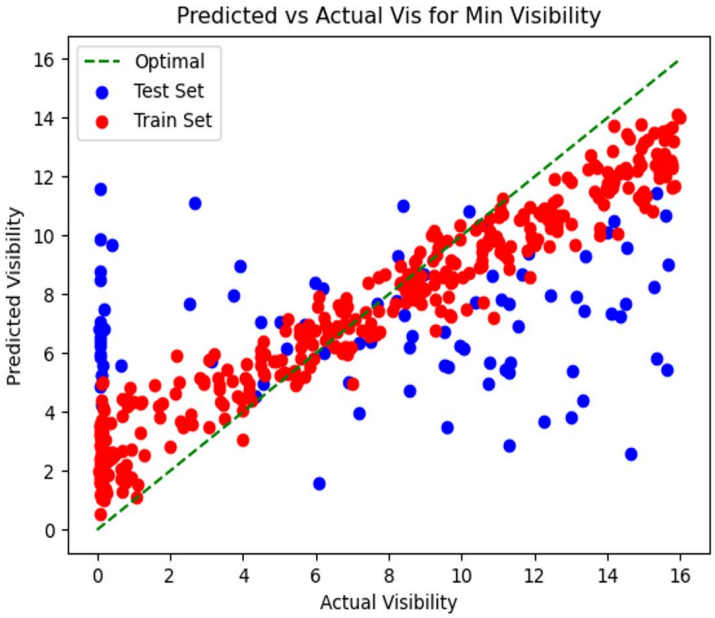

Figure 2: Plot of predicted visibility vs actual visibility in kilometers illustrating the 1-day predictive capability of the Random Forest algorithm. Values below 1.6km are the point at which site operations are affected.

	Binary classification	Continuous visibility value
Elastic Net	0.16	0.47
Cat Boost	0.467	0.35
Light GBM	0.467	0.38

Table 1: Equitable threat scores (ETS) for various classification/ regression methods when forecasting next-day fog.

Contributing Postdoctoral Researchers

Eric Hoar Stephanie Gamble

Contributing Student Researcher

Ajay Kumar Gogineni

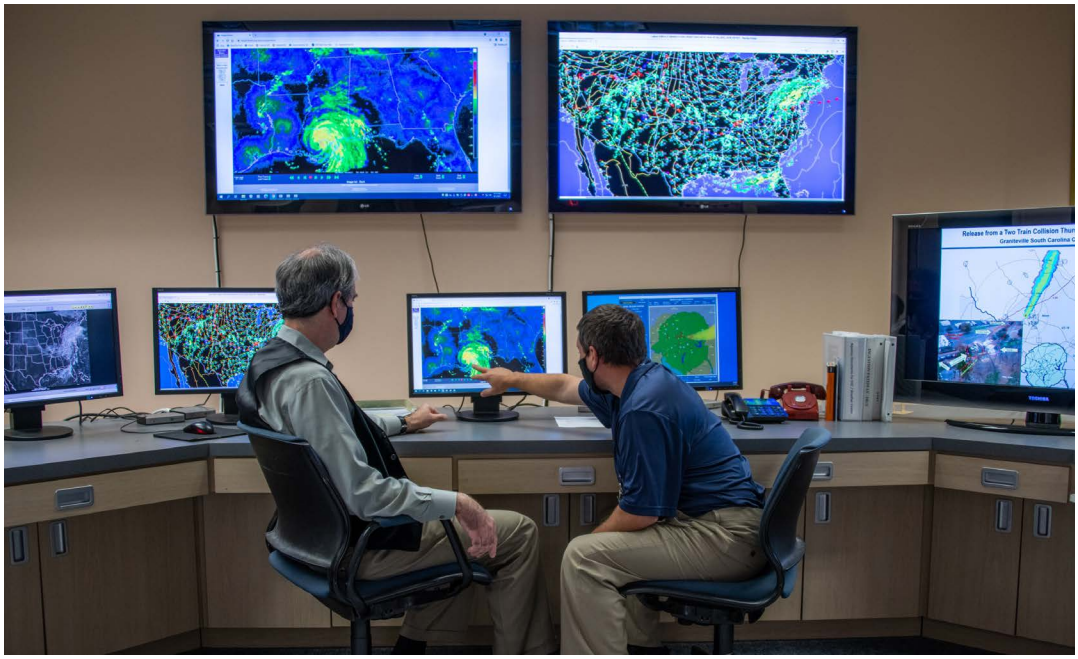

AI to predict glass compositions satisfying property and cooling rate criteria

Anna d'Entremont

Project Highlight

Machine learning models were developed to predict glass properties based on their composition and temperature and showed promise for providing greater prediction accuracy than a traditional regression model on the same data. Custom computer code was developed to filter and process the data from a large database of empirical glass data to make it usable for this project and future glass research.

Project Team

Principal Investigator Anna d'Entremont

Team Members
Bruce Hardy
Lindsay Roy
Eric Hoar

External Collaborators
Charles Daniels (USC)
Jason Bakos (USC)
Joseph Cammarata (USC)

Abstract

This project aimed to develop a predictive, artificial intelligence/machine learning-based model to identify glass compositions satisfying specified property requirements. Such a model would provide a systematic approach for narrowing down the nearly infinite range of possible compositions for glasses and minimize unnecessary experimental trial and error.

A large empirical data set for training and testing the algorithm was obtained from the SciGlass database. It contains glass compositions and corresponding property data from a wide range of literature sources. However, the currently available form of this data, recently released under an open database license, is not conducive to easy querying and use. The data structure was deciphered and a customized parsing code developed to make this data more usable for the current and future work. Neural network models were developed and trained on viscosity data from the database and demonstrated potential for improving prediction accuracy over a traditional regression model.

Objectives

- Develop machine learning methods to connect glass composition and cooling rate to the resulting glass properties in order to predict compositions that will yield desired properties.
- Identify a suitable data set for training containing large quantities of glass composition and property data.
- Choose preliminary targets of properties to predict.
- Identify physics-based models to incorporate into the algorithm.
- Process training data for input to model; train and test ML algorithms.
- Use molecular modeling as needed to generate additional training data and/or physical insights.
- Evaluate final model.

Introduction

This project aimed to develop a predictive, artificial intelligence/machine learning-based model to predict envelopes of glass compositions that will yield acceptable properties for a given application. Such a model would provide a systematic approach for narrowing down the "nearly infinite" [1] range of possible compositions for glasses and thus accelerate progress compared to the traditional empirical approach. Data-driven approaches for advancing glass science, particularly those coupling data-driven (e.g. machine learning), physics-based, and/or empirical modeling, have been identified as a key opportunity space in the field [2].

A challenge for effective use of machine learning models (or any complex data-driven model) is obtaining a suitably large and representative data set for the model application. The ability to learn unknown and complex patterns within data without needing to define the expected dependence of the data a priori is a major strength of machine learning approaches, but learning meaningful patterns relies on large amounts of training data that can be fed into the algorithm in consistent format. As a result, large collections of glass data covering broad ranges of compositions are invaluable if data-driven techniques are to be applied in glass science. The SciGlass database, a formerly proprietary database recently released under an open database license, is one such collection. Unfortunately, this data was released in an outdated proprietary file format with very limited functionality and documentation. As part of preparing the data for machine learning, code was developed to extract this data from the original database files, parse it according to structure, and store it in an open-source format designed to be readily queried and formatted for either human readability or for input into another algorithm. In addition to enabling the current machine learning work, this upgraded database format will help to keep this valuable data set accessible and usable for future data analysis efforts and glass research.

Machine learning models to predict glass viscosity as a function of composition and temperature were trained and tested on empirical data from the SciGlass database. Glass melt viscosity-temperature relationships are an important factor in glass manufacturing since various glass processing and forming steps must be performed in certain viscosity ranges. Preliminary results indicate that a neural network model can provide accuracy improvements over an existing traditional regression model when trained on similar data sets.

Approach

Machine learning algorithms require large data sets for training and testing. The data set for this project is existing empirical data from the literature, already compiled in the SciGlass database. This large and varied set of glass data was developed as a proprietary database and recently made available under an open database license. It contains data from more than 422k glasses, from a wide variety of published sources including journal articles, technical reports, and patents, from as early as 1878 to as recent as 2019. Unfortunately, the open-database release is stored in an outdated proprietary file format (Microsoft Access 2.0), lacks functionality of the proprietary database even when opened with the specified software, and has minimal documentation, making it difficult to effectively find data and understand the entries. As a result, the first step to using this data was to decipher the format and develop custom parsing code to interpret the database files and convert it into a more usable format. The new data format facilitates searching and filtering based on various attributes of the data, such as the glass composition, the properties reported for the glass, or the original reference for the data. This enables extraction of subsets of data meeting specified criteria. For example, to compare our machine learning algorithm results to a traditional regression model, we were able to filter based on the references cited for the existing model in order to isolate roughly the same data set.

Neural network models were trained on data extracted from the SciGlass database to predict glass viscosity as a function of the glass composition and temperature. The data set is divided into training and testing sets. The training set is used to train the model and determine the model parameters to best fit the data. The testing set data is never seen by the algorithm during model training and instead enables evaluation of the model performance by testing how well the model can generalize, i.e., make predictions for inputs it was not trained on. The training and testing sets were split based on individual glass compositions rather than individual viscosity data points to ensure that the learned model can generalize to previously unknown compositions. Hyperparameters such as the number of model layers and number of neurons in each layer were varied and the resulting accuracy assessed to identify what combinations of hyperparameters (and corresponding model complexity) would enable the model to learn a good fit for the data. A traditional regression model from the literature [3], also developed using viscosity data from the SciGlass database, was used as a benchmark for the machine learning model. The Fluegel model is provided as a spreadsheet [4]. It fits the composition dependence of viscosity using three polynomial functions of the mole fractions of 54 glass components and interpolates between these polynomial relationships based on the temperature-dependence defined by the Vogel-Fulcher-Tammann equation [3]. The Fluegel model spreadsheet contains a large number of constraints on allowable compositions; these model limits were taken into account when comparing the performance of the models.

Accomplishments

- Developed custom parsing code to extract and transform the data from the SciGlass database from a difficult-to-use and poorly documented format to an open-source format allowing for straightforward querying and filtering of the data.
- A publication and code repository are being developed to document the data parsing and new data format to make this data readily usable for future research.
- Performed training of machine learning algorithms, demonstrating potential for improved accuracy in predicting glass viscosity as a function of composition and temperature over a traditional linear regression model developed using data from the same database. **Figure 1** shows a comparison of the root mean squared error (RMSE) of machine learning (MLP) and traditional (Fluegel) model predictions of

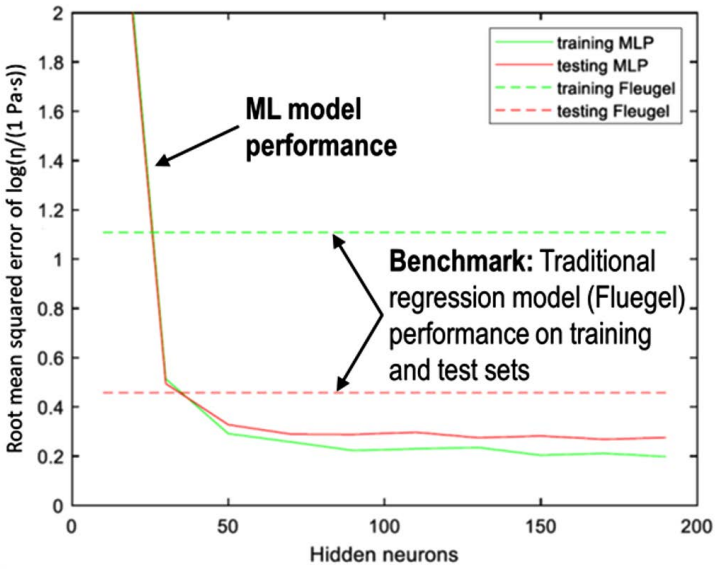

Figure 1: Comparison of root mean squared error (RMSE) of model predictions for the machine learning model (solid curves) and a traditional regression model from the literature [3] (values marked with dashed lines) on training and testing sets taken from 332 glass compositions meeting the Fluegel model's composition limitations. ML prediction error drops below that of benchmark model as number of neurons increases.

logη(η), where η is the viscosity in Pa·s. The training and testing data sets were split from a set of 332 glasses within the composition limits for the Fluegel model and believed to be part of the data set it was developed on. For models with at least 50 hidden neurons, the machine learning model outperformed the Fluegel model on both training and testing sets. The similar accuracies for the training and testing sets indicates that the model was able to generalize to new compositions.

Contributing Postdoctoral Researcher

Eric Hoar

Contributing Student Researchers

Charles Daniels Joseph Cammarata

References

1. Mauro. "Grand challenges in glass science." Frontiers in Materials 1(20), pp. 1-5 (2014).
2. De Guire, et al. "Data-driven glass/ceramic science research: Insights from the glass and ceramic and data science/informatics communities". J. Am. Ceram. Soc. 102, pp. 6385–6406 (2019).
3. Fluegel. "Glass viscosity calculation based on a global statistical modelling approach." Glass Technology-European Journal of Glass Science and Technology Part A 48.1, pp. 13-30 (2007).
4. https://glassproperties.com/viscosity/#_edn2, accessed 9/2/2021.

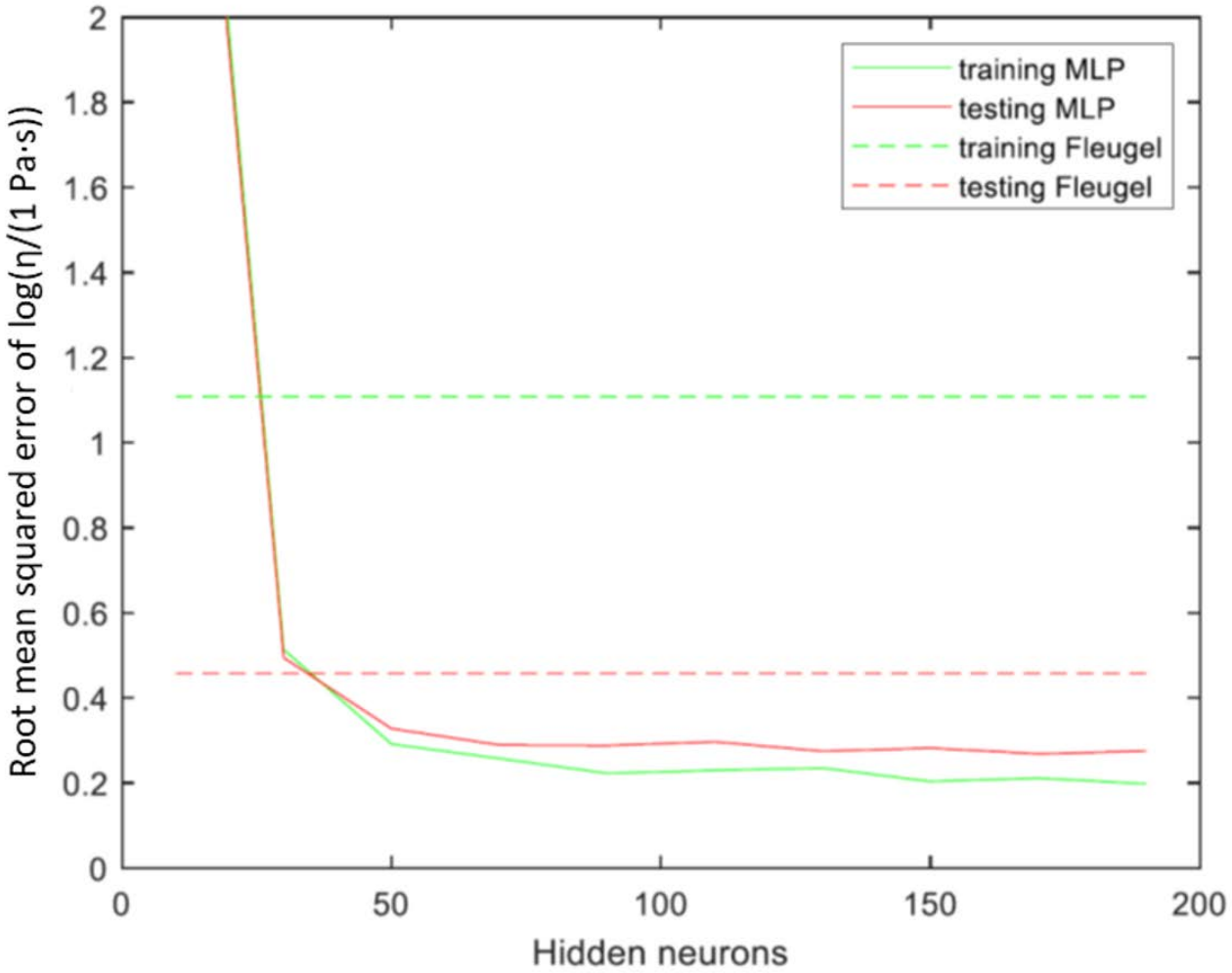

Figure 2: Comparison of root mean squared error (RMSE) of model predictions for the machine learning model (solid curves) and a traditional regression model from the literature [3] (values marked with dashed lines) on training and testing sets taken from 332 glass compositions meeting the Fluegel model's composition limitations.

Molecular Radiation Resistance Markers in Microorganisms

Brady Lee

Project Highlight

Research will help with understanding of microbiological response mechanisms to radiation resistance and associated genetic loci for response to radiation in individual prokaryotes and microbial communities. Identification of important genetic determinants will allow for development biosensors for application for nonproliferation, environmental and medical purposes.

Project Team

Principal Investigator Brady Lee

Team Members
Robin Brigmon
Samantha Waters
Stephanie Jacobs

External Collaborators
Linda DeVeaux
Hannah Lambertson
Katheryn Perea
Katherine Persinger
(New Mexico Institute of Mining and Technology)

Abstract

Radiation resistance is a trait common across all domains of life, yet molecular resistance mechanisms are not well understood. The objective of the proposed work is to understand how expression of single-stranded deoxyribonucleic acid binding proteins are central to radiation resistance. Expression of Single-stranded deoxyribonucleic acid binding proteins in a highly-radiation resistant microorganism is hypothesized to be a model of radiation resistance across the three domains of life. Expression of these proteins will be analyzed on environmental samples from chronic and acute radiation environments. Research will compare mechanisms/markers of radiation resistance in a microbe able to survive high levels of radiation, to similar marker in environmental samples following acute or chronic radiation exposure. This approach is one of the first efforts to assign a radiation resistance mechanism across all domains of life. Signatures that are part of this mechanism are important to the Department of Energy because the information can then be used as a signature for radiation biology, non-proliferation, and preventing corrosion in nuclear storage environments.

Objectives

- Identify microbiological response mechanisms to radiation resistance and associated genetic loci for response to radiation in individual prokaryotes and microbial communities.

Introduction

Prokaryotic organisms (bacteria) have been found in very high radiation areas, waste tanks and basins, where ɣ-radiation dose rates are 100 Gy h^{-1}. Populations found in these areas appeared to be thriving and tolerant to dose rates as high as 3.5 kGy[1]. Biofilms, a consortium of microbes of either a single species or a mixture of species, have also been found adhered to spent nuclear fuel rods in cooling/holding pools [2] as well as isolated in contaminated vadose sediments near high-level waste tanks[3]. Many of these resistant bacteria were found to be gram-positive. The plume contained high concentrations of alkali, nitrate, aluminate, Cr (VI), ^{137}Cs, and ^{99}Tc. These organisms were found to be radiation resistant up to 20 kGy of gamma radiation and cells were high in G+C content. Radiation resistant bacteria have also been isolated from extreme environments including desert sands[4]. Overall, the ability of these microorganisms to thrive in high radiation areas is not well understood nor are its potential applications to understanding environmental implications, human cell cycle progression and repair mechanisms.

Repair of DNA damage caused by extreme radiation exposure requires concerted interaction of an array of proteins, including single-stranded DNA (ssDNA) and binding proteins (SSB/RPA). These proteins have been shown to play both a passive and active role in protecting DNA during replication and repair of damaged DNA. Homologs of SSB/RPA have been found in all three domains of life: Eubacteria, Archaea, and Eukarya. Homology of these proteins typically occurs in the oligonucleotide/oligosaccharide binding domain (OB-fold). We hypothesize that the transcription of DNA for these proteins, along with homology across the three domains of life, will represent a universal tool to understand radiation exposure and resistance in the environment. Further, expression of SSB in *H. salinarum*[5] will be used as a model to understand SSB expression in Eubacteria and Eukarya. As an example, SSB has been shown to be integral to both cell survival and extreme radiation resistance in Deinococcus radiodurans as well as *H. salinarum*[5].

Approach

Research for the project will be performed in two parallel tasks; 1) Presence of SSB/RPA signatures in metatranscriptomes of environmental samples under chronic and acute radiation exposure, and 2) Determination of biological relevance of transcriptional changes in *H. salinarum*[5] to allow assignment of functional roles in radiation resistance.

The objective of the research will be to identify similarities in general gene expression, and specifically expression of SSB/RPA in Eubacteria, Archaea and Eukarya caused by chronic and acute radiation exposure. We hypothesize that microbial communities from chronic radiation environments will show higher SSB/RPA expression than those from environments with low, or background levels of radiation. Likewise, exposure of microbial communities from background radiation environments will show increased SSB/RPA expression when exposed to radiation. These hypotheses will be proven using a metatranscriptomic response based on enrichment of mRNA from microbial communities from chronic radiation environments, as well as communities from samples before and after radiation exposure. Complementary DNA (cDNA) generated from the mRNA transcripts will then be sequenced using next generation sequencing techniques.

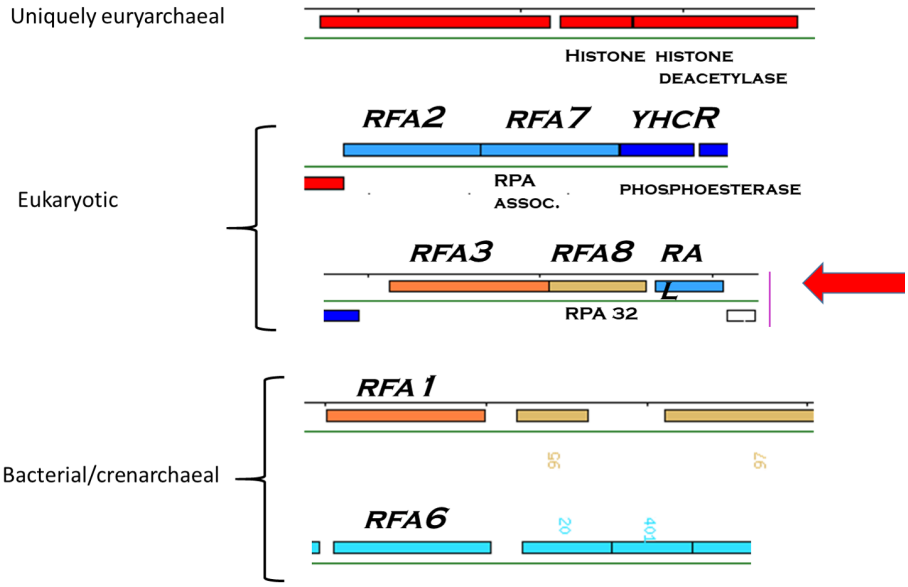

Figure 1: Halobacterium contains 5 Replication Protein A (RPA)/ DNA single-stranded binding protein (SSB) homologs.

Accomplishments

- Identification of potential radiation-resistance determinants in evolved strains of *Halobacterium* (**Figure 1**) *salinarum*
  - *ecp* gene which is annotated as surface glycoprotein (**Figure 2A**)
  - *erc* gene which is annotated as ATP-dependent RNA helicase homolog eIF-4A (**Figure 2B**)
  - *tnp1* gene – annotated as transposase (**Figure 2C**)
  - *vng41* gene – no annotation (**Figure 2C**)
  - *prtr1* gene – annotated as predicted transcriptional regulator (**Figure 2C**)
  - *arl1* gene – annotated as transcriptional regulator (**Figure 2C**)

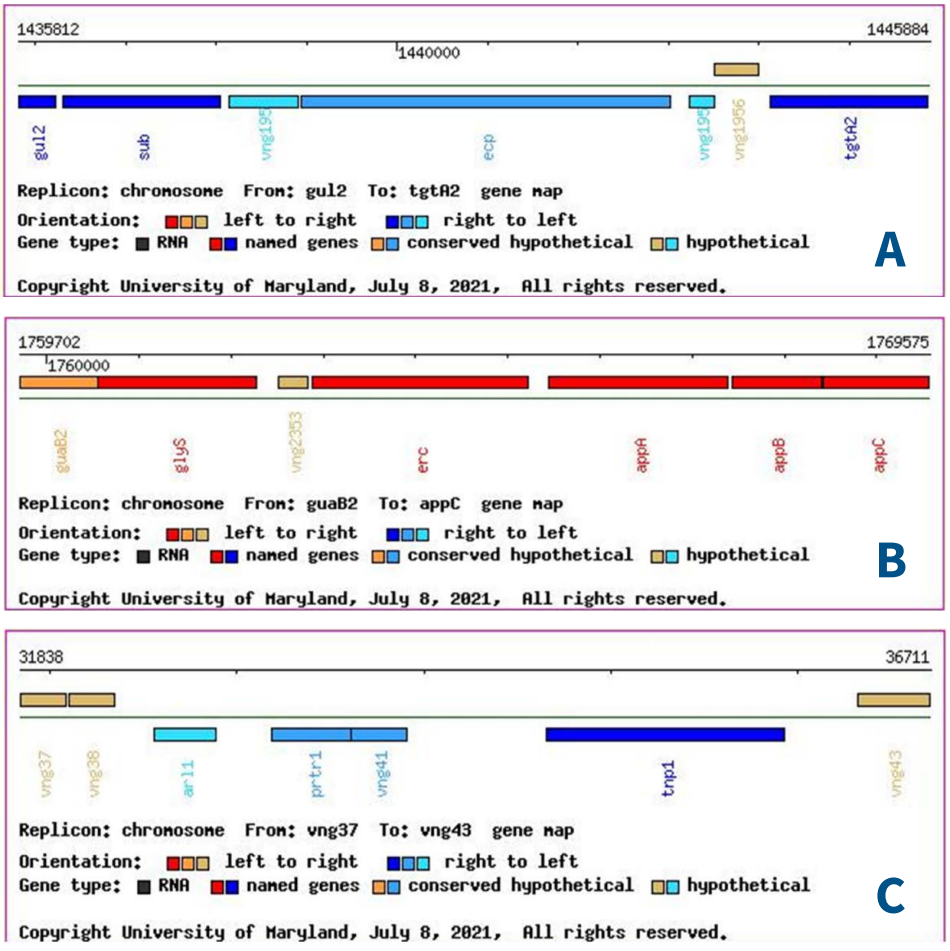

Figure 2: Genes in which SNPs were found in all 6 radiation-resistant Halobacterium genomes A) ecp gene; B) erc gene; C) tnp1, prtr1, vng41 and arl1 genes.

- Creation of deletion allele plasmids of ecp, erc, and vng41 genes for genomic replacement into parent strain NRC-1 (**Figure 3**)
- Isolation of genomic DNA from halophilic communities for species identification and subsequent SSB/RPA characterization
- Single stranded DNA binding proteins important in radiation resistance across all domains
  - Radiation resistance in fungi
  - Whole mouse models and radiation resistance in cancer cells
- Planned Gamma irradiation experiments at ORNL-HFIR (high dose, and SRNL Calibration Facility (low dose)
- L-Basin sample transfer planned:
  - Filters containing basin bioinorganic samples (**Figure 4**)
- Supported two new strategic hires for SRNL Biology Program
-

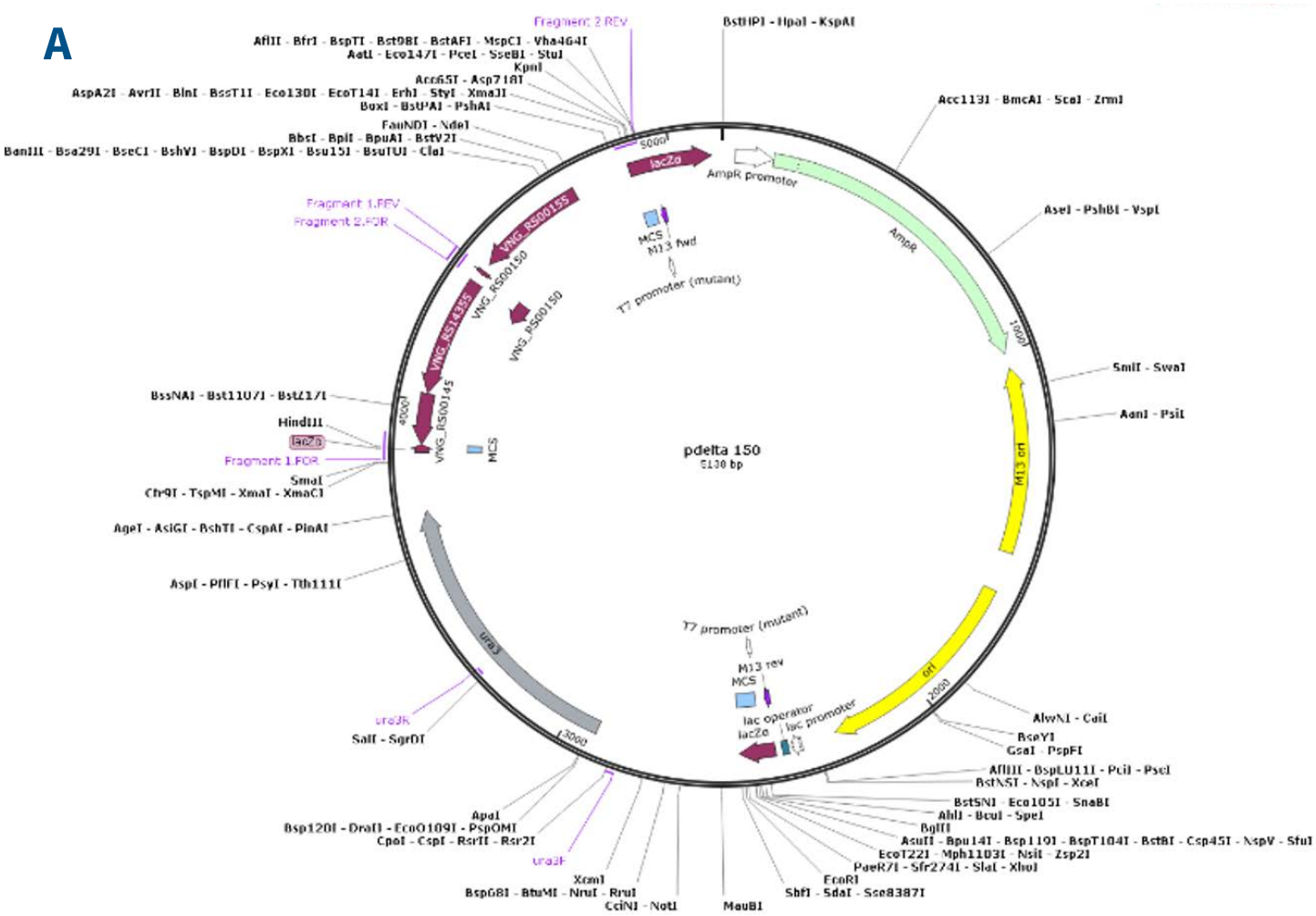

Figure 3: Restriction maps of constructed deletion allele plasmids. A. Deletion plasmid of gene prtr1. B. Deletion plasmid of gene erc. C Deletion plasmid of gene ecp. All deletion plasmids are constructed by combining approximately 500 bp of upstream and downstream sequences of the gene to be deleted into plasmid pMPK4081, which contains an E. coli origin and selectable marker (ampR), a Halobacterium selectable marker (ura3), but no Halobacterium origin of replication.

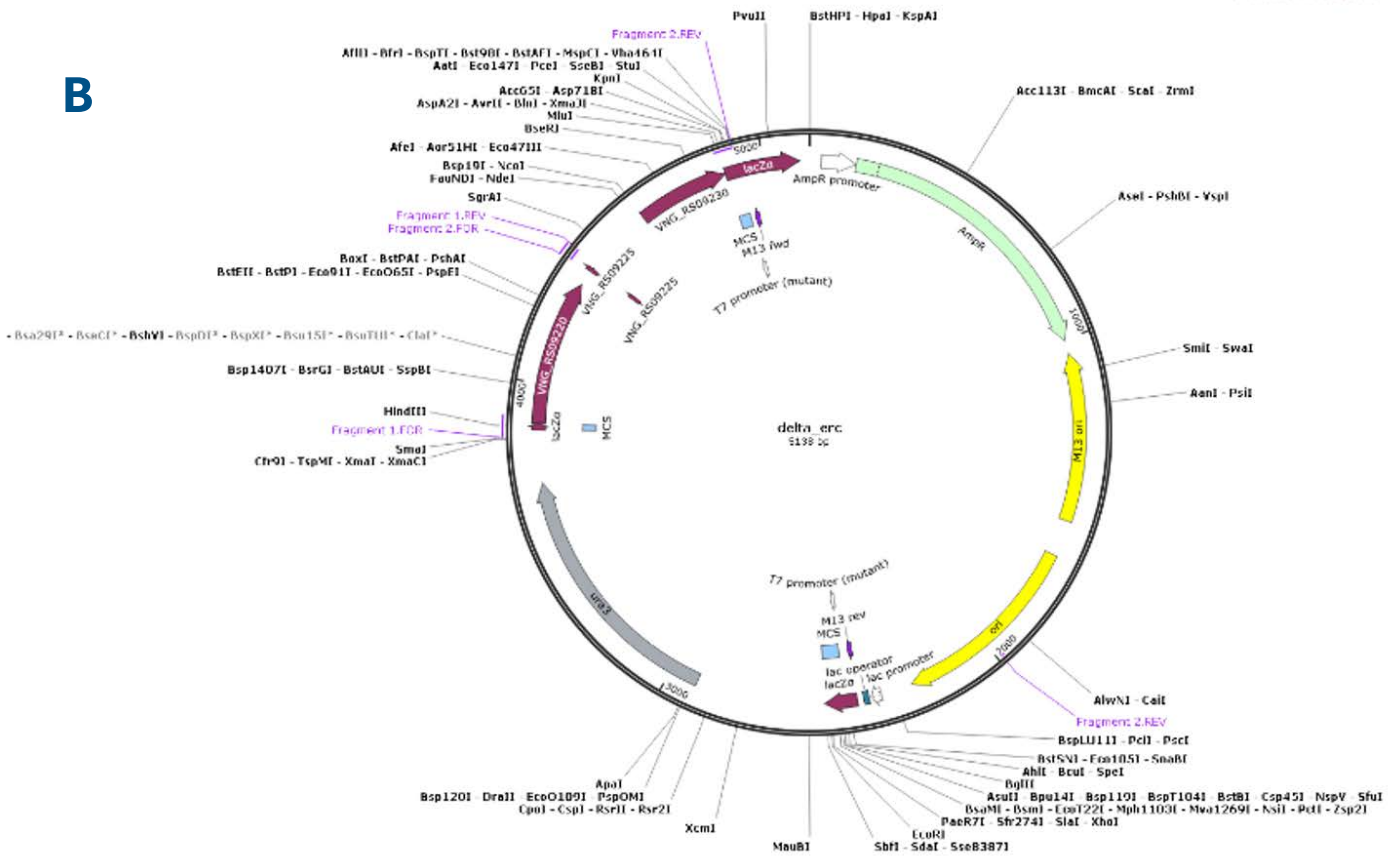
B
delta_erc
5138 bp
lacZα
AmpR promoter
AmpR
MCS
M13 fwd
T7 promoter (mutant)
VNG_RS09230
VNG_RS09225
M13 ori
ori
T7 promoter (mutant)
M13 rev
lac operator
lac promoter
Fragment 2.REV
Fragment 1.REV
Fragment 2.FOR
Fragment 1.FOR
PvuII
BstHPI - HpaI - KspAI
Acc113I - BmcAI - ScaI - ZrmI
AseI - PshBI - VspI
SmiI - SwaI
AanI - PsiI
AlwNI - CaiI
BspLU11I - PclI - PscI
BstSNI - Eco105I - SnaBI
AhlI - BcuI - SpeI
BglII
AsuII - Bpu14I - Bsp119I - BspT104I - BstBI - Csp45I - NspV - SfuI
BsaMI - BsmI - EcoT22I - Mph1103I - Mva1269I - NsiI - PctI - Zsp2I
PaeR7I - Sfr274I - SlaI - XhoI
EcoRI
SbfI - SdaI - Sse8387I
MauBI
XcmI
ApaI
Bsp120I - DraII - Eco0109I - PspOMI
CpoI - CspI - RsrII - Rsr2I
HindIII
SmaI
Cfr9I - TspMI - XmaI - XmaCI
Bsp1407I - BsrGI - BstAUI - SspBI
BstEII - BstPI - Eco91I - Eco065I - PspEI
BoxI - BstPAI - PshAI
SgrAI
Bsp19I - NcoI
FauNDI - NdeI
Afe1 - AorS1HI - Eco47III
AflII - BfrI - BspTI - Bst98I - BstAFI - MspCI - Vha464I
AatII - Eco147I - PceI - SseBI - StuI
KpnI
Acc65I - Asp718I
AspA2I - AvrII - BluI - XmaJI
MluI
BseRI

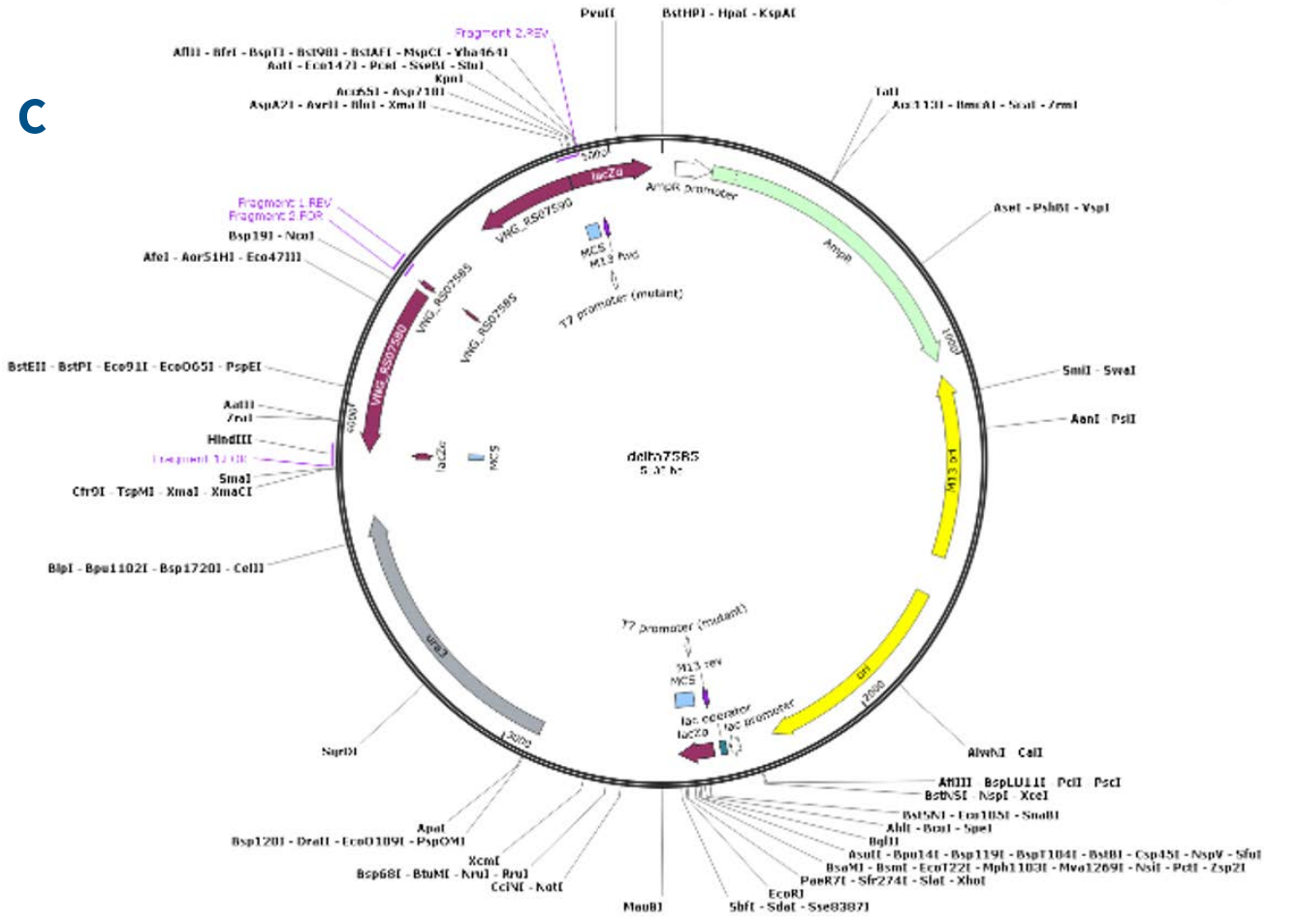
C
delta7585
lacZα
AmpR promoter
AmpR
MCS
M13 fwd
T7 promoter (mutant)
VNG_RS07590
VNG_RS07585
M13 ori
ori
T7 promoter (mutant)
M13 rev
lac operator
lac promoter
Fragment 2.REV
Fragment 1.REV
Fragment 2.FOR
PvuII
BstHPI - HpaI - KspAI
Acc113I - BmcAI - ScaI - ZrmI
AseI - PshBI - VspI
SmiI - SwaI
AanI - PsiI
AlwNI - CaiI
AflIII - BspLU11I - PclI - PscI
BstNSI - NspI - XceI
BstSNI - Eco105I - SnaBI
AhlI - BcuI - SpeI
BglII
AsuII - Bpu14I - Bsp119I - BspT104I - BstBI - Csp45I - NspV - SfuI
BsaMI - BsmI - EcoT22I - Mph1103I - Mva1269I - NsiI - PctI - Zsp2I
PaeR7I - Sfr274I - SlaI - XhoI
EcoRI
SbfI - SdaI - Sse8387I
MauBI
XcmI
ApaI
Bsp120I - DraII - Eco0109I - PspOMI
Bsp68I - BtuMI - KruI - RruI
CciNI - NotI
SgrDI
BlpI - Bpu1102I - Bsp1720I - CelII
HindIII
SmaI
Cfr9I - TspMI - XmaI - XmaCI
BstEII - BstPI - Eco91I - Eco065I - PspEI
AatII
ZraI
BglII
AflII - BfrI - BspTI - Bst98I - BstAFI - MspCI - Vha464I
AatII - Eco147I - PceI - SseBI - StuI
KpnI
Acc65I - Asp718I
AspA2I - AvrII - BluI - XmaJI

Contributing Postdoctoral Researcher

Alex Kugler

Total Number of Student Researchers

Katheryn Perea
Katherine Persinger
Olivia Berding
Hannah Lambertson
Benjamin Wilson

References

1. Robert W Phillips, Juergen Wiegel, Christopher J Berry, Carl Fliermans, Aaron D Peacock, David C White, and Lawrence J Shimkets, *Kineococcus radiotolerans* Sp. Nov., a Radiation-Resistant, Gram-Positive Bacterium', 52 (2002), 933-38.
2. M. I. Sarro, A. M. Garcia, and D. A. Moreno, 'Biofilm Formation in Spent Nuclear Fuel Pools and Bioremediation of Radioactive Water', *Int Microbio*l, 8 (2005), 223-30.
3. James K. Fredrickson, John M. Zachara, David L. Balkwill, David Kennedy, Shu-mei W. Li, Heather M. Kostandarithes, Michael J. Daly, Margaret F. Romine, and Fred J. Brockman, 'Geomicrobiology of High-Level Nuclear Waste-Contaminated Vadose Sediments at the Hanford Site, Washington State', 70 (2004), 4230-41.
4. F. A. Rainey, K. Ray, M. Ferreira, B. Z. Gatz, M. F. Nobre, D. Bagaley, B. A. Rash, M. J. Park, A. M. Earl, N. C. Shank, A. M. Small, M. C. Henk, J. R. Battista, P. Kampfer, and M. S. da Costa, 'Extensive Diversity of Ionizing-Radiation-Resistant Bacteria Recovered from Sonoran Desert Soil and Description of Nine New Species of the Genus *Deinococcus* Obtained from a Single Soil Sample', *Appl Environ Microbio*l, 71 (2005), 5225-35.
5. J. S. Lockhart, and L. C. DeVeaux, 'The Essential Role of the Deinococcus Radiodurans Ssb Gene in Cell Survival and Radiation Tolerance', PLoS One, 8 (2013), e71651.
6. Ronald F. Peck, Shiladitya DasSarma, and Mark P. Krebs, 'Homologous Gene Knockout in the Archaeon *Halobacterium Salinarum* with Ura3 as a Counterselectable Marker', *Molecular Microbiology*, 35 (2000), 667-76.

Figure 4: Filter units used to collect L-Basin samples.

Microbially Influenced Separation of Uranium Isotopes

Beth Lewczyk

Project Highlight

This project explores the use of microorganisms to separate uranium-236 from spent nuclear fuel through metal reduction processes.

Project Team

Principal Investigator Beth Lewczyk

Team Members
Robin Brigmon David DiPrete
Lisa Ward

External Collaborators Ken Czerwinski (UNLV)

Abstract

The US nuclear industry is on the cusp of significant growth in the areas of advanced reactors, SMRs, and microreactors. The existing commercial nuclear reactor fleet is considering expanding the life of the reactor cores by slightly increasing enrichment of their fuel. The common thread is the demand for High Assay Low Enriched Uranium (HALEU). A technical challenge exists with a blend down of Highly Enriched Uranium (HEU) from spent nuclear fuel (SNF) to meet the American Society for Testing and Materials (ASTM) and the "Y12" specifications. U-236 impacts reactor performance and is not desired in fresh fuel cores. In order to meet tight specifications, U-236 must be diluted by addition of fresh HEU. Fresh HEU is highly sought after and not plentiful in the US. A solution to this issue lies in the application of a technology to selectively remove the U-236 with non-hazardous microorganisms, which will be evaluated in this project by experimentally separating different isotopes of uranium.

Objectives

- Explore an alternate method of isotopic separation of uranium through microorganisms
- Use microorganisms with planned application to HALEU production by looking to remove U-236 from SNF

Introduction

Currently many studies of uranium isotopic separation focus on the separation of U-235/U-238 without taking into consideration U-236. By looking at separating U-236 there is added technical difficulty as U-236 is generally seen concentrating alongside U-235 and U-233 as well as U-234 and U-232. Additionally, U-236 is found only in SNF and reprocessed uranium, giving the Savannah River National Laboratory (SRNL) a unique opportunity to use its available reserve of materials to perform microbiological separations of U-236 from SNF.

The methods for uranium isotopic separation currently in place are not expected to have commercial availability until 2023-2024, while demands for HALEU expecting to reach almost 600 MT by 2030 as noted in a 2018 letter from the Nuclear Energy Institute (NEI) to Energy Secretary Perry. Having an additional method of HALEU production is imperative for SRNL as the electrochemical processing is only estimated to deliver approximately 5 MT of 19.75% U – 10Zr fuel by 2023, and by 2020 ZIRCEX is only at a ¼ scale facility, leaving a wide margin of need left unfulfilled. Currently, the H-Canyon processes SNF to eventually create a uranyl nitrate solution. If applied here, microorganisms in a bioreactor would be able to work with an already dissolved form of uranium to begin an isotopic separation and partially purify the uranyl nitrate from the U-236 poison. The utilization of microorganisms in order to separate uranium isotopes is a way to help alleviate the increasing need for HALEU production while advancing SRNL's potential in the field of microbial heavy metal reduction, by looking specifically at U-236, then applying the process to reactor fuel production.

Approach

In the first phase of the project, microorganisms have been cultured and media obtained and formulated for the metabolic needs of each microorganism to allow for the most optimal metal reduction environments. The microbial cultures have successfully been maintained such that live cells are always available for testing. Once the capabilities of these microorganisms are assessed in initial trials of uranium metal reduction, the approach will be refined to observe the potential for isotopic separation of U-236 in SNF.

The second phase of the project includes the isotopic analysis of the media. It is expected based on previous evidence that the microorganisms will successfully reduce soluble uranium into an insoluble form, creating a precipitate. The precipitate should have a different concentration of uranium isotopes than in the original solution, therefore demonstrating a microbially influenced separation of uranium isotopes to be analyzed by Inductively Coupled Plasma Mass Spectrophotometry (ICP-MS).

Accomplishments

- Microorganisms with previously proven U235/ U238 separation have been procured. Additional microorganisms with uranium metal reduction capabilities have been procured for testing
- Microorganisms' viability in testing media has been established for a period of up to 7 days
- Metal reduction testing apparatus has been designed and installed
- Highly Enriched Uranium with the isotopes U-234, U-235, U-236 and U-238 has been procured for testing
- Specialized medium has been prepared for U biotransformations
- Hazard Analysis complete for FY22 isotopic separation experiments

Growth and Development of Quantum Materials

Utpal N. Roy

Project Highlight

The project focuses on the growth of single crystals and thin films that are expected to display non-trivial symmetry-protected topological order and allow for fabrication of mesoscale nanostructures and devices from the films using a SEM Focused Ion Beam (FIB) microscope. (**Figure 1** shows the crystal growth system).

Project Team

Principal Investigator Utpal N. Roy

Team Members

Robert Lascola
Henry Ajo
Patrick O'Rourke
Binod Rair

Abstract

Topological insulators (TIs) display a new state of quantum matter, which is broadly known as quantum materials. The TIs have a unique property of being an insulator as a bulk property and having conducting surface states, which are symmetry-protected Dirac Fermions and well isolated from the bulk valence and conduction bands. Ideally, these topological surface states and bulk electronic states should act independently. The degree to which they intermix depends on the crystalline quality, composition and defects present in the material. These materials thus demand very high-quality crystals to observe the desired quantum properties. We proposed growth of high-quality single crystals and thin films to enhance the ability to fabricate devices with unique performance attributes. Two separate approaches will be made to make the thin films, one is exfoliation of 2D monolayer from the grown single crystals and the second is thin films grown by pulsed laser deposition. Both techniques will subsequently allow for fabrication of meso structures using a Focused Ion Beam technique.

Objectives

- Growth of both n-and p-type topological insulators.
- Characterization of the crystals for their structural, electrical and magnetic properties.
- Growth of thin film by a pulsed laser deposition technique.
- Fabrication of p-n junction and meso structures using a focused ion beam technique.
- Use of machine learning to predict better understanding of the growth and synthesis of topological materials.

Introduction

TIs are narrow-gap insulators with the unique property of having conducting Dirac cone surface states, which are remarkably long lived "spin locked" and "symmetry-protected". At energies near the Fermi level (EF), the valence band and conduction bands take the shape of upper and lower halves of a conical surface called the Dirac cone, and the meeting point of the two cones is called the Dirac point. Here, massless charge carriers called Dirac Fermions are produced. These massless Fermions lead to quantum effects with very high carrier mobilities.

Figure 1: Crystal growth station installed at SRNL facility.

In topological insulating materials experimental realization of such Dirac Fermions has been achieved, which makes TIs very attractive for future advanced devices including quantum computation. The critical criterion for selecting the near ideal topological material is the ability to tune the Dirac point while keeping the Fermi level within the bulk band gap.

The growth of TI single crystals was planned to start after completion of the crystal growth facility at SRNL. However, due to the unanticipated COVID-19 epidemic, the progress in establishing the crystal growth facility was severely impacted, causing a few milestones to be missed due to the lab-construction delay. The facility is now established, and growth of single crystalline quantum materials is underway.

Approach

To conduct the research effectively, a versatile crystal growth facility was established. Two units of crystal growth stations have been installed. The furnaces were designed and fabricated by the vendor in accordance with this design. Each furnace has three-zone separately controlled heating elements incorporated into it. The three zones facilitate different temperature gradients as required for customized control of the temperature profile for growth of different material systems. The furnace can also be used for growth by the vertical Bridgman growth technique, physical vapor deposition (PVD), or traveling heater method (THM). The facility can grow up to three-inch diameter ingots weighing more than 2.5 kg. Figure 1 shows a typical unit for the crystal growth station.

Accomplishments

- Identified project logistics and path forward for synthesis and crystal growth.
- Identified prospective candidate materials to pursue crystal growth process.
- Designed/Developed/Established crystal growth facility.
- Procured all the raw materials and crucibles for performing crystal growth experiments.
- Two crystal growth furnaces/systems have been installed to grow TIs.
- Hazard analysis is complete.

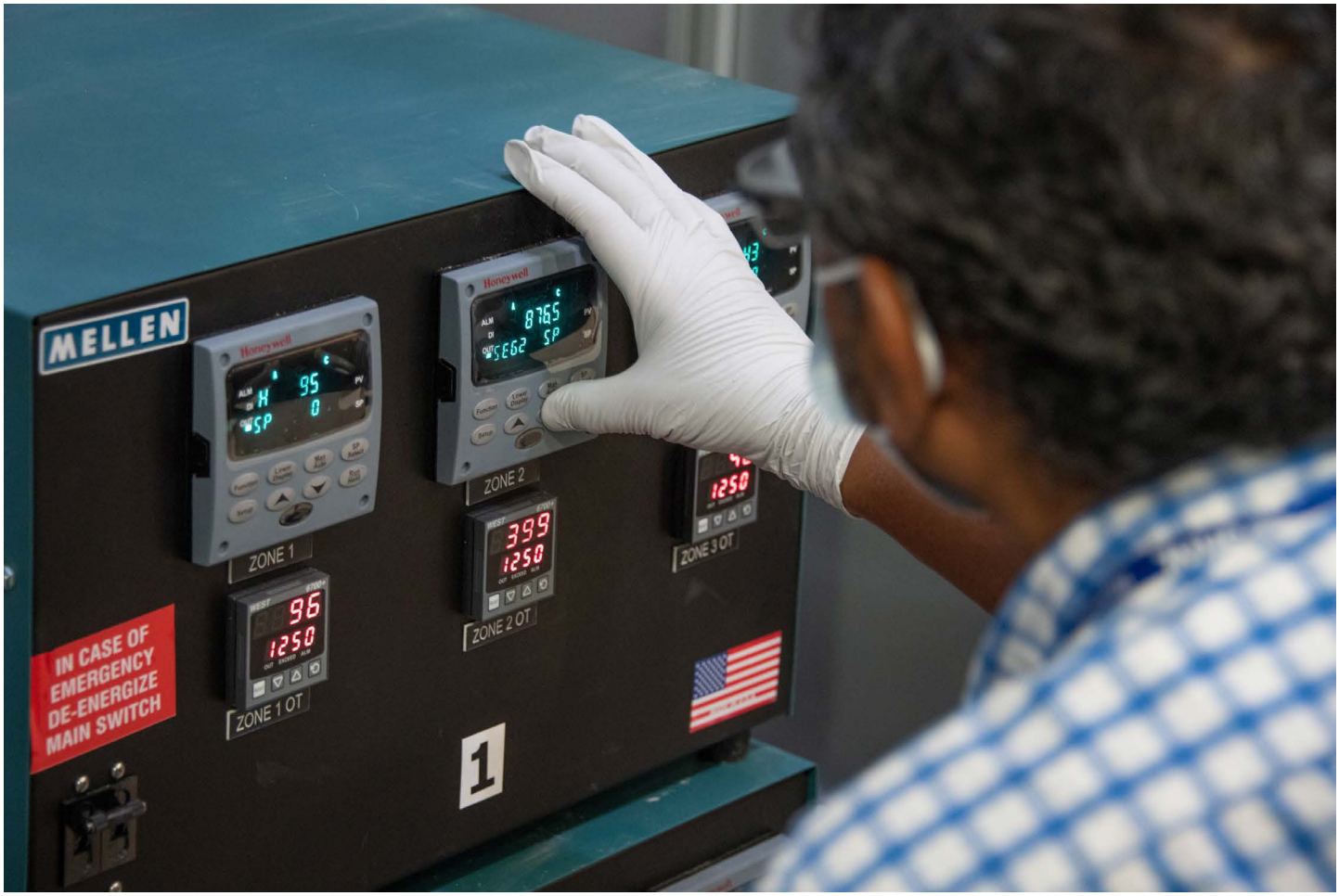

Molecular and Microstructural Bases for Understanding Microplastic Origin, Transport, and Fate

George Larsen

Project Highlight

The formation of micro and nanoplastics from parent plastics is one of the most challenging ecological threats since plastic pollution reaches even the most desolate places on earth and is expected to double by 2030. The goal of this project is to understand physico-chemical properties on microplastics formation, transport, and fate by analyzing the microplastics found in environmentally collected samples at Savannah River Site (SRS), supported by lab-based experiments.

Project Team

Principal Investigator *George Larsen*

Team Members

George Larsen
Wendy Kuhne
Eric Doman
Kimberly Price
Kaitlin Lawrence
Teresa Eddy
Shane Shull

Abstract

The formation of micro and nanoplastics from parent plastics is one of the most challenging ecological threats since plastic pollution reaches even the most desolate places on earth and is expected to double by 2030. The goal of this project is to understand physico-chemical properties on microplastics formation, transport, and fate by analyzing the microplastics found in environmentally collected samples at SRS, supported by lab-based experiments. An initial assessment found and identified microplastics and micronizing plastics in Fourmile Branch and the Savannah River. Fourmile Branch also carried trace-level radioactive contaminants associated with the Site's legacy missions, which may incorporate into entrained microplastics.

Objectives

- Set up process to collect and receive field samples from SRNS Environmental Monitoring Group
- Develop method for recovering and processing microplastics in SRNL based on established guidelines
- Begin assessing microplastic inventories in SRS waterways

Introduction

The ubiquitous use of plastics has led to one of the worst human created environmental disasters of our time, leading to millions of tons per year of plastic waste.[2] Plastics generally are not biodegradable and accumulate in vast amounts in the environment, including the plastic island found off the coast of California that is composed of over 1.8 trillion pieces of plastic. As plastics break down, they form into micro and nanoplastics that are persistent in the environment, even reaching secluded environments such as polar regions and the deep ocean floor.[3] Microplastics are integrated into most water sources, making their way through the food chain. It is estimated that most Americans consume hundreds of thousands of microplastics annually through the standard diet.[4] There are significant unknowns regarding their impact on human and environmental health as well as in the source, transport, and fate of microplastics and nanoplastics.[5] In order to understand the fate and risk of such particles, there is a need to assess the relationships between polymer structural characteristics and the formation of smaller plastic particles in nature. There is also a need to develop markers and approaches to causally link micro- and nanoplastics found in different environmental compartments to their origin. The goal of this project is to understand physico-chemical properties on microplastics formation, transport, and fate by analyzing the microplastics found in environmentally collected samples at SRS and evaluating the biological materials study on different types of plastics. Further, laboratory-based studies have been employed to support field collection data.

Approach

Surface water samples were collected from Fourmile Branch at three locations (FM-2B, FM-A7, and FM-6) and an additional three locations along the Savannah River using plankton nets and grab samples (**Figure 1a**). Samples were collected through a collaboration with the SRS Environmental Monitoring Group. Sample processing followed the standard NOAA procedure, which includes sieving to remove large fractions (4000-2000 µm) and to analyze fractions <500 µm, followed by gravimetric separation. Initial analyses of selected micronizing samples were conducted and included identification using Fourier-transform infrared (FTIR) spectroscopy and microscopic imaging. Further gamma measurements were conducted and determined the presence of trace radioactive elements in the water matrix. samples were conducted and included identification using Fourier-transform infrared (FTIR) spectroscopy and microscopic imaging. Further gamma measurements were conducted and determined the presence of trace radioactive elements in the water matrix. samples were conducted and included identification using Fourier-transform infrared (FTIR) spectroscopy and microscopic imaging. Further gamma measurements were conducted and determined the presence of trace radioactive elements in the water matrix.

Results/Discussion

Initial processing and separation of the samples has been conducted and stored for future characterization. Micronizing plastic particles removed from the first sieving process were separated and identified using FTIR spectroscopy. The samples were identified as polypropylene and polyethylene (**Figure 1b**). Low level gamma counting was conducted on the water grab samples from Fourmile Branch, and Cs-137 and I-129 were clearly identified. Additional naturally occurring radioactive elements were detected above background levels. Further analyses are required to determine the uptake of these radioactive tracers in entrained plastic particles.

In order to better understand the degradation effects of microplastics, accelerated aging tests using UV light and X-rays were conducted on lab-derived polyamide microparticles. X-ray diffraction (XRD) data were obtained on polyamide before and after ultraviolet (UV) light exposure had similar spectra, with a slight decrease in the ratio between the (200) and (002) reflections (2θ=20 and 24 respectively) from 1.19 to 1.16. This may indicate a slight decrease in crystallinity with UV exposure but not significant (**Figure 2a**). To investigate the damage of the micro polyamide sample under higher powered light (X-rays) for accelerated ageing, the XRD of the polyamide was measured over time. As the results show, the ratio between the (100) and (110) reflections exponentially decreased

Figure 1(a): Plankton net deployed in a Savannah River sampling location.

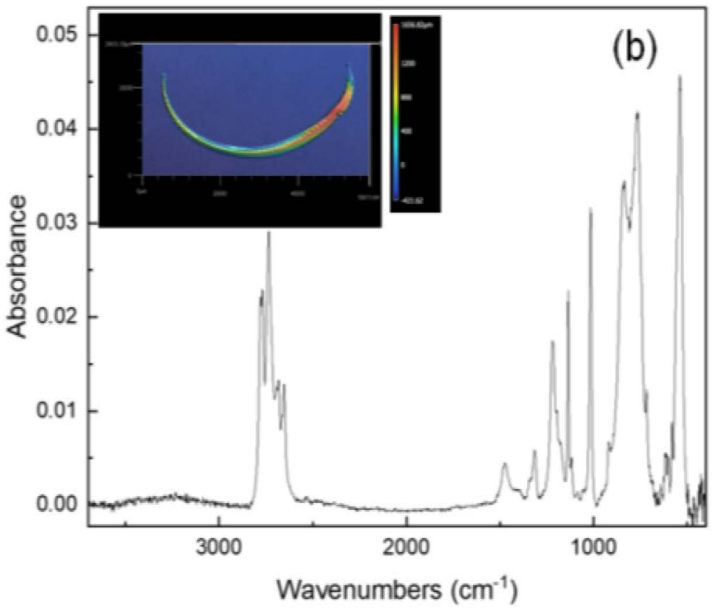

Figure 1(b): FTIR spectrum of polypropylene particle retrieved from plankton net; (Inset) macroscope height image of the retrieved polypropylene particle.

(**Figure 2b**). Over time, X-ray exposure led to a decrease in crystallinity for the polyamide sample (**Figure 2c**). This is consistent with previous results where long exposure to UV light caused a decrease in crystallinity as measured by glass transition temperatures.

FY21 Accomplishments

- Developed process to coordinate through SRNS Environmental Monitoring group to collect and deliver microplastic samples to SRNL
- Contacts have been made through other government agencies and at SRS to further develop collaboration and support programmatic growth
- Detected Cs-137 and I-129 in the water grab samples, which may be incorporated into any microplastics as well

Acronyms

FTIR — Fourier Transform Infrared Spectroscopy
NOAA — National Oceanic and Atmospheric Administration
UV — Ultraviolet
XRD — X-ray diffraction

Contributing Postdoctoral Researcher

Candace Langan

External Collaborator

SRS Environmental Monitoring Group

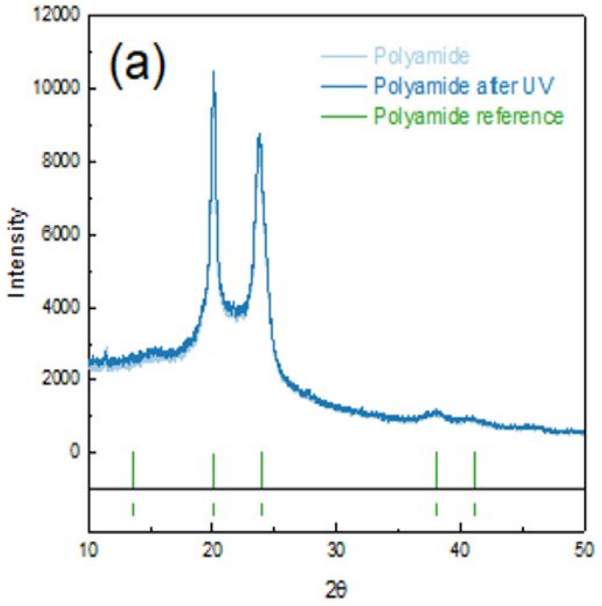

Figure 2(a): XRD spectra of polyamide (a) before and after UV exposure.

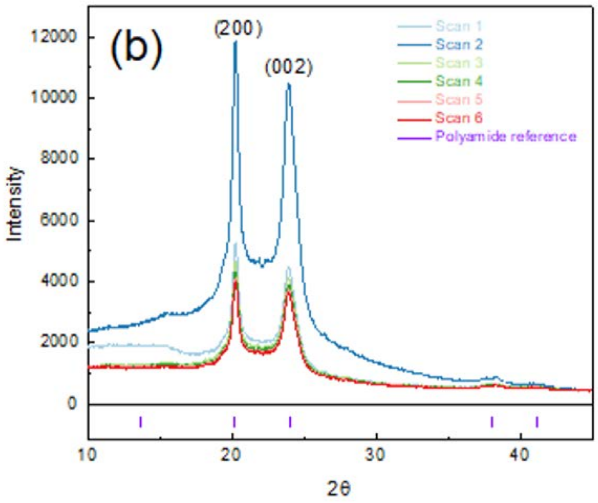

Figure 2(b): Before and after successive X-ray exposure.

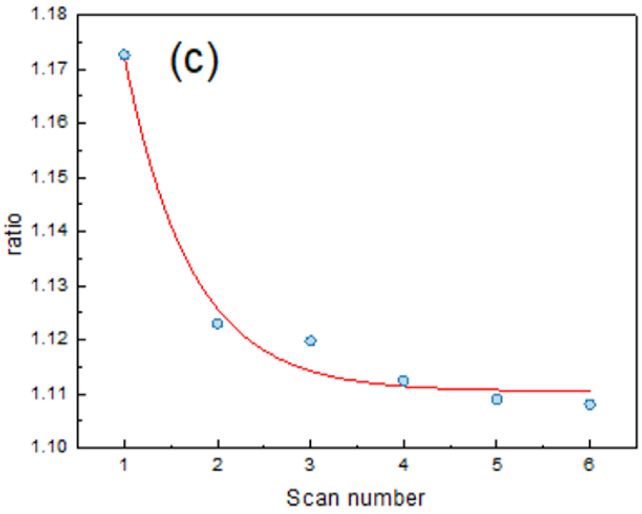

Figure 2(c): Change in (200)/(002) peak ratios with increased X-ray exposure.

Photon Entanglement Spectroscopy and Imaging in Actinide Research

Eliel Villa-Aleman

Project Highlight

This project aims to develop advanced imaging techniques by leveraging quantum entangled photons to provide a mechanism to provide imaging capabilities for applications in which other techniques are not applicable. A breadboard system to generate quantum entangled photons was constructed and used to demonstrate unique imaging capabilities.

Project Team

Principal Investigator Eliel Villa-Aleman

Team Members
Patrick Ward Don DeWayne Dick

Abstract

Quantumly entangled particles are capable of affecting the quantum state of their entangled counterpart instantaneously once one particle has changed. Herein, quantumly entangled photons are generated by spontaneous parametric down conversion through a temperature controlled non-linear crystals. This process generates two pairs of photons of lower energy of which the sum of energy equals the energy of the pump photons. These entangled photons can be separated and provide imaging capabilities by using one set of photons for imaging and the other set of photons for detection.

Introduction

Second order non-classical interference has been demonstrated previously with indistinguishable photon pairs. [1,2] The generation of photon pairs from a non-linear optic (signal and idler) by spontaneous parametric down conversion provides photons which can be separated based on their wavelength by dichroic mirrors. When idler photons are perfectly aligned with another set of idler photons generated in a second non-linear optic, the photons are now indistinguishable and therefore satisfy the indistinguishability requirement necessary for quantum interference. This allows for interference to be observed in the signal photons generated from the first non-linear optic and therefore imaging of an object from photons which have never actually physically interacted with that object. This methodology opens a multitude of possibilities for imaging solutions since the photons interacting with the object of interest do not need to be detected directly. Instead, their entangled photons can be observed to provide the image of the interest.

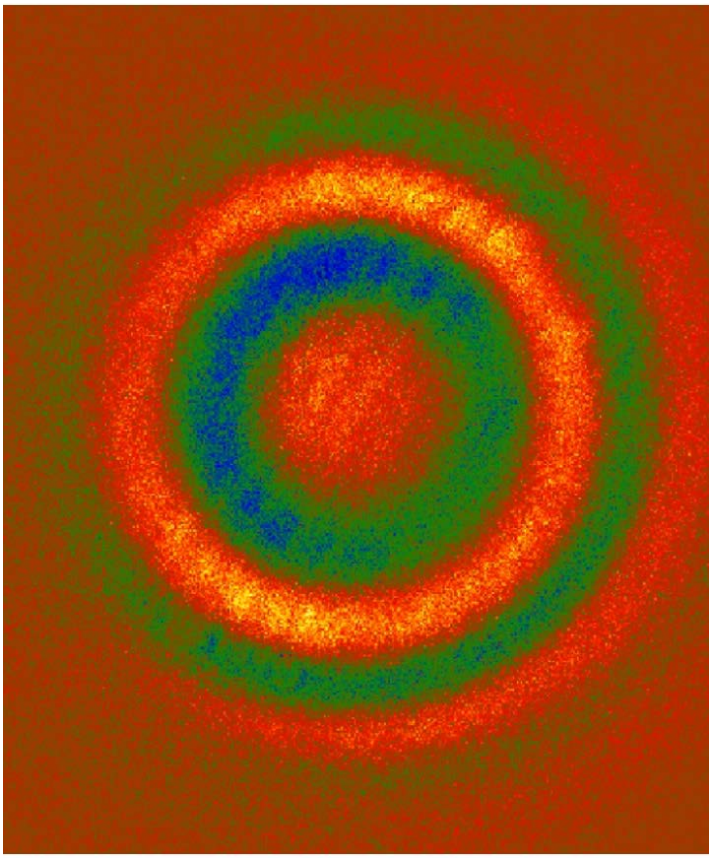

SRNL's first quantum image detected.

Inspired by recent illustrations of this ability to image using undetected photons [3,4], we have set out to develop our own breadboard quantum imaging system and advance the technique to provide application in practice.

Objectives

- Improve system stability (allows interference to be better observed)
- Optimize system alignment
- View quantum entanglement image of various slits (ultimately, this still needs further refinement)

Approach

A 532nm signal longitudinal mode (SLM) laser is used to generate quantum entangled photon pairs by spontaneous parametric down conversion in a pair of periodically poled potassium titanyl phosphate (ppKTP) crystals. A SLM laser and bandpass filters for the signal photons are used to significantly reduce the bandwidth of the beams and therefore increase the coherence length. A breadboard system was constructed to focus idler photons from the first non-linear optic onto the beam profile of idler photons generated from a second non-linear optic. The wavelengths generated from each non-linear optic were measured in a spectrometer and the temperature of the ppKTP (non-linear optic) adjusted to provide identical wavelengths for photon pairs generated from each non-linear optic. The idler photons from non-linear optic 1 were aligned to pass through an object of interest and the signal photons aligned with the signal photons from the second non-linear optic. The signal photons were then split in a 50:50 beamsplitter and half of the beam sent to a CCD detector for imaging and the other half dumped.

Accomplishments

- Breadboard quantum imaging system was modified to dampen vibrations that were preventing entangled image via interference pattern from being seen (see **Figure 1**).
- Verified the generation of entangled photons by observing a change of interference fringes while slightly varying the 1550nm light path.
- SRNL's first quantum image detected
- Taken the quantum image of slits with various sized openings (see **Figure 2**).
- Demonstrated a dynamic shift in interference patterns for gases with different indices of refraction.
- Setup an advanced quantum imaging system based on the literature that is simpler in design, requiring only one crystal, and allows for a larger sample/fiber optic cavity. In principle, this would allow for remote sensing much more readily than the first design.

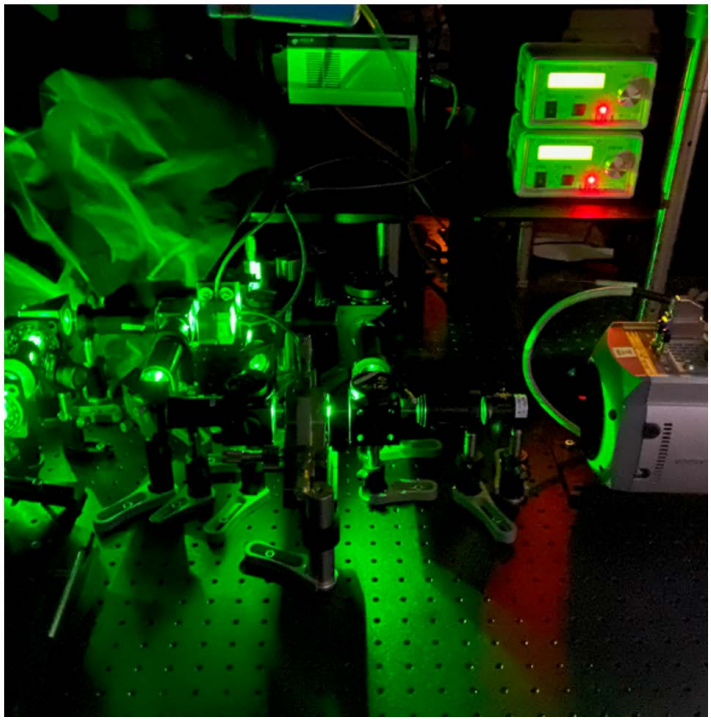

Figure 1: Image of breadboard system during operation.

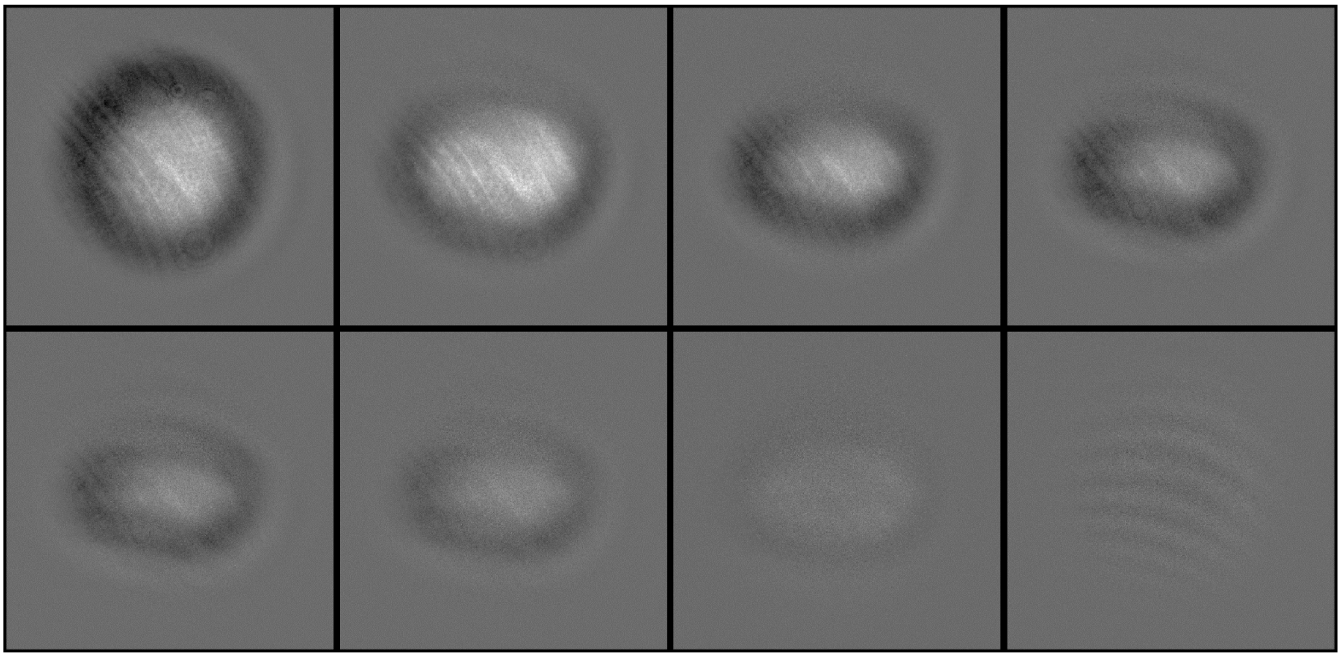

Figure 2: Quantum entangled image of 1550 nm passing through 8 different slits opening. As the narrowest slit opening visible is ~1 mm, this shows that the image resolution needs to be improved.

Contributing Postdoctoral Researcher

Don DeWayne Dick

References

1. Zou, X.Y.; Wang, L. J.; Mandel, L. Induced Coherence and Indistinguishability in Optical Interference. Phys. Rev. Lett., 1991, 67, (3), 318-321.
2. Wang, L. J.; Zou, X. Y.; Mandel, L. Induced Coherence without Induced Emission. Phys. Rev. A 1991, 44, (7), 4614-4622.
3. Lahiri, M.; Lapkiewicz, R.; Lemos, G. B.; Zeilinger, A. Theory of Quantum Imaging with Undetected Photons. Phys. Rev. A 2015, 92, 013832-1 - 1013832-8.
4. Lemos, G. B.; Borish, V.; Cole, G. D.; Ramelow, S.; Lapkiewicz, R.; Zeilinger, A. Quantum Imaging with Undetected Photons. Nature 2014, 512, 409-412.

Acronyms

CCD – Charge coupled device

ppKTP – periodically poled potassium titanyl phosphate

SLM – Single longitudinal mode

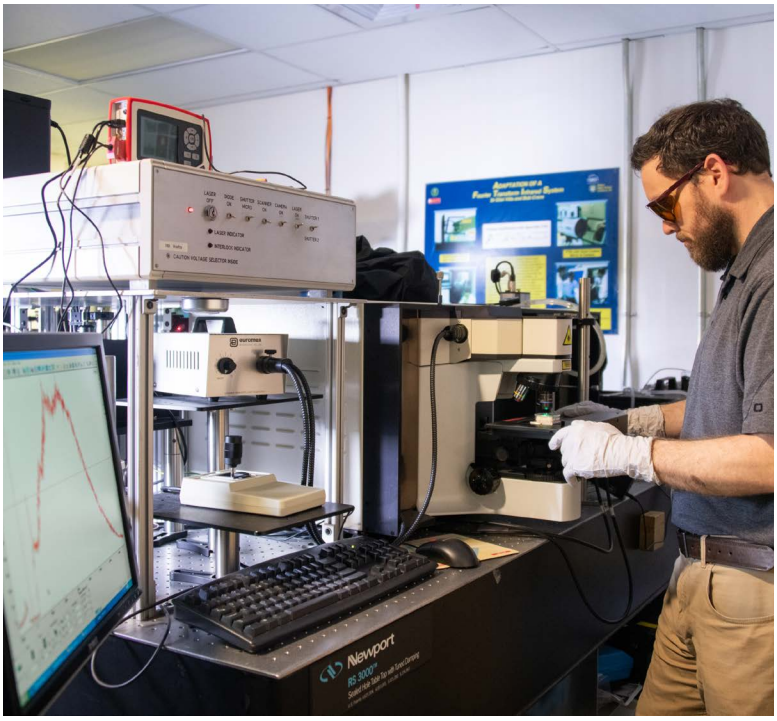

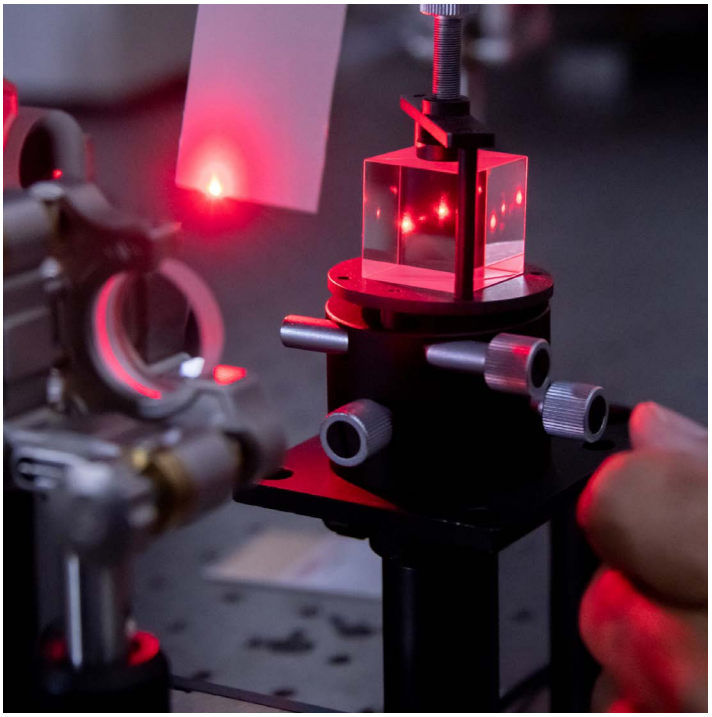

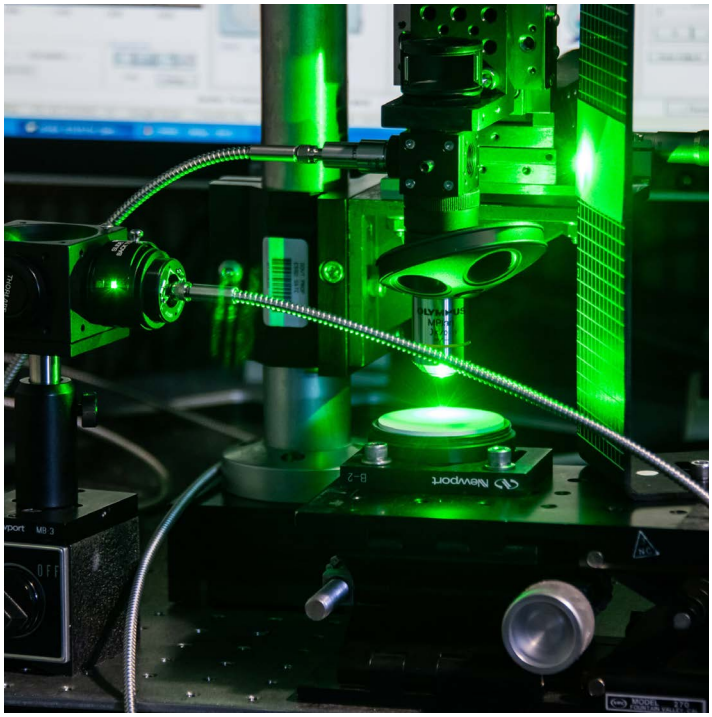

Reinforced Learning Feedbacks for reinforcement learning

Steve Xiao

Project Highlight

The use of Machine learning (ML) and artificial intelligence (AI) was investigated utilizing algorithms developed on a simple insect robot to determine the source of dropping gas pressures in the TCAP system. A deep neural network was utilized and trained to utilize the internal weights for identifying the cause of dropping pressures.

Project Team

Principal Investigator Steve Xiao

Team Members
Matthew Folsom Caleb Scott
Vincent Dinova

Abstract

Use of a deep neural network to determine the cause of an event is a unique method of determination. Determination is commonly executed through ML algorithms specifically regression-based ML or Bayesian networks. These methods limit the complexity of the systems that can be analyzed. The deep neural network methodology, though more complex and unpredictable, can allow for analysis of the system with orders of magnitude more complexity than previous methods.

Objectives

- Acquire TCAP data
- Develop software to sort TCAP events
- Create and train AI
- Retrieve and interpret results for analysis

Introduction

The TCAP system in SRNL utilizes a heating and cooling process to separate isotopes. The mini-TCAP development collects about 100 parameters every two seconds. As illustrated in **Figure 1**, the test system separates gas between two tanks (Feed/Recycle Tank1 and Feed/Recycle Tank2). Once a certain pressure is reached the system swaps the source and product tanks. This allows the system to continue testing with the same gas. Throughout this testing, the total pressure of these tanks (1+2) was dropping as shown in Figure 1. Eventually the pressure drops below the switching threshold and the system test is discontinued. The objective of this AI is to determine which input parameter affects the pressure of these tanks as shown in **Figure 2**.

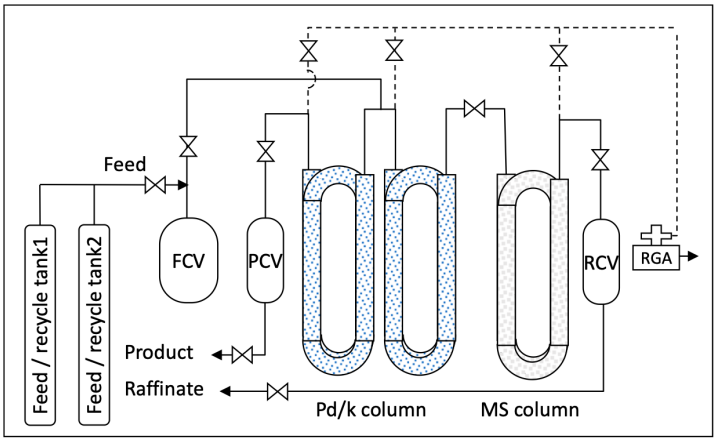

Figure 1: Gas Transfer between tanks (top) and total gas pressure dropping (bottom).

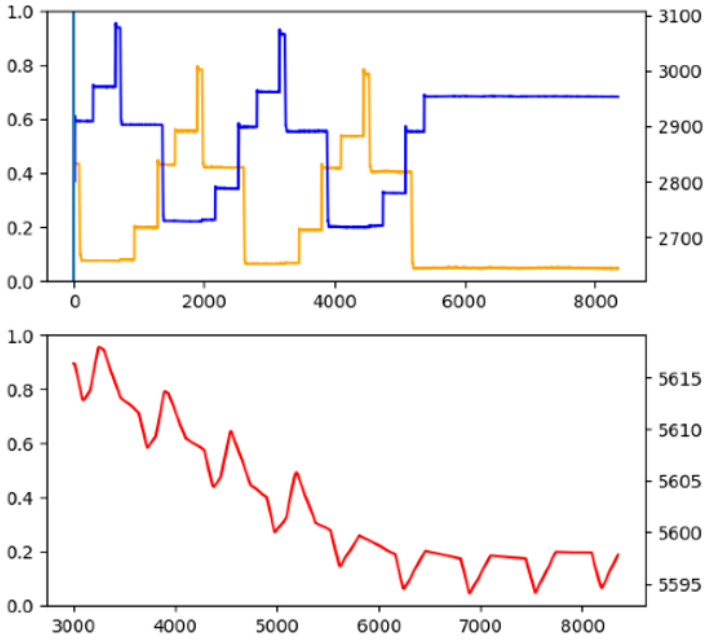

Figure 2: A simplified Schematic of mini-TCAP.

Approach

A deep neural network was chosen due to the complexity of the problem set. Most causal problems are solved with Bayesian networks or regressions-based ML. This is due to the simplicity of the algorithm's internals. A deep neural network was trained utilizing the methodology shown in **Figure 3**. The dataset and the weights of the first layer are stored. This process is completed multiple times with multiple loss functions. The weights of each parameter are then averaged to produce the result. This allows the network to train with multiple internal configurations. A library was created to allow quick changes to these parameters and utilize a custom acceptance algorithm for training. Utilization of the library follows the login in **Figure 4**.

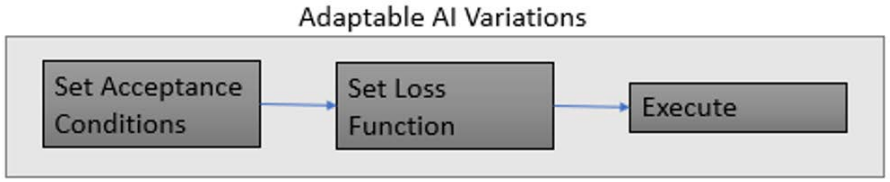

Figure 3: AI Training Methodology.

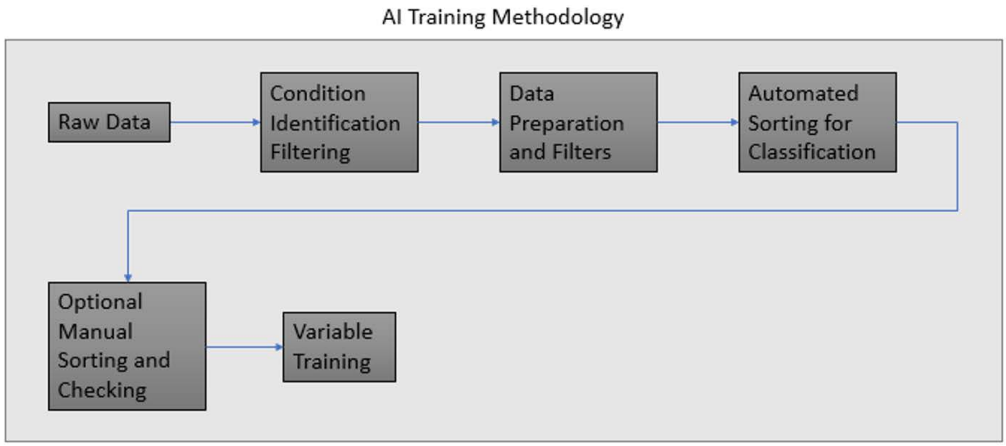

Figure 4: Custom AI Library Usage.

The results produced were valid. The selected parameter was the amount of gas transferred. This would be a valid result given the parameter set of interest. This does not indicate the exact problem. Given more time, the algorithms should be adjusted and executed with this parameter left out to determine a less obvious cause. However, the neural network approach of causation functioned with acceptable results as shown in **Figure 5**.

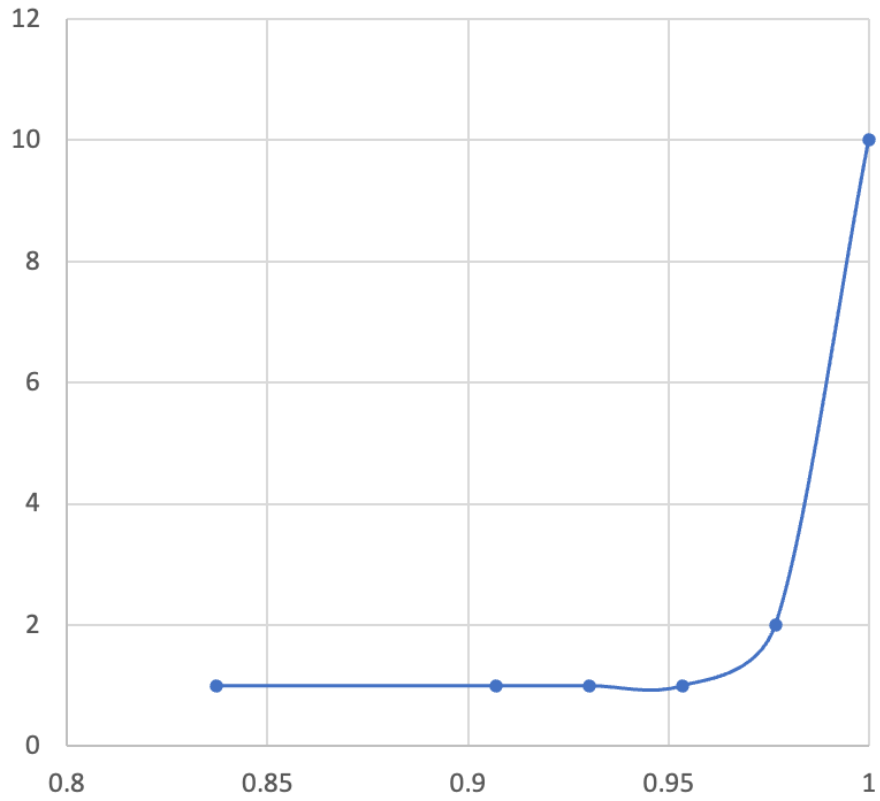

Figure 5: Distribution of amount of gas transferred parameter from multiple loss functions (value of one being the most influential parameter).

Accomplishments

- Acquired TCAP data
- Developed software to automatically sort TCAP events from multiple years of data
- Developed automated and with manual methods of verification to sort TCAP events in which gas pressure is dropping in the pattern of interest
- Developed neural network helper library for quick changes to the system
- Create neural network topology
- Trained neural network
- Retrieved and interpreted results for analysis

Contributing Postdoctoral Researcher

Vincent Dinova

Contributing Student Researchers

Henry Salgado
Henry Goff
Wesley Martin
Reva Fowler
Ashley Van Ausdale
Anna Hawcroft
Christopher Laborde

Acknowledgements

A. Boone Thompson provided TCAP raw data and some helpful discussions.

Characterization of Properties for a Gamma-Irradiated 'Revised' International Simple Glass

Charles L. Crawford

Project Highlight

Simulated high-level waste borosilicate glasses were irradiated with gamma dose to simulate in-situ radiation exposure and damage in the glass. After irradiation, several measurements of optical, physical and corrosion properties were determined to compare with the unirradiated glass

Project Team

Principal Investigator Charles L. Crawford

Team Members
Robert J. Lascola Katie A. Hill

External Collaborators
Jose Lugo Jimenez (Augusta University)

Abstract

Simplified surrogate high-level waste glasses from recent national and international testing were irradiated to gamma doses of 100 Mrad and 200 Mrad. Properties of the irradiated glass were measured for comparison to the pristine unirradiated glass. Glass transition temperatures as well as infrared and Raman spectroscopy measurements show no change in the irradiated glass. Short-term aqueous corrosion tests on the glass powders also indicate no measurable differences comparing the irradiated to pristine samples. Some corrosion differences were observed in the pristine glasses due to slight compositional changes. As expected from the observed radiation darkening of the glass, absorbance spectra of the irradiated glass with the pristine glass used as reference indicates a broad absorbance over the range of 400 to 700 nm that is centered around 550-600 nm.

Objectives

- Irradiate International Simple Glass (ISG) with SRNL Gamma Irradiator to nominal dose of 200 Mrad
- Irradiate 'revised' ISG glasses (ISG-1 and ISG-2) to nominal dose of 100 Mrad
- Compare measured properties of the unirradiated and irradiated glasses
- Measure optical properties with Raman spectroscopy and Photoluminescence (PL)
- Apply the American Society for Testing and Materials (ASTM) static powder glass leach test to measure corrosion properties of all glasses

Unirradiated 500-gram glass bar vs. irradiated bar: top view of bars (left) and unpolished cross sections (middle left & right); Revised ISG-1 plate glass (right). Ionizing radiation discolors the original dull lime-green hue of the ISG glass and the clear ISG-1 glass to a darkened color.

Introduction

Borosilicate glass has been adopted internationally for the treatment of nuclear waste with the object of long-term stabilization of the waste through vitrification [1,2]. Still, the effects of self-radiation through radioactive element decay over hundreds or even thousands of years on glass composition can only be modeled or simulated [3]. Accelerated tests considering worst-case scenarios are therefore useful for understanding glass behavior on the longer time scales in the interest of future generations. Accordingly, the object of the proposed research is to gain understanding of the effects of gamma radiation resulting from radioactive element decay on the physical properties of borosilicate glass for use in the vitrification process. To this aim, the well characterized glass system referred to as International Simple Glass (ISG) [4] agreed upon by the international community as representative glass will be employed. The ISG, a 6- component (Si, B, Na, Al, Ca, Zr) glass available at the Savannah River National Lab (SRNL), was originally subjected to a 100 Mrad dose via a Co-60 gamma irradiation and an additional 100 Mrad dose to attain a cumulative 200 Mrad dose. Revised ISG glasses were obtained that introduce minor chemical additives of La and Mg, and these glasses were also irradiated to a 100 Mrad dose.

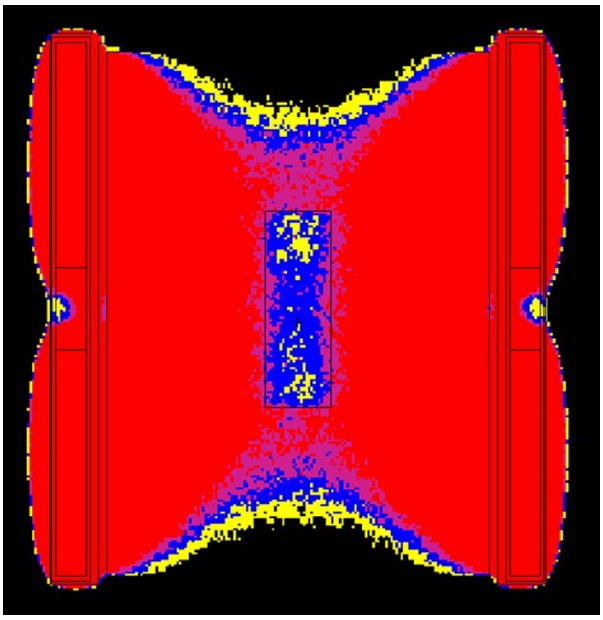

Figure 1:. Modeled dose rate to the central/vertical glass bar.

The effects of gamma rays on the ISG glasses were then studied by spectroscopic analysis methods, dilatometry/ calorimetry and corrosion, in comparison with the unirradiated reference. The primary methods included optical absorption, Raman spectroscopy, glass transition temperature and short-term corrosion performance. The research is expected to provide insights into the long-term effects of gamma radiation emitted during radioactive waste decay.

Approach

This study examined a 100 Mrad and 200 Mrad dose to the original ISG glass, as well as 100 Mrad doses to revised ISG glasses (ISG-1 and ISG-2). A 500-gram bar of the ISG was irradiated in the SRNL Co-60 gamma irradiator for a duration of 1,096 hr at a dose rate of ~ 9E+04 rad/hr to obtain a cumulative gamma dose of ~ 100 Mrad. A portion of the original ISG dosed glass was further irradiated to attain cumulative 200 Mrad dose. **Figure 1** shows the modeled dose rate from the Co-60 source to the central bar of glass. The colors shown in the central rectangle indicate expected dose rates of ~9.15E+04 rad/hr (yellow), 9.45E+04 rad/hr (blue) and 9.75E+04 rad/hr (purple). After irradiation exposure several 'slices' of the glass were cut/ polished by the SRNL Glass Shop using a wet diamond cut blade and manual polishing aids including Silicon Carbide (SiC), Cerium impregnated discs and 3-9 micron Al2O3 grinding sheets. Photographs of the ~ 800 grit and ~ 8,000 grit (clear) cross section slides from the unirradiated glass are shown in **Figure 2**. A comprehensive physico-chemical evaluation was carried out comparing the three pristine ISG specimens. The different characterizations performed were the following: XRD and vibrational spectroscopy (structural properties); static dissolution PCT (chemical durability); dilatometry and calorimetry measurements (thermal behavior); photoluminescence spectroscopy with decay kinetics assessment (optical properties). **Table 1** shows the chemical composition of the revised ISG-1 and ISG-2 glasses vs. the original ISG glass. Trace La was added into ISG-1 and Mg was substituted for some of the Ca in the ISG-2 glass.

Figure 2: Low (left) and high polish (right) unirradiated glass corrosion section specimens.

Accomplishments

- The original ISG glass that had been dosed to 100 Mrad in FY20 was further irradiated to achieve a cumulative 200 Mrad dose. Samples of the newer ISG-1 and ISG-2 glass plates were both dosed to 100 Mrad.

Oxide	ISG[a]		ISG-1[b]		ISG-2[b]	
	Target	Actual	Target	Actual	Target	Actual
SiO_2	56.2	56.30	56.2	56.38	56.54	56.87
B_2O_3	17.3	17.65	17.3	17.31	17.40	17.38
Al_2O_3	6.1	5.90	6.1	5.94	6.14	5.96
Na_2O	12.2	12.40	12.2	12.06	12.27	12.10
MgO	—	0.03	—	0.04	1.8	1.76
CaO	5.0	4.57	5.0	4.88	2.52	2.51
ZrO_2	3.3	3.20	3.3	3.29	3.32	3.31
La_2O_3	—	—	0.1	0.15	0.10	0.12
Density (g/cm^3)	2.516 ± 0.013		2.508 ± 0.001		2.475 ± 0.001	

[a] Impurity of note: Fe (equivalent to 0.065-0.068 mass% oxide)

[b] Impurities of note: Sn, Hf (0.05-0.09 mass% oxides)

Table 1: Compositions (mass%) of the various ISG Specimens.

- Corrosion testing (**Table 2**) indicates that the three pristine glasses (ISG, ISG-1 and ISG-2) display measurable differences in normalized release of B and Na. Similar comparisons amongst pristine vs. irradiated samples indicate no measurable differences in corrosion behavior.
- Raman spectroscopy (**Figures 3 – 5**) shows similarity in the three pristine glasses (ISG, ISG-1, ISG-2) as well as very similar spectra comparing the ISG to the 100 Mrad (ISG 1x) and 200 Mrad (ISG 2x). The 100 Mrad irradiated ISG-1 and ISG-2 also show similar Raman spectra to their pristine samples.

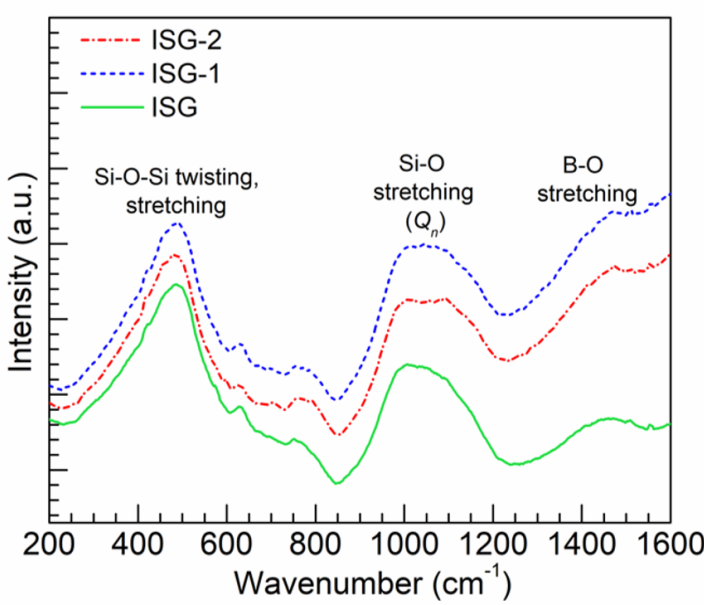

Figure 3: Raman Spectra obtained with 532 nm excitation for the various ISG samples.

Glass ID	NL B	NL Na	NL Si
ISG	2.4	2.3	0.5
St. Dev.	0.04	0.03	0.004
%RSD	1.7	1.3	0.8
ISG-1	2.2	1.9	0.5
St. Dev.	0.1	0.1	0.02
%RSD	4.4	3.9	4.8
ISG-2	4.3	3.2	0.4
St. Dev.	0.29	0.13	0.003
%RSD	7.3	4.3	0.7
ISG 100 Mrad	2.3	2.3	0.5
St. Dev.	0.06	0.08	0.007
%RSD	2.5	3.7	1.6
ISG 200 Mrad	2.5	2.1	0.5
St. Dev.	0.05	0.04	0.009
%RSD	2.3	2.1	1.9
ISG-1 100 Mrad	2.2	1.9	0.5
St. Dev.	0.02	0.01	0.003
%RSD	1.2	0.6	0.7
ISG-2 100 Mrad	4.2	3.2	0.4
St. Dev.	0.38	0.25	0.01
%RSD	9.9	8.5	2.7

Table 2: Corrosion test normalized concentration (g/L) results on pristine and irradiated glasses.

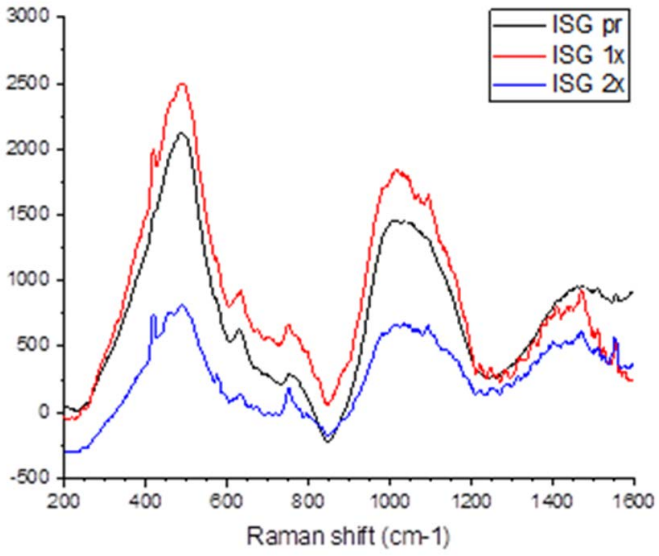

Figure 4: Raman Spectra of the original ISG and the 100 Mrad and 200 Mrad samples.

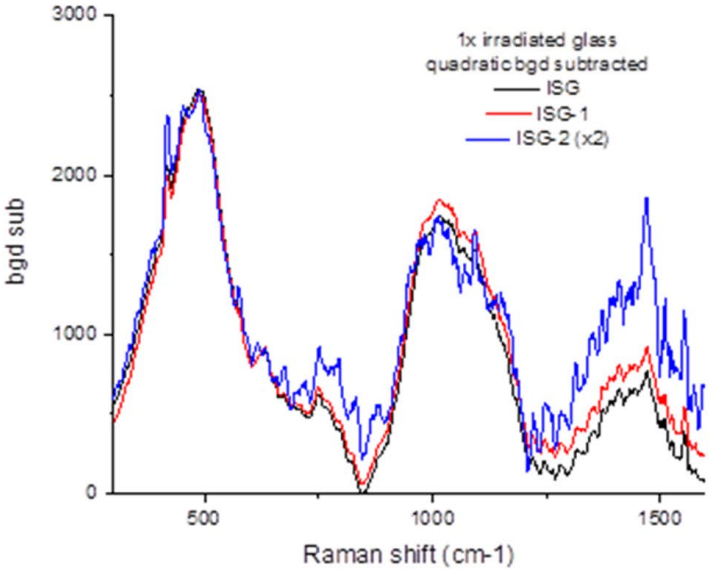

Figure 5: Raman Spectra of the pristine and irradiated ISG-1 and ISG-2 samples.

- Photoluminescence (PL) emission spectra (**Figures 6 – 9**) were collected for all glasses to enable comparison of the pristine glasses and the irradiated samples. PL spectra for the ISG and irradiated samples do not show new PL peaks. New PL peaks and peak shift were noted for the irradiated ISG-1 and ISG-2 glasses vs. the pristine samples.

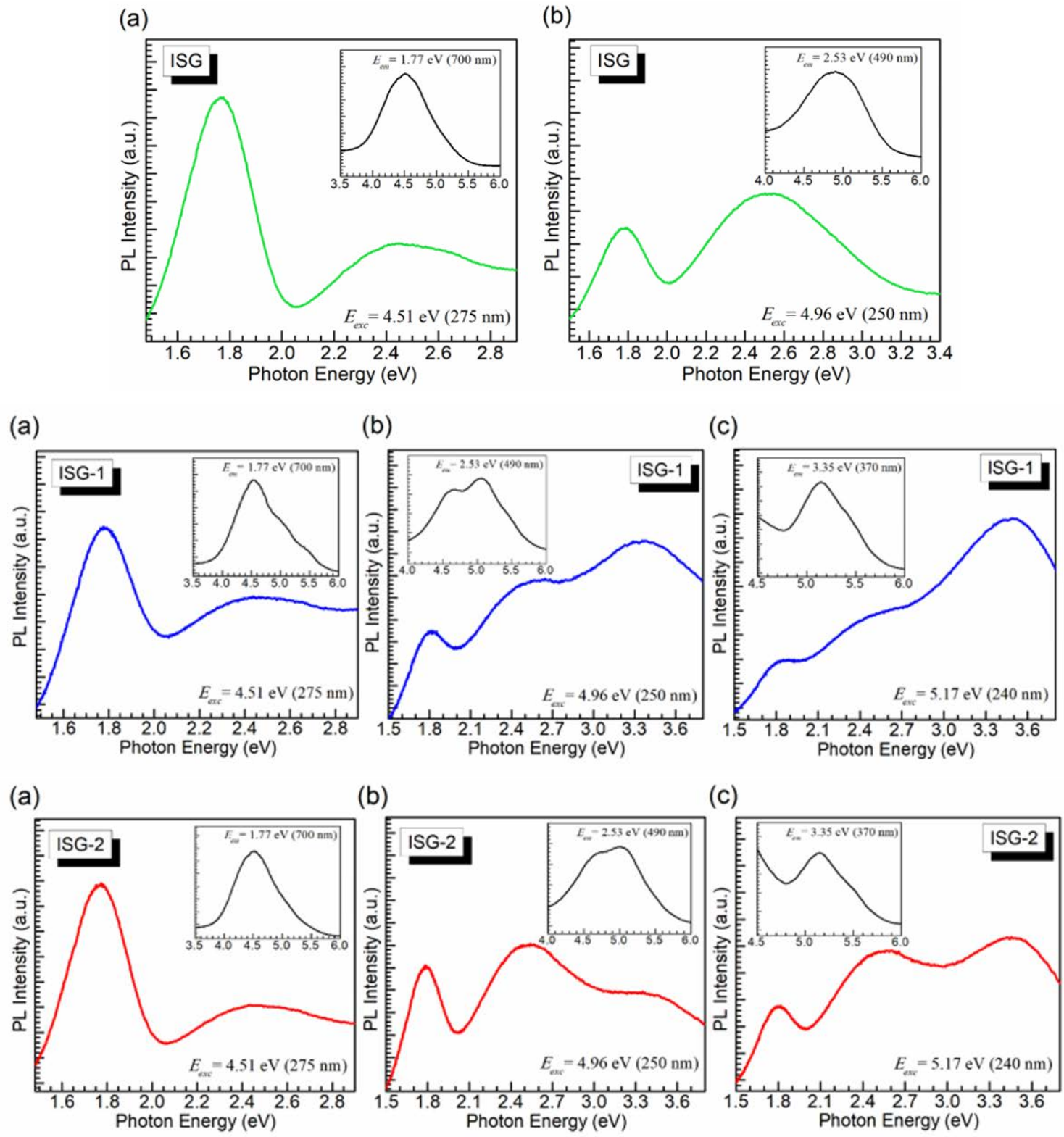

Figure 6: PL emission spectra obtained for the ISG (top), ISG-1 (middle) and ISG-2 (bottom)

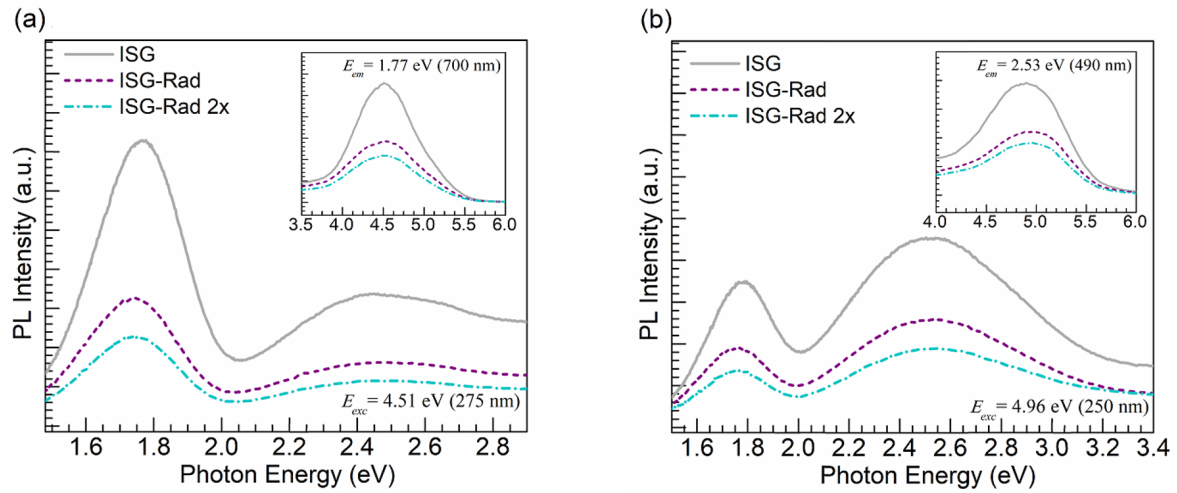

Figure 7: PL emission spectra obtained for ISG and irradiated (100 Mrad and 200 Mrad) samples. The irradiated ISG samples did not show any new luminescence.

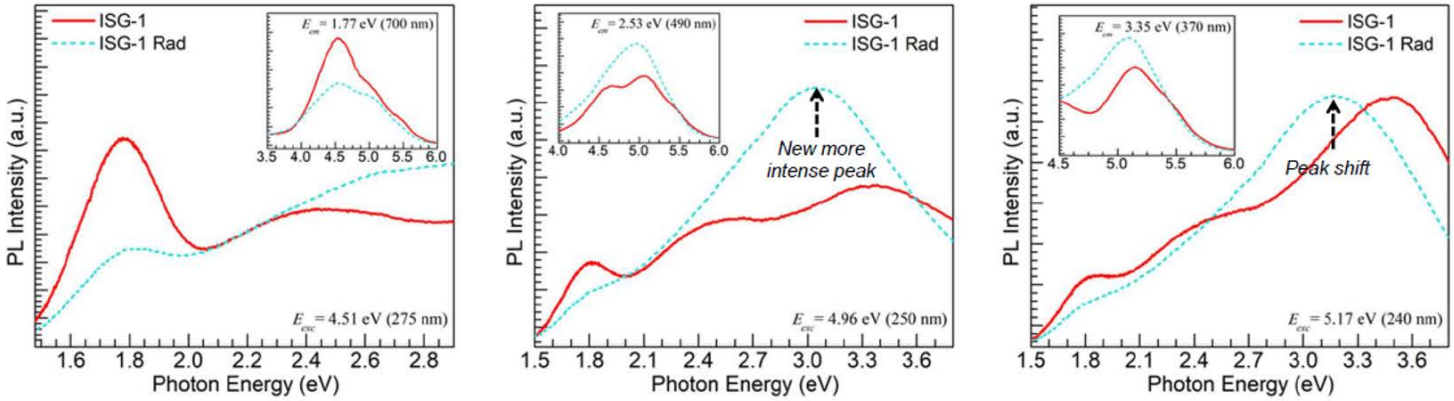

Figure 8: PL emission spectra obtained for ISG-1 and irradiated samples. A PL increase (middle spectra) and shift (right spectra) occurs for irradiated ISG-1.

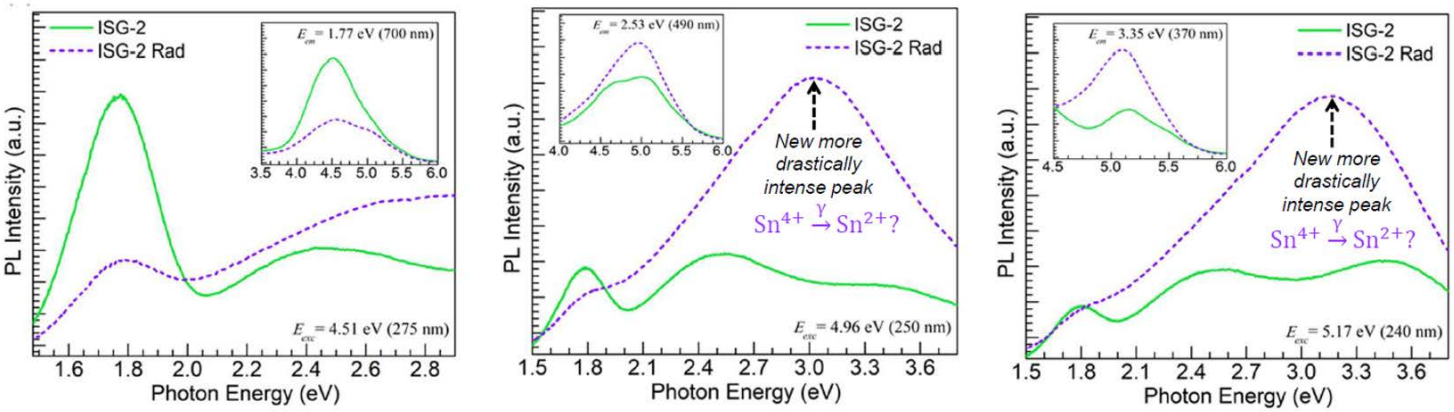

Figure 9: PL emission spectra obtained for ISG-2 and irradiated samples. New more intense PL observed for irradiated ISG-2 (middle & right spectra).

Corrosion Detection of Material Surfaces Using a Java-Based Software

Holly B. Flynn

Project Highlight

The main milestone of performing a proof of principal test was reached, by getting access to the data and extracting out significant features of a crack defect using the Java-based software, Fiji™ (ImageJ). The data was also used to programmatically identify the width of cracks by using Gaussian fits.

Project Team

Principal Investigator Holly B. Flynn

Team Members
Raymond G. Belliveau
Michael Martinez-Rodriquez

Abstract

Automation techniques for recognizing material defects are very common in fields like infrastructure survey and civil engineering; however, the defects are usually easily distinguishable from their background, on a larger scale (e.g. cement bridges), and very specific. Extracting information about a defect that is near or equal to the background of the data can be extremely difficult. Images with heavy background corrosion, pitting, cracking, and man-made defects (such as welding) makes extracting information on a specific defect near-impossible. This is especially true when the defect is on the micron level and the dynamic range of your image taking instrument is low. So, a simplified, Java-based Fiji™ (ImageJ) defect detection program, dependent on a 'flag' system, was proposed for data that has a micron level hairline crack that is near or equal to the background. The utilization of the built-in functions, plugins, and macro scripting capability of the Java-based software sends a series of flags to the user that help to identify if the surface contains a defect of interest and to characterize that defect.

Objectives

The main milestone was to perform a proof of principle test. This is demonstrated by:

- Extracting data (images) from the measurement instrument.
- Processing the images through the Java-based software and identifying the defect of choice (crack).
- Using the information from the Java-based software, Fiji™ (ImageJ), to process through Gaussian fitting routines and other processing techniques.

Introduction

Automation techniques for recognizing material defects are very common in fields like infrastructure survey and civil engineering; however, the defects are typically easily distinguishable from the background surface, occur on large structures, and due to the size of the defect can be imaged with a camera. In many of these cases the analysis approach is either computationally heavy such as a neural network or the feature extraction is overly complicated and very specific. It is proposed that a simple flag-based system using a macro program written in a Java-based software can identify the location of a crack and extract the relevant feature information for analysis and machine learning.

Cylindrical stainless-steel containers for radiological materials at the Savannah River Site become compromised over time due to extensive radiation exposure. The containers consist of a cylindrical body and welded lid, and in preparation for study are cut into sections. Individual sections are imaged using a laser confocal microscope (LCM). Due to the curvature of the container the LCM is used to 'flatten' the images for analysis and defect detection. The areas of interest are also nearest the lid weld location, which has been indicated as the region most likely to develop cracks. The cracks are typically only a few microns wide. Due to the small size of the cracks and the curvature of the containers, the LCM is a great instrument for extracting data; however, the LCM takes a very long time to image the samples and often produces sample images with low dynamic range. In combination with the problems due to the welding defects, corrosion, and pitting that has also occurred during the radiation and heat exposure, the crack is often difficult to differentiate from the rest of the sample surface.

A simplified, Java-based Fiji™ (ImageJ) defect detection program, dependent on a 'flag' system was proposed. The utilization of the built-in functions, plugins, and macro scripting capability of the Java-based software (ImageJ) sends a series of flags to the user that help to identify if the surface contains a defect of interest. Further analysis and examination of the region can be had through x, y location estimation and Gaussian fits. This contributes a less-computationally heavy way of extracting out features from an image that can be used as is or can be further used in supervised learning.

Approach

The image analysis process is based on identifying flags that tell the user and the program that a defect has potentially been identified. The more flags that are weighted the higher the probability that a defect has been found amongst the background noise. The flags are based on key facts about what a specific defect is. For the purpose of this study, the defect of interest is a crack, defined as an object that ideally has the lowest intensity in its local area, has a high directionality, can be reduced to a single thread or skeleton, and has a distinguishable Gaussian-shaped profile.

Accomplishments

- An in-house written stitching routine was built to extract the data from the VK4 files that the laser confocal microscope generates. This stitching routine is demonstrated by three steps in **Figure 1**.
- A flag-based system was proposed and performed on the images. This approach is a simpler, less computationally intense approach to defect detection especially in low-dynamic range, noisy images.
- **Figure 2** includes images of two separate cracks with varying levels of background noise. The x, y locations determined by the flag-based system are drawn on each image as small squares. The images show that the estimated x, y locations determined to be the crack center by the flag-based system is a very good estimate.

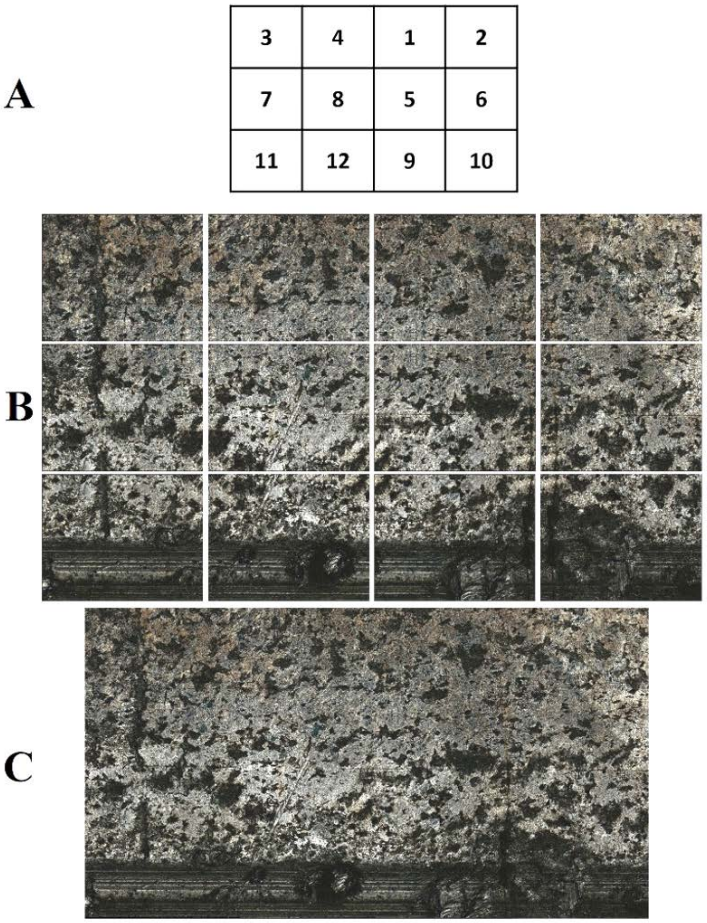

Figure 1: A: Map of the relative locations of each image based on the filename convention. B: Twelve optical-intensity images that cover a region of interest. Each image overlaps partially with the adjacent images. C: Result of the stitching routine on the twelve images in B.

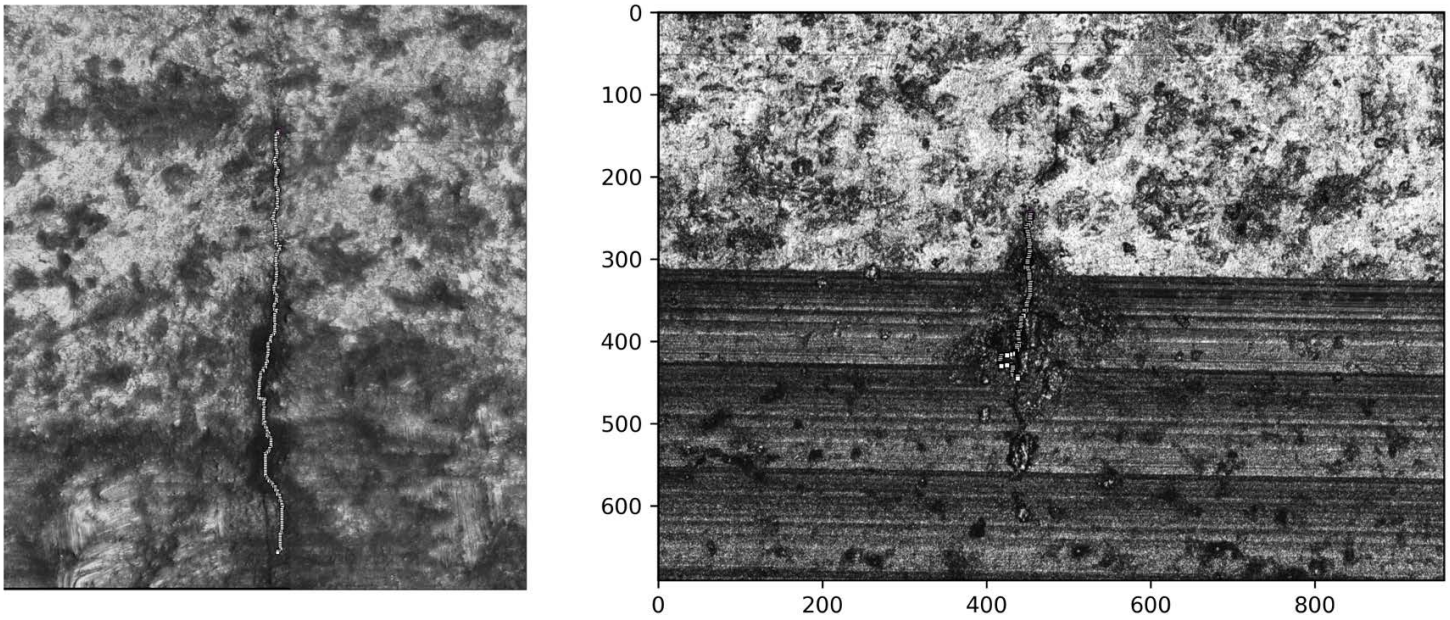

Figure 2: (Left) Estimated x, y position of the crack determined by the flag-based software for an image with corrosion and pitting present. (Right) Estimated x, y position of the crack determined by the flag-based software for an image with welding defects present (darker region at bottom).

- The determined x, y values were then used to fit Gaussian routines to the estimated crack locations. **Figure 3** shows two histograms that plot the frequency that each FWHM is measured. A red line is drawn to indicate prior analysis determination of crack width.
- The short project successfully completed the proof of concept.

Contributing Postdoctoral Researchers

Holly B. Flynn Raymond G. Belliveau

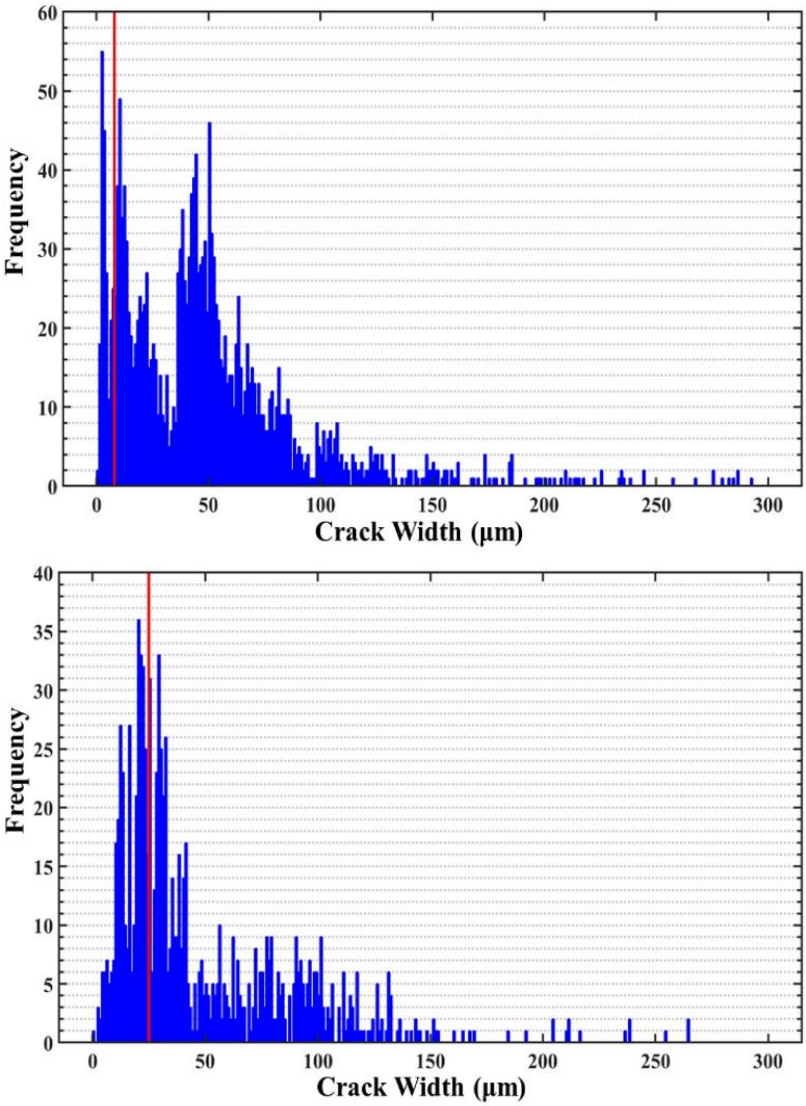

Figure 3: Histograms of the FWHM values calculated using Gaussian fits and the estimated x, y crack location determined by the flag-based system. The red line is the size of the crack determined by a prior analysis. Each Histogram relates to the images in Figure 2, respectively. The dual peaks in the top hand image is due to the heavy corrosion regions that the crack passes through, whereas, the image with weld defects has less corrosion.

Enhanced Filter Material for Pathogen Removal

Wendy Kuhne

Project Highlight

It was determined that spherical silver (Ag) nanoparticles either bound to 316 stainless-steel filter material or as unbound nanomaterials in deionized water had anti-microbial activity on Escherichia coli K-12 (*E. coli*) cultures when aerosolized or waterborne. This effect however was attenuated when in the presence of the high-salt growth media. Nanoparticles are known to agglomerate in high salt solutions and this may have limited their ability to cross the cell membrane of the microorganisms and cause fatal damage.

Project Team

Principal Investigator Wendy Kuhne

Team Members
Candace Langan Simona Murph

Abstract

In this project we evaluated two spherical nanoparticles, gold (Au) and silver (Ag), embedded separately on 316 stainless steel (SS) filter materials to remove potentially pathogenic microorganisms from airborne and waterborne environments. Escherichia coli K-12 (*E. coli*) was chosen for airborne experiments where an aerosol stream was generated for 75 sec using deionized water (DI) in a nebulizer (fan speed set to ~11.2 L per min, sonication at 50%). *E. coli* were collected on agar plates 1" from the nebulizer with and without filter material present. Treatment conditions were SS alone, SS + Ag, and SS + Au, and no filter conducted in triplicate. Ag filter material showed a 90% reduction in colony forming units (CFUs) in the aerosolized stream using DI water. Waterborne experiments, using liquid *E. coli* cultures in DI water exposed to SS, SS + Ag, and SS + Au filters resulted in a statistically significant reduction of CFUs compared to the no filter material control. When evaluated using a high salt growth media as a delivery source instead of DI water, the reduction in viable colonies was not present. Comparison of the SS filter alone vs the SS + Ag show similar levels of CFU reduction (~70-79%) in the aerosolized stream of DI water.

Objectives

- Determine suitable viral pathogen surrogates relevant and ensure that adequate analytical tools exist.
- Create and functionalize nanoparticles (different geometries and compositions; native or coated with surrogate-specific receptors) on filter materials, such as polypropylene fibers and/or stainless-steel wool.
- Create relevantly sized microorganism waterborne/airborne environments (surrogates) and filters, the ability to entrain them in fluid streams, and a way to reliably detect them with the surrogate to deactivate them and determine the efficacy of the treatment.

Introduction

Controlling and preventing air-and water-borne infections from exposure to pathogenic microorganisms is of global concern. The COVID-19 pandemic highlighted the need for development of novel filtering technologies for deactivation of human viral pathogens and surrogates present in airborne, foodborne and/or waterborne environments. Herein, we address fundamental questions to develop an effective means for the capture, removal and deactivation of human pathogens and surrogates through attraction to activated nanoparticles (NPs), with subsequent destruction and decontamination. The small particle size and high surface areas of nanomaterials are attractive additives as they can dramatically alter performance at low loadings. Metal and metal oxides, e.g. silver (Ag) and cuprous oxide nanoparticles, have been known for decades to display antiseptic characteristics, including antibacterial, antifungal, and antiviral properties.[1] They are efficient in wound management, various coatings for medical devices, and impregnating textile fabrics. Moreover, it has been shown to have increased efficacy at limiting viral infectivity on material bound viruses in clinical trials. Prior reports have indicated the Ag nanoparticles at 3-6 nM concentration had antimicrobial effects on yeast (isolated from bovine mastitis) and Escherichia coli (*E. coli*) O157:H8 (ATCC 43886). A higher concentration (33 nM) was required for inactivation of Staphylococcus aureus (ATCC 19636).[2] The mechanism by which Ag nanoparticles are thought to function as antimicrobial agents is linked to damage caused to the microorganisms cell membrane either through electrostatic forces[3] or by internal physical damage by passage of the nanomaterials through cell membranes or by the formation of pits leading to leaking of the cells.[4] We investigated Ag and gold (Au) nanomaterial bound to stainless-steel filter materials, as well as unbound nanomaterials, for their antimicrobial activity in both airborne and waterborne environments.

Approach

Airborne pathogen approach:

Initial tests were completed to determine the optimal distance from nebulizer and amount of time required for collection and formation of colony forming units (CFU). Varying distances and timepoints were collected on tryptic soy agar plates and incubated overnight to determine a dilution factor that would allow for countability (between 50-200 colonies/plate) pf the CFUs.

E. coli K-12 (ATCC, Manassas, VA), were diluted in deionized (DI) water (1:250,000 from stock culture) and loaded into a nebulizer to generate an aerosol stream. The nebulizer fan was set at 50% sonication to deliver the aerosol stream containing *E. coli* at 11.2 L min-1. The aerosol stream containing *E. coli* was set up 1 inch away from the filter material covering a tryptic soy agar plate (**Figure 1**).

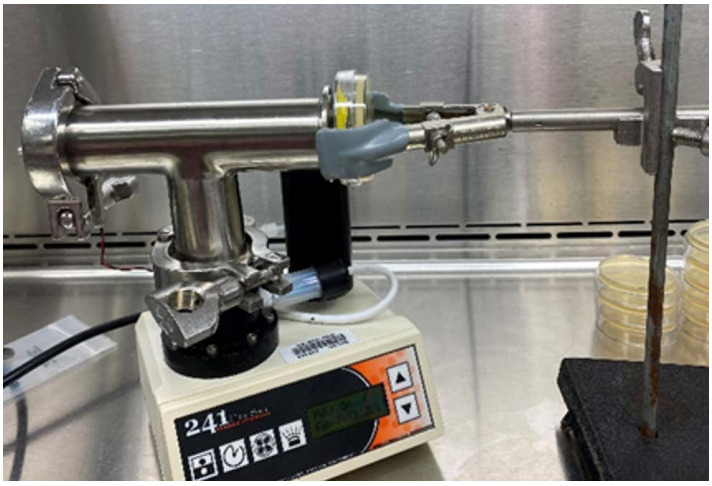

Figure 1: E. coli aerosol delivery to the filter material covering an agar plate.

Each agar plate was exposed for 30 seconds, and all experimental conditions were performed in triplicate. Filter material tested included spherical silver (Ag) nanoparticle-coated 316 stainless steel, spherical gold (Au) nanoparticle-coated, 316 stainless steel without nanoparticles bound, and no filter material as a positive control. Aerosolized *E. coli* that had traveled through the filter material was collected onto agar plates and incubated overnight. Colonies were allowed to form for 24-h post collection at 37°C and CFUs were imaged and counted using a AlphaImager.

Waterborne pathogen approach:

E.coli were diluted in DI water or Tryptic Soy Broth (TSB) growth media (1:250,000 from stock culture) and 10 mL of diluted culture were placed in a petri dish and incubated with varying filter materials: Ag nanoparticle-coated stainless steel, Au nanoparticle-coated stainless steel, stainless steel without nanoparticles bound, and no filter material as a positive control, or unbound spherical nanoparticles (Ag and Au) while shaking on a rocker table (**Figure 2**). Timepoints were taken over the course of incubation by taking 20 µL of the incubated *E. coli* culture and plating it onto a tryptic soy agar plate. Colonies were allowed to form for 24-h post plating at 37°C and CFUs imaged and counted using an AlphaImager.

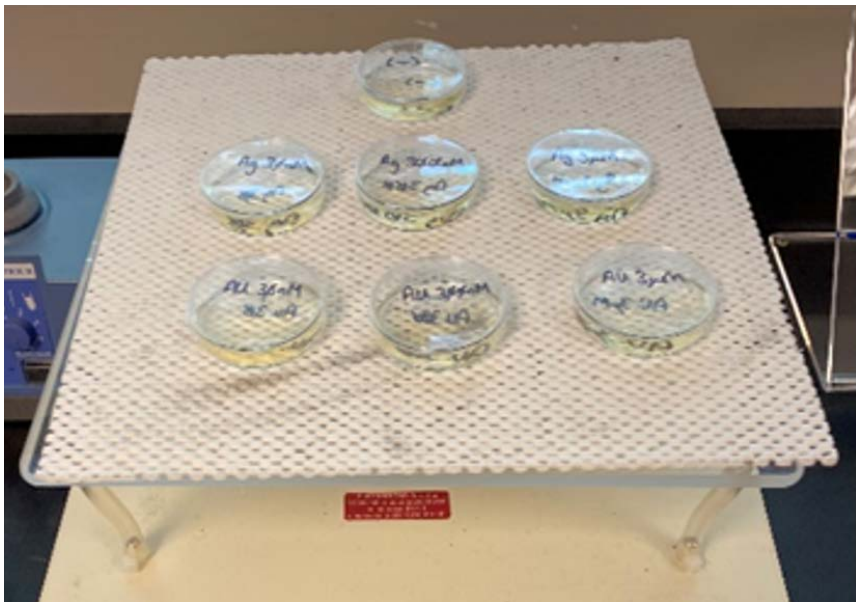

Figure 2: E. coli waterborne incubation with bound nanoparticle filter materials and unbound nanoparticles at room temperature on shaker.

Accomplishments

- Airborne: A log-reduction (~90%) in CFUs of aerosolized E.coli in DI water was measured with filter materials embedded with Ag nanoparticles versus the control with no filter present (T-Test one-tail p-value <0.01). The stainless-steel filter alone and stainless steel embedded with Au reduced CFU by ~70-79% and was measured to be statistically significant vs the control no filter test (p-values = 0.01, p-value = 0.03) respectively. A marginal difference was measured in comparing the antimicrobial effect of the stainless-steel filter alone vs the stainless-steel embedded with Ag (T-Test one-tail p-value=0.05) (**Figure 3**).
- Waterborne: Statistically significant reductions (p<0.05) in colony formation were observed with filters embedded with spherical Ag nanoparticles at a minimum of 1 h of exposure. Exposures performed using dilute TSB growth media containing salts showed little to no reduction in CFUs. Salts are known to cause agglomeration of nanoparticles[5] and could have reduced their efficacy by not allowing the Ag to pass through the cell membrane to cause damage. Efficacy of Au is driven by the size and shape of the nanoparticles, with rod shapes being the most effective[6], and in this study the spherical shape and size were not as effective for bacterial reduction (**Figure 4**).

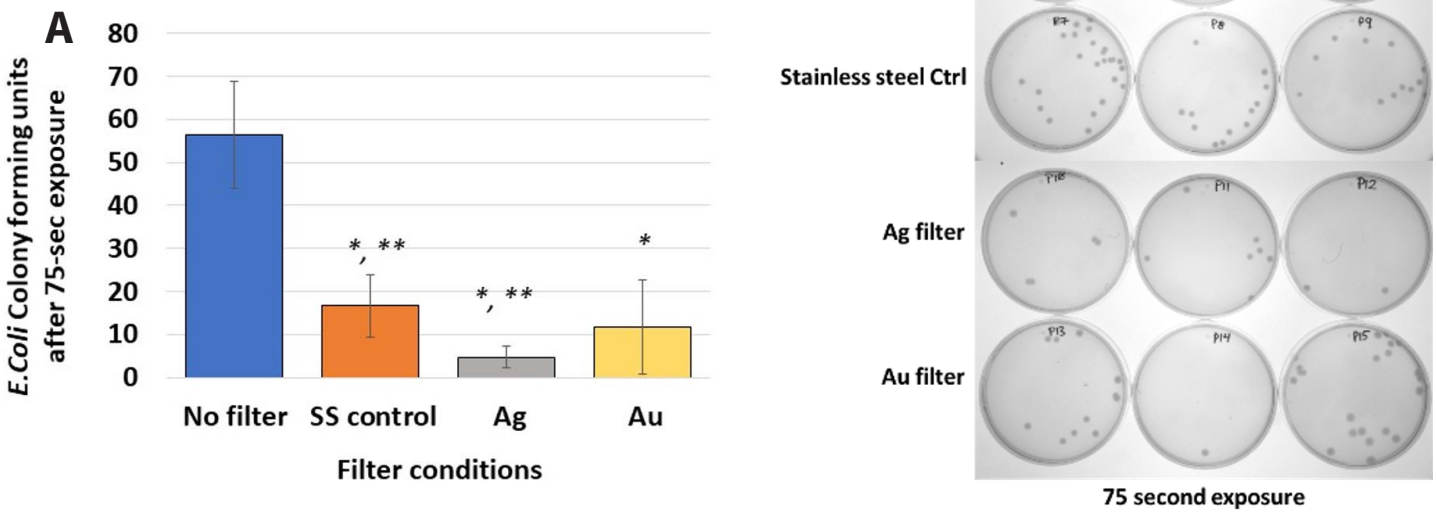

*Figure 3: (A) Colony Forming Units (CFUs) of aerosolized E. coli exposed to filter materials containing embedded silver (Ag) or gold (Au) spherical nanoparticles compared to stainless steel (SS) filter control and no filter. (B) Post-24hr collection of exposed E. coli to filter material on agar plates. Nebulizer positive controls were included (n=3). *All filter conditions were statistically significant vs the no filter control (AVOVA p-value <0.01). **A marginal difference was measured between the SS control and the Ag filter (p-value = 0.05) and no difference between the Ag and Au filters (p-value >0.05)*

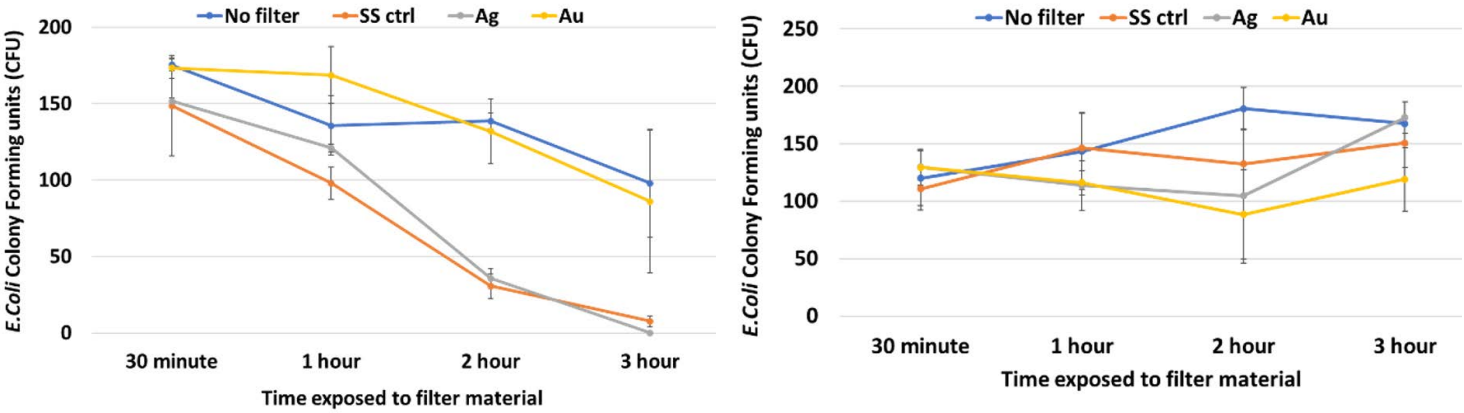

Figure 4: (Left) Colony Forming Units (CFUs) of waterborne E. coli in deionized water exposed to filter materials containing bound silver (Ag) or gold (Au) nanoparticles compared to 316 stainless steel (SS) filter control and no filter control (n=3). (Right) CFUs of waterborne E. coli in growth media exposed to filter materials containing bound silver (Ag) or gold (Au) nanoparticles compared to 316 stainless steel (SS) filter control and no filter (n=3).

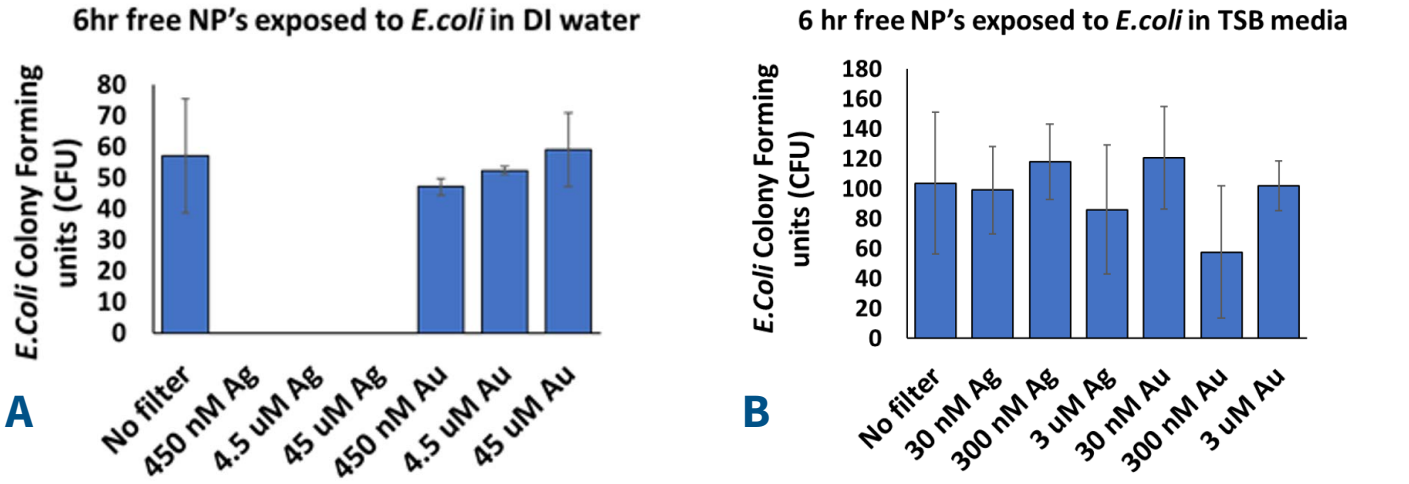

Figure 5: (A) CFUs of waterborne E. coli in DI water exposed to unbound spherical silver (Ag) or spherical gold (Au) nanoparticles compared to control culture with no nanoparticles (n=3). (B) CFUs of waterborne E. coli in TSB growth media exposed to unbound spherical silver (Ag) or spherical gold (Au) nanoparticles compared to control culture with no nanoparticles (n=3).

- Unbound nanoparticles alone were tested at concentrations of 450 nM, 4.5 µM, 45 µM in DI water for 6 h with 100% reduction of CFUs with the stainless steel + Ag filters and no statically significant difference in CFUs measured vs the control ($p > 0.05$). Using a dilute concentration of nanoparticles (30 nM, 300 nM and 3µM Ag and Au) in TSB growth media containing salts no statistically significant reduction in CFUs vs the control ($p > 0.05$) was measured (**Figure 5**).

Contributing Postdoctoral Researcher

Candace Langan

References

1. Dizaj, S. M.; Lotfipour, F.; Barzegar-Jalali, M.; Zarrintan, M. H.; Adibkia, K., Antimicrobial activity of the metals and metal oxide nanoparticles. Materials Science and Engineering: C 2014, 44, 278-284.
2. Kim, J. S.; Kuk, E.; Yu, K. N.; Kim, J.-H.; Park, S. J.; Lee, H. J.; Kim, S. H.; Park, Y. K.; Park, Y. H.; Hwang, C.-Y.; Kim, Y.-K.; Lee, Y.-S.; Jeong, D. H.; Cho, M.-H., Antimicrobial effects of silver nanoparticles. Nanomedicine: Nanotechnology, Biology and Medicine 2007, 3 (1), 95-101.
3. Dibrov, P.; Dzioba, J.; Gosink, K.K.; Häse, Chemiosmotic mechanism of antimicrobial activity of Ag+ in Vibrio cholerae. Antimicrob Agents Chemother. 2002, 46(8), 2668-2670.
4. Sondi, I; Salopek-Soni, B., Silver nanoparticles as antimicrobial agent: a case study on *E. coli* as a model for Gram-negative bacteria. J Colloid and Interface Sci. 2004, 275, 177-182.
5. Williams, D.N.; Ehrman, S.H.; Pulliam Holoman, T.R., Evaluation of the microbial growth response to inorganic nanoparticles. J Nanobiotechnology. 2006, 4:3, 1-8.
6. Chatterjee, T; Chatterjee, B.K.; Chakrabarti, P.; Modelling of growth kinetics of Vibrio cholerae in presence of gold nanoparticles: Effect of size and morphology. Sci. Rep. 2021, 7, 9671.

Analysis of Microplastics in Bivalves along Fourmile Branch

Wendy Kuhne

Project Highlight

Water and bivalves were collected at Fourmile branch sampling locations along the length of the branch to evaluate the formation of microplastics from site operations. Fourmile Branch is a site stream with historical and current industrial effluent from site operations and receives effluent from the site's wastewater treatment facility. This research is the first to explore microplastics environmental transport on the Savannah River Site, allowing SRNL to expand capabilities to a new field that is expanding as the deleterious effects of plastics on the environment is becoming more apparent.

Project Team

Principal Investigator Wendy Kuhne

Team Members

Grayson Walker
Kaitlin Lawrence
Heather Brant
George Larsen
Joseph Mannion

Abstract

Microplastics are commonly found near wastewater treatment facilities with the source originating typically from fibers associated with laundry detergents. Fourmile branch would have limited laundry associated effluent and does not receive any input from water originating from upstream industry sources, therefore microplastics would have originated from Site operations or through atmospheric deposition which are both unexplored pathways. In order to assess environmental inventory effects on the biota, water samples were collected from sampling locations along Fourmile Branch on the Savannah River Site using plankton nets and grab samples at Fourmile Branch locations (i.e., FM-2B, FM-A7, and FM-6). Fourmile Branch has a long history of receiving industrial effluents from site operations as well effluent from the site's wastewater treatment plant. Water samples and the debris collected in the nets were rinsed with deionized water and sieved to remove the larger fractions of plastics (4000-2000 µm) and retain fractions <500 µm. The water samples were analyzed for the type and size of plastics by µ-Raman, mass spectrometry, and Fourier Transform Infrared Spectroscopy (FTIR) methods. Previously collected bivalves were prepared into thin sections and analyzed using microscopy

Objectives

- Develop a method to analyze and measure microplastics from SRS streams
- Analyze surface water samples collected along Fourmile Branch using plankton nets for the presence of microplastics.
- Analyze the tissue of previously collected bivalves from Fourmile Branch for microplastics taken into organism.

Introduction

Plastics in the environment are recognized as a global environmental health problem. The majority of our daily one-use items (cups, food containers, and drink bottles) are made of monomers that are NOT totally biodegradable. Many of these items are not involved in recycling programs and end up in sanitary landfills or discarded to the local environment. Over time, these materials end up fracturing through processes of photodegradation and physical abrasion into smaller and smaller size fractions, going from macro scale (>5 mm)1 to microplastic (1 µm to 5 mm) 2 and finally to nano-size particles (<1 µm) 3. These particles are often referred to as micronizing plastics.

Figure 1: (Left) Fourmile Branch location FM-2B. Upper most location with the lowest flow rate 1909 gpm. (Right – Top) Location FM-A7, below the wastewater treatment facility with a stream flow with flow rate of 7371 gpm. (Right – Bottom) Location FM-A6 furthest location downstream before entering the Savannah River. Flow rate measured at 9777 gpm.

Fourmile branch (FMB) is a tributary on the upper coastal plain of South Carolina and historically received thermal effluent from C Reactor on the Savannah River Site from 1955 to 1985. It also received discharges from the F- and H-area Chemical Separations facilities and today from the Site's only sanitary wastewater treatment facility. To our knowledge levels of microplastics in SRS Site streams have not been investigated. This study would be the first to evaluate microplastics in FMB along three locations representing a clean "background" location (FM-2B), just below the wastewater treatment facility (FM-A7), and furthest away from site operations, but prior to entering the Savannah River (FM-6) (**Figure 1**).

Microplastics were evaluated in surface water collected from the locations using grab samples and plankton nets. Sieving was performed to remove larger fractions (4000-2000 µm) and to retain fractions <500 µm. Bivalves that had been collected previously were investigated for levels of microplastics in the tissue at these same locations (**Figure 2**). Both water and biota tissue samples were analyzed by microscopy and spectrometry (micro-Raman, FTIR, mass spectrometry) techniques to determine quantity, size, and type.

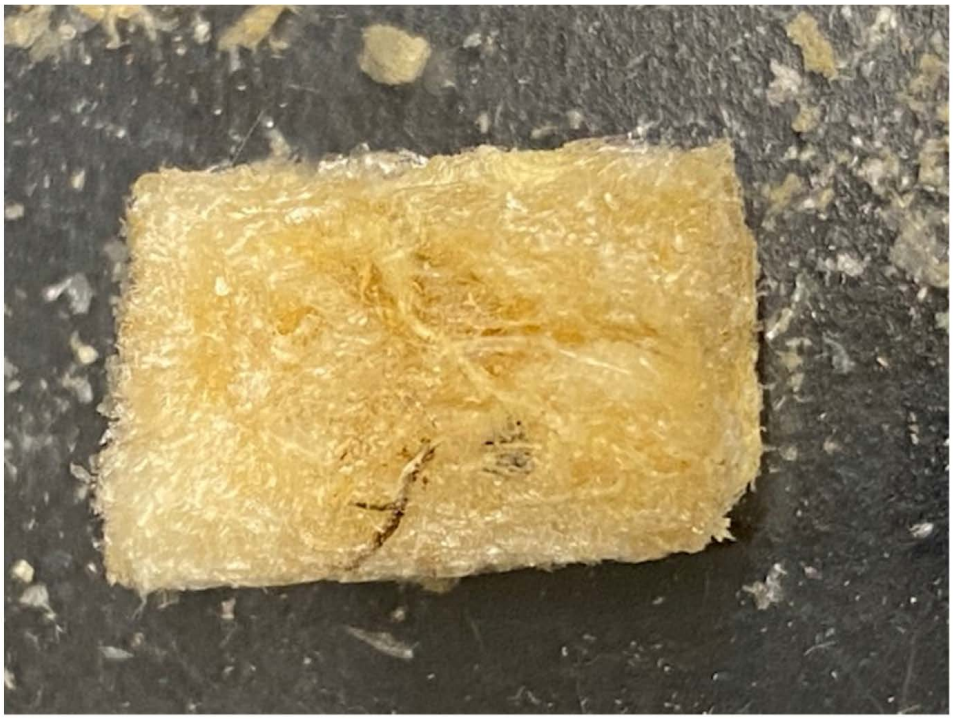

Figure 2: Tissue section from bivalve collected at FM-6.

Approach

1. Determine levels of microplastics in water collected from FMB. Microplastics will be evaluated in previously collected surface water samples along the FMB (i.e., FM-2B, FM-A7, and FM-6). A 10 L grab sample and plankton nets were deployed to the main channel of the stream for collection times of ~4.5 h.
2. Determine levels of microplastics in archived bivalves from FMB. Filter feeder organisms are proving to be a valuable resource for understanding MPs in the environment. Histological sections of the Bivalve tissue were made and submitted for micro-Raman analysis.
3. Recovered microplastic particles from both water and bivalves were analyzed using bright field microscopy and spectrometry (micro-Raman, FTIR, mass spec) techniques to determine quantity, size, and type.

Accomplishments

- Water samples were collected at each of the three locations for an average collection time of ~4.5 h. The flow rate of the mainstream channel ranged from 1909 gallons per minute (gpm) at FM-2B, the upper most control location, to 7371 gpm at FM-A7, and finally a peak flow of 9777 gpm at FM-6 (**Figure 1**).
- Bivalve histological sections (**Figure 2**) could not be evaluated using micro-Raman due to intense background fluorescence levels.
- Polyamide bead standards were measured with micro-Raman for single particle measurements (**Figure 3**).
- Fluorescence microscopy was used with dye tagged polymer beads to investigate the utility of fluorescence microscopy for polymer imaging (**Figure 4**).
- Plastic particulates were found in the streams and FTIR was used to identify their chemical composition (**Figure 5**).

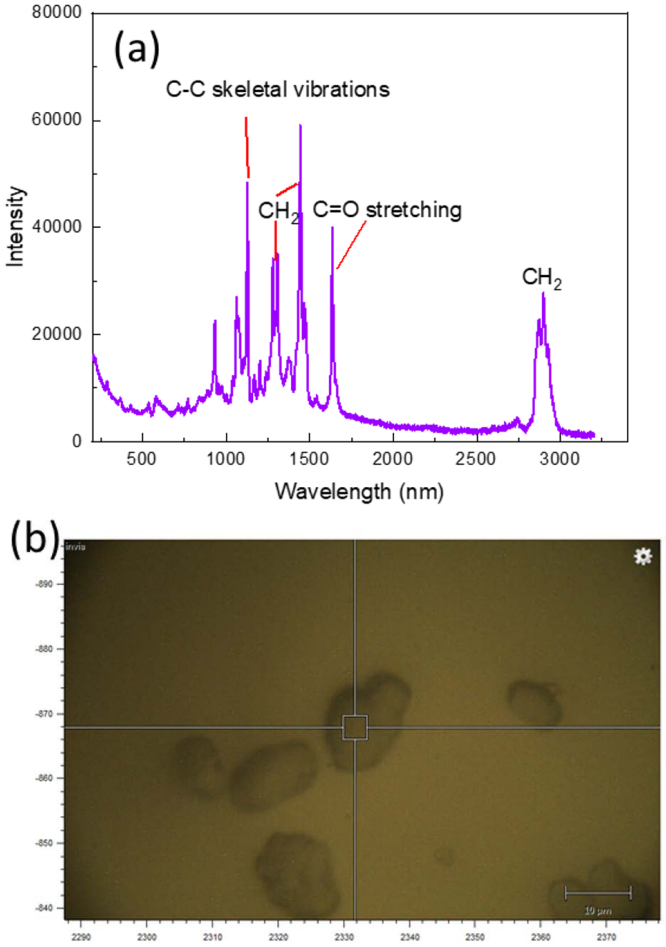

Figure 3: (a) micro-Raman of standard polyamide (b) single particle map for Raman measurements.

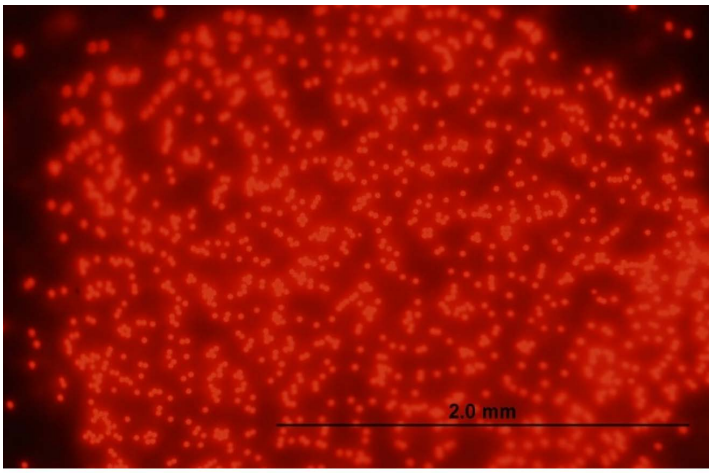

Figure 4: Fluorescence microscope image of dye tagged polystyrene beads.

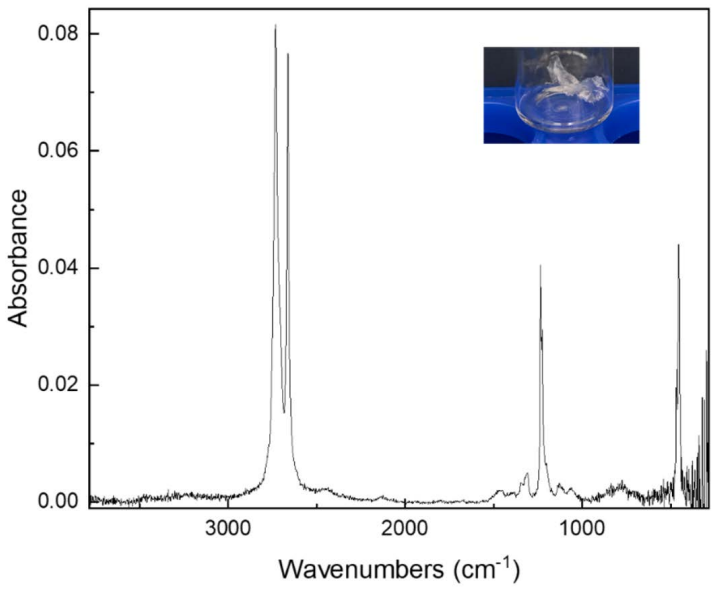

Figure 5: FTIR of plastic particulate found in FM2B, which was identified as polyethylene (inset: photo of collected plastic particulate).

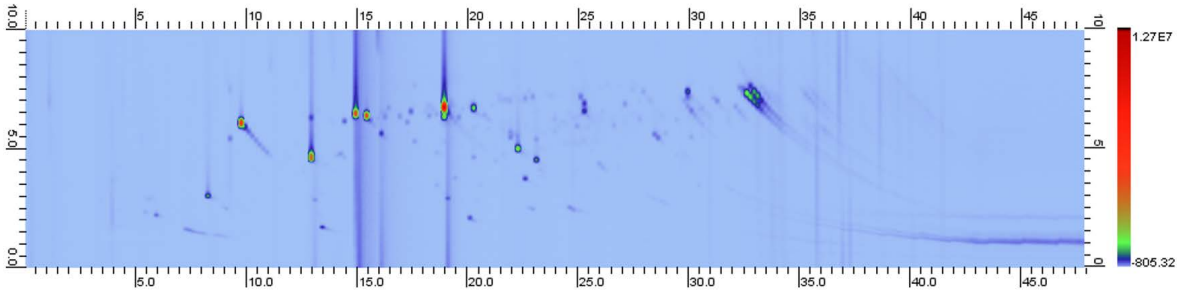

Figure 6: 2D GCxGC-MS for FM2B.

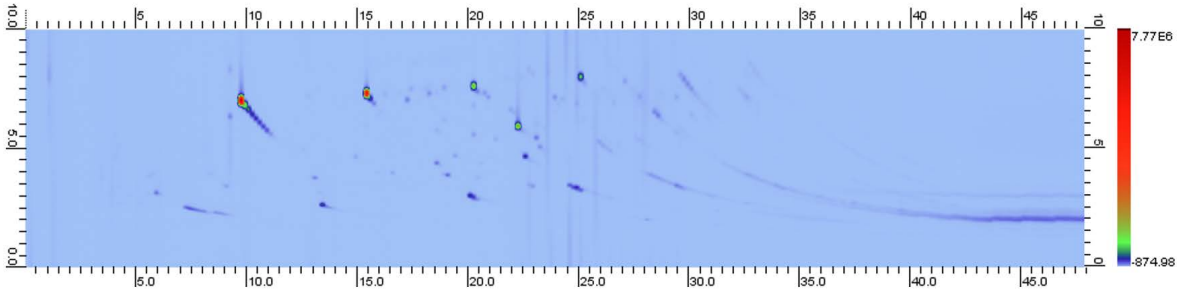

Figure 7: 2D GCxGC-MS data for FMA7.

- Water samples were oxidized to remove biological material then filtered and imaged using bright field microscopy (**Figure 8 – Figure 10**)
- Two-dimensional gas chromatography coupled with mass spectrometry (GCxGC-MS) data was measured using sorbent stir bars to identify the chemicals present in the water to help identify the types of plastics and chemicals found in the water streams (**Figure 6** and **Figure 7**). Chemical compositions were compared to a NIST library for positive chemical identification. Different styrene-based fragments were measured in FM-A7 (**Figure 7**). The sampling location for FM-A7 is near a roadway, where tire treads are one possible source of the styrene. The sample nets are made of nylon, the floats attached to the net and the grab sample carboy are both made of polyethylene.

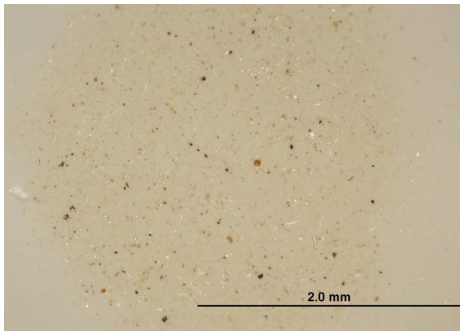

Figure 8: Bright field images of FMA7 after filtration and wet peroxide oxidation.

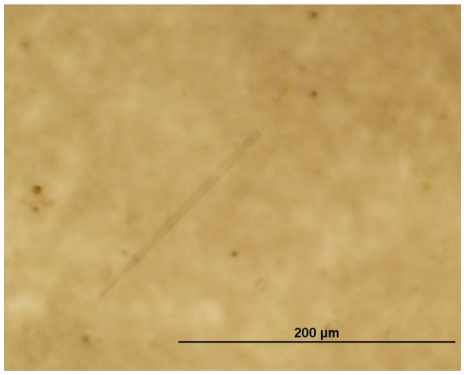

Figure 9: Brightfield image closeup of suspected microplastics from FM2B.

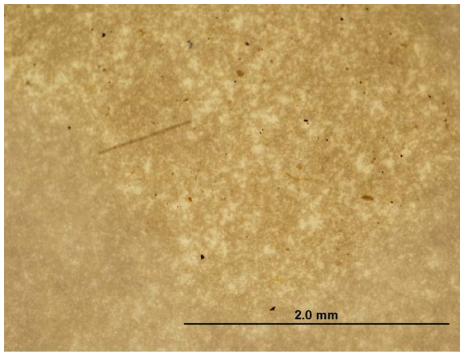

Figure 10: Brightfield image of FM6.

References

1. Lebreton, L., Egger, M. & Slat, B. A global mass budget for positively buoyant macroplastic debris in the ocean. Sci. Rep. 9, 1–10 (2019).
2. Peeken, I. et al. Arctic sea ice is an important temporal sink and means of transport for microplastic. Nat. Commun. 9, 1505 (2018).
3. Wagner, S. & Reemtsma, T. Things we know and don't know about nanoplastic in the environment. Nat. Nanotechnol. 14, 300–301 (2019).

Savannah River National Laboratory

FY21 LDRD ANNUAL REPORT

SRNL
SAVANNAH RIVER NATIONAL LABORATORY

LDRD
LABORATORY DIRECTED RESEARCH & DEVELOPMENT

For more information, go to *www.srnl.doe.gov*